Studies of the assembly pathway of human ATP synthase

Corsten Perrie Louise Claire Douglas

Medical Research Council

Mitochondrial Biology Unit

University of Cambridge, Murray Edwards College

A thesis submitted to the University of Cambridge for the degree of Doctor of Philosophy

March 2017

Declaration

The work presented in this thesis was carried out at the Mitochondrial Biology Unit between December 2012 and March 2017, and is the result of my own work, except where stated. This thesis has not been submitted to any other institution. The word limit has been adhered to.

Corsten Douglas

March 2017

Acknowledgements

First and foremost, I thank my supervisor, Professor Sir John Walker, for giving me the opportunity to study one of the most fascinating enzymes discovered, and for his guidance with the writing of this thesis.

I would also like to give thanks to all the past and present members of the proteomics and ATP synthase labs, who have helped my understanding of ATP synthase, and enjoyment of research, grow over the years. Specifically, I thank to Dr. Joe Carroll and Dr. Ian Fearnley for investing time and effort to discuss both the technical and practical aspects of research. Thanks is also given to other members of the lab: Holly, Tobias, Byron, Tom, Shujing, Mike, Ian W, Martin, Virginie, Leo and Jay for their help.

Appreciation is also given to the administrators, IT support, research support staff and custodians of the MBU for their hard work ensuring that staff and students are cared for and fully equipped to carry out their work.

Dan Douglas also deserves commendation, for the tremendous effort he has made to keep me safe and healthy throughout my time at the University of Cambridge.

I am also grateful to my close and distant relatives for their love and support.

There are many others whom I owe a great deal to for supporting me over the years, and the list is so long that I wish to thank them all anonymously.

Abstract

Human mitochondrial ATP synthase is an enzyme containing 18 unlike subunits located in the inner mitochondrial membrane (IMM), where the catalytic F_1 domain extends into the mitochondrial matrix and the F_O domain, which contains the c_8-ring rotor, the a-subunit and the supernumerary subunits, is anchored in the IMM. All the subunits, apart from the a- and A6L-subunits, are encoded in the nucleus and require transport into the mitochondria before being assembled. The a- and A6L-subunits are encoded on the mitochondrial genome. The respiratory complexes generate the proton motive force (PMF), which ATP synthase uses to generate ATP from ADP and P_i. Rotation of the α- and β-subunits with the central stalk γ-, δ- and ε-subunits is prevented by coupling the F_1 domain to the F_O domain via the peripheral stalk (the OSCP-, F_6-, d- and b-subunits). ATP hydrolysis is prevented by the natural inhibitor of the enzyme, IF_1, binding to the F_1 domain. In addition to the a- and, b-subunits, the F_O domain contains the c_8-ring and six supernumerary subunits not involved in the catalytic activity of ATP synthase. The roles of five of these subunits in the assembly of ATP synthase, the e-, f-, g-, DAPIT- and 6.8 kDa proteolipid-subunits, were investigated by suppressing or disrupting their expression individually. The e-subunit is the first of the supernumerary subunits to assemble, then the g-subunit followed by the f-, 6.8 kDa proteolipid- and DAPIT-subunits. All five supernumerary subunits investigated were required to facilitate the dimerisation and oligomerisation of ATP synthase. The e-, f- and g-subunits were found to be important for maintaining mitochondrial respiratory capacity.

Table of contents

Abbreviations

6.8 PL	6.8 kDa proteolipid
°C	degrees Celsius
ΔΨ	electrical gradient
ΔG	Gibbs' free energy change
ΔpH	pH gradient
2DG	2-deoxy-D-glucose
A	adenine
Å	$1x10^{-10}$ meters
ADP	adenosine diphosphate
ANT	adenine nucleotide transporter
AO	aridine orange
ATP	adenosine triphosphate
ATPAF1	ATP synthase assembly factor 1
ATPAF2	ATP synthase assembly factor 2
ATTC	American type culture cells
BCA	bicinchoninic acid
BN-PAGE	blue native polyacrylamide gel electrophoresis
bp	base pairs
BSA	bovine serum albumin
C	cytosine
Ca	calcium
cDNA	complementary deoxyribonucleic acid
Cl	chlorine

C-termini	carboxyl-termini of peptides or proteins
CRISPR	clustered regularly interspaced short palindromic repeats
Da	Dalton
DAPI	2-(4-amidinophenyl)-1H -indol-6-carboxamide
DAPIT	diabetes associated protein in insulin sensitive tissues
DDM	n-dodecyl-beta-D-maltoside
ΔpH	pH gradient
DMEM	Dulbecco's modified eagle medium
DMSO	dimethyl sulfoxide
DNA	deoxyribonucleic acid
dPBS	Dulbecco's phosphate buffered saline
Drp1	dynamin related protein 1
DTT	1,4-dithiothreitol
EB	elution buffer
ECL	enhanced chemiluminescence
EDTA	(ethane-1,2-diyldinitrilo)tetraacetic acid
EM	electron microscopy
ETF	electron transferring flavoprotein
F	Faraday constant
FACS	fluorescence assisted cell sorting
FAD	flavin adenine dinucleotide
FAM	6-carboxyfluoriscein
FBS	fetal bovine serum
fMol	femto mole
FNSN	familial bilateral striatal necrosis

FCCP	4-(trifluoromethoxy(phenylhydrazone)
Fis1	mitochondrial fission protein 1
G	guanine
g	gravitational force
GFP	green fluorescent protein
GRACILE	growth retardation, aminoaciduria, cholestasis, iron overload, lactic acidosis and early death
gRNA	guide ribonucleic acid
GTP	guanosine triphosphate
HBSS	Hank's buffered saline solution
HCl	hydrochloric acid
HPLC	high pressure liquid chromatography
IF_1	inhibitory factor 1
IMDM	Iscove's modified Dulbecco's medium
IMM	inner mitochondrial membrane
IMS	intermembrane space
INAC	inner membrane assembly complex
kDa	kilo Dalton
L	litre
LB	lysogeny broth
LC-MS	liquid chromatography-mass spectrometry
M	moles per litre
m/z	mass per charge
mA	milli amps
MALDI TOF	matrix assisted laser desorption/ionisation time of flight

MELAS	mitochondrial encephalomyopathy, lactic acidosis, and stroke-like episodes
Mff	mitochondrial fission factor
Mfn1	mitofusin 1
Mfn2	mitofusin 2
mg	milli gram
Mg	magnesium
MiD49	mitochondrial dynamics protein of 49 kDa
MiD51	mitochondrial dynamics protein of 51 kDa
min	minutes
mL	milli Litre
mM	milli Mole
mPTP	mitochondrial permeability transition pore
mRNA	messenger ribonucleic acid
mtDNA	mitochondrial DNA
NADH	nicotinamide adenine dinucleotide
NARP	neuropathy, ataxia and retinitis pigmentosa
NDUFS1	NADH dehydrogenase (ubiquinone) iron sulfur protein 1
NEB	New England Biolabs
ng	nano gram
nm	nano meter
N-termini	amino-termini of peptides or proteins
OCR	oxygen consumption rate
OMM	outer mitochondrial membrane
OSCP	oligomycin sensitivity conferral protein

OPA1	optic atrophy 1
PAM	protospacer adjacent motif
PCR	polymerase chain reaction
PD	Parkinson's disease
pH	- log $[H^+]$
P_i	inorganic phosphate
PINK1	PTEN-induced putative kinase 1
PMF	proton motive force
PTEN	phosphatase and tensin homologue
PVDF	polyvinylidene-difluoride
qPCR	quantitative polymerase chain reaction
Q	quinone
QH_2	ubiquinone
R	universal gas constant
RET	reverse electron transfer
ROS	reactive oxygen species
SDS-PAGE	sodium dodecyl sulfate poly acrylamide gel electrophoresis
SILAC	stable isotope labelling of amino acids in cell culture
siRNA	small intefering ribonucleic acid
SOC	super optimal broth
SQ	semiquinone
sRNA	scaffold RNA
SRB	sulphorhodamine B
T	thymine

TAMRA	tetramethylrhodamine
TBE	Tris borate EDTA
TCA	trichloroacetic acid
TCEP	Tris (2-carboxyethyl) phosphine
TEMED	tetramethylethylenediamine
TIM	translocase of the inner mitochondrial membrane
TOM	translocase of the outer mitochondrial membrane
Tris	2-amino-2-hydroxymethyl-propane-1,3-diol
RNA	ribonucleic acid
rRNA	ribosomal RNA
tRNA	transfer RNA
μL	milli Litre
μM	micro molar
UV	ultra violet
V	volts
v/v	volume pervolume
VDAC	voltage gated anion channel
WT	wildtype
w/v	weight per volume

1. Introduction

1.1. Bioenergetics

All living things require a mechanism to convert the energy they consume as food into chemical energy to do useful work for the organism, such as growth and reproduction. Energy conversion can be in the form of photophosphorylation for plants and photosynthetic bacteria during photosynthesis, and oxidative phosphorylation for respiring organisms [1]. Most of the energy consumed by eukaryotes is converted to adenosine triphosphate (ATP) in mitochondria by the ATP synthase using the proton motive force (PMF) generated by enzymes in the respiratory chain. The remaining ATP is produced by glycolysis [2] and other substrate-level phosphorylation events including those catalysed by succinyl-coA synthetase [3], and creatine kinase [4]. The bioenergetic cost of making an ATP molecule in the mitochondria of mammals is 2.7 protons translocated through ATP synthase /ATP molecule. When the transport of phosphate through the phosphate/H^+ symporter is considered, the cost increases to 3.7 protons/ATP synthesised [5]. Furthermore, there is the requirement to transport one proton to the IMS to replace the loss of membrane potential when ATP^{4-} is exchanged for ADP^{3-} by the adenine nucleotide transporter [1].

The action of respiratory chains can be explained by chemiosmosis, which describes the coupling between the proton translocating and electron transferring respiratory complexes and the reversible ATP synthase, which catalyses the reaction in Equation 1 [6].

Equation 1. $ADP + Pi + H_2O \leftrightarrow ATP$

According to chemiosmosis, the components required for ATP synthesis are the reversible ATP synthase, the respiratory chain complexes in bacteria and mitochondria, or

photophosphorylation complexes in chloroplasts, the mitochondrial transporters and a solute and ion impermeable inner mitochondrial membrane, (1, 2, 3 and 4 in Fig. 1.1, respectively) [1, 6, 7].

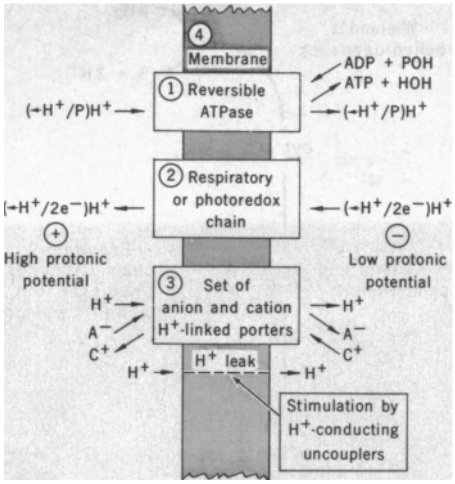

Fig. 1.1 The chemiosmotic hypothesis. ADP: adenosine diphosphate, POH: inorganic phosphate, ATP: adenosine triphosphate, A^-: anions, C^+: cations, H^+: protons. Figure adapted from ref. [6].

The ability of an organism to use ATP to do useful work requires the ATP:ADP ratio to be large, indicating that the reaction in Equation 1 is displaced far from equilibrium in the direction of ATP synthesis. In mitochondria, the ADP/ATP translocator and the phosphate transporter continuously supply and remove the reactants and products of ATP synthesis, while the respiratory chain provides the proton motive force (PMF) that ATP synthase requires to synthesise ATP via rotary catalysis. This is related to the Gibbs free energy change as shown in Equations 2 and 3:

Equation 2. $\Delta G = -F\Delta\Psi + 2.3RT \log_{10} ([H^+_{matrix}]/[H^+_{IMS}])$

Equation 3. $\Delta\tilde{\mu}_{H^+} = -F\Delta\Psi + 2.3RT\Delta pH$

Where ΔG is the Gibbs free energy change, F = the Faraday constant, ΔΨ = the electrical gradient (membrane potential), R = the universal gas constant, T = the temperature at atmospheric pressure measured in Kelvin and ΔpH is $[H^+_{matrix}]/[H^+_{IMS}]$. IMS = intermembrane space [1].

1.2.Mitochondria

Mitochondria are essential for aerobic respiration in eukaryotic life and are also involved in many important cellular processes including regulation of the cell cycle [8], apoptosis [9], the permeability transition [10], amino acid and fatty acid metabolism [1], and are the site of essential processes such as iron-sulphur cluster (Fe-S) [11] and haem biosynthesis [12], and the citric acid cycle [13].

The evolution of eukaryotic life is a controversial subject, and there are many different theories which try to explain it [14]. One theory, the hydrogen hypothesis for eukaryotic evolution, suggests that an α-proteobacterial cell capable of facultative anaerobic respiration was the symbiont for an obligate anaerobic methanosome host that used geologically available hydrogen as a substrate for methanogenesis and ATP synthesis. The theory suggests that the geological hydrogen source became unavailable to the host methanosome and that the host obtained its hydrogen from the symbiont instead. This event may have resulted in the host engulfing the symbiont (endocytosis) and the subsequent transfer of genes from the symbiont to the host [15]. From this point, it is hypothesised that the first eukaryote began to evolve, leading to the transfer of genes from the mitochondria to the host cell nucleus. This event resulted in the requirement to translate nuclear encoded mitochondrial proteins in the cytosol and then to transfer the proteins into mitochondria through the outer and/or inner membrane of the organelle. The process of protein import into mitochondria is carried out by the TOM-TIM twin-pore translocase complex [16, 17],

which uses the membrane potential generated by the respiratory complexes to insert proteins into the inter-membrane space (IMS), inner mitochondrial membrane (IMM) or the mitochondrial matrix. Mitochondrial import sequences are recognised by subunits of the twin-pore translocase and this sequence determines which compartment of the mitochondrion the protein will eventually reside in. In human mitochondria, the genes that remain on the mitochondrial genome encode 13 hydrophobic proteins, all of them components of the respiratory chain complexes, 22 transfer RNA (tRNA) molecules and 2 ribosomal RNA (rRNA) molecules that are used during the translation of the mitochondrially encoded proteins. [18]. The organisation of genes on the human mitochondrial genome is present in Fig. 1.2.

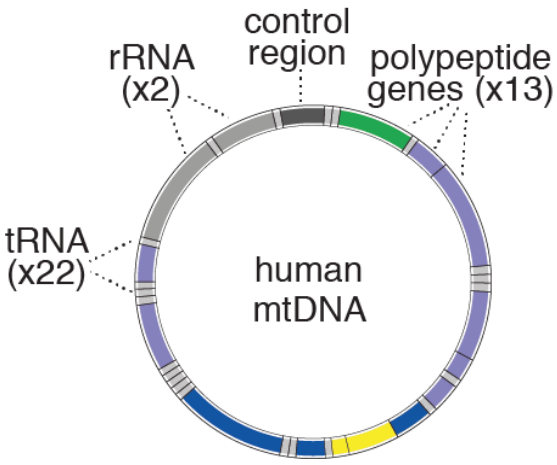

Fig. 1.2 The human mitochondrial genome. Control region in dark grey, ribosomal RNA in medium grey, transfer RNA in light grey, complex III gene CYB in green, complex I genes ND6, ND5, ND4, ND4L, ND3, ND2 and ND1 in purple, ATP synthase genes ATP8 and ATP6 in yellow, complex IV genes COX1, COX2 and COX3 in blue. Figure supplied by Martin Montgomery, MRC-MBU.

Mitochondria are the site of many metabolic processes that require substrates including fatty acids, keto acids, amino acids, nucleotides and vitamins. These molecules need to be transported from or to the cytoplasm or mitochondrial matrix through the mitochondrial carriers [19–21]. Mitochondria require substrates to carry out their functions, and are the

site of synthesis of many enzyme co-factors and substrates including ATP, iron-sulphur clusters and haem groups that are required by enzymes outside of the mitochondrion [22, 23]. In addition, active transport of substrates across the IMM is needed because the IMM is impermeable to molecules such as fatty acids, keto acids, amino acids, nucleotides and vitamins. Therefore, a mechanism of transport between the mitochondrial matrix and cell cytoplasm is required. Members of the mitochondrial carrier family [24] function as monomers and contain three points of contact that mediate binding between the carrier and substrate [25]. The carriers exist in one of three states at any one time, open to the cytoplasm, substrate occluded or open to the mitochondrial matrix [25].

1.3. Dynamics and morphology of mitochondria

Mitochondria are dynamic organelles that are constantly changing shape or size [26] via different mechanisms, including swelling and shrinking, fusion of numerous mitochondria into a larger reticulated mitochondrial network, and fission of mitochondria into multiple smaller punctate organelles [27]. The number of mitochondria in cells ranges from zero in red blood cells to around 2000/cell in liver, heart and skeletal muscle cells [1]. Mitochondria possess two membranes, the IMM surrounded by the outer mitochondrial membrane (OMM) with the intermembrane space in between the two, and the mitochondrial matrix contained inside the IMM [1]. During each cell cycle, the cell's mitochondrial population needs to double, so that each daughter cell is endowed with a mitochondrial population akin to that of the parent cell, highlighting the requirement for mitochondrial dynamics to be tuned to the cell cycle. Mitochondria are motile within the cell, interacting with microtubules that transport the organelles predominantly to areas of the cell with high energy usage [27]. The entire mitochondrial network interacts with the cellular actin network, where association of mitochondria with actin filaments is linked to

rapid Drp1-mediated fission of the mitochondrial network, followed by immediate fusion once the interaction is abolished. It is thought that interaction of actin with mitochondria is one of the factors that regulates the homeostasis of mitochondrial morphology [28]. Fission is the process of mitochondria dividing and becoming smaller punctate structures, where larger, elongated mitochondria have split into multiple smaller organelles. Fission is regulated by the dynamin-related GTPase Drp1 [29]. Monomers of Drp1 form helical multimers around mitochondria in response to recruitment by a number of factors including Fis1, Mff, MiD49 and MiD51 [30], followed by GTP dependent division of the mitochondrion into a punctate network consisting of small dot-like mitochondria. Fusion of mitochondria results from two or more mitochondria integrating with each other to become a larger reticulated mitochondrial network [26]. Fusion relies on the coordination of separate events involving the fusion of the OMM and IMM, and allows exchange of matrix contents [31]. Proteins known to mediate mitochondrial fusion include the mitofusins Mfn1 and Mfn2, and OPA1, which are GTPases. Outer membrane fusion is mediated by Mfn1 and Mfn2, and precedes inner membrane fusion, resulting from the action of OPA1 [32]. The IMM contains the mitochondrial carriers and respiratory complexes and displays two notable structural features: numerous tubular or lamellar cristae which increase the surface area, and, therefore, the space available for the membrane bound proteins, and a boundary membrane (Fig. 1.3). Cristae display a range of morphologies depending on factors including the stage of the cell cycle, cell type and disease status of the mitochondrion [33]. The morphology of the cristae in mitochondria is linked to the presence of rows of ATP synthase dimers at the apices of the cristae in a range of species including cows, potatoes, fungi [34, 35] and the alga *Polytomella* spp [36]. When the gene encoding the e-subunit of ATP synthase is deleted in yeast, the cristae display onion-like concentric ring structures [37], which may indicate that the cristae have become

disrupted. In *Saccharomyces cerevisiae*, the e-subunit and also the g-subunit are required for dimerisation of ATP synthase [37]. Mgm1p, the yeast homologue of human OPA1, is also involved in mitochondrial fusion and is thought to regulate the stabilisation of ATP synthase dimers by the e-subunit [38].

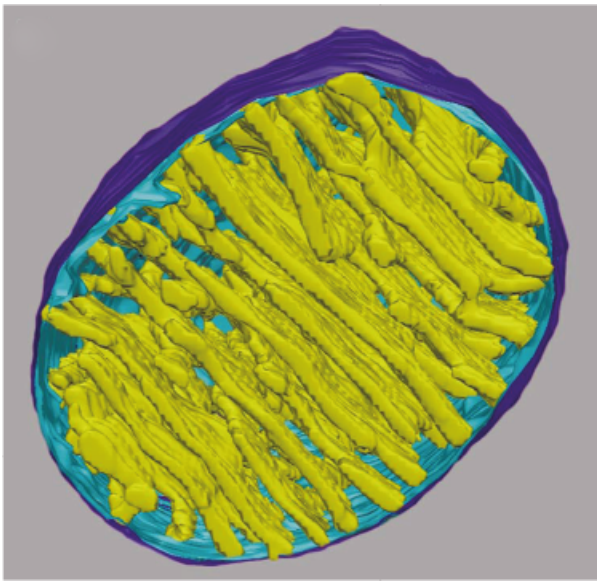

Fig. 1.3 Electron microscopic tomograph of mitochondria from chicken cerebellum. The IMM is shown with two structural features, the cristae (yellow), the boundary membrane (light blue) which is surrounded by the OMM (dark blue). At the interfaces between the cristae and the boundary membrane are cristae junctions. Figure adapted from Frey, 2000 [33].

1.4. The respiratory chain enzymes

For ATP synthase to synthesise ATP, a PMF across the inner mitochondrial membrane is required, which is generated when protons are pumped from the mitochondrial matrix into the intermembrane space by respiratory complexes I, III and IV using redox energy. Complexes I, II, III and the electron transferring flavoprotein (ETF) contribute to the QH_2 pool in the IMM, (Fig. 1.4). The quinone pool facilitates the mobility of electrons from complex I, complex II and the ETF oxidoreductase. The QH_2 pool is utilised by complex III in the Q cycle [39]. Electrons are transferred from complex III to complex IV by

cytochrome c [1]. The mechanisms of proton pumping differ between respiratory complexes. They result in the transport of electrons from low potential redox couples, such as the NAD^+/NADH couple through higher potential redox couples to the final electron acceptor O_2 (comprising the $O_2/2H_2O$ redox couple) [1].

The electrons transported through the respiratory chain are donated by substrates including NADH and succinate, which are generated by the citric acid cycle. Electron transfer and proton translocation by the respiratory chain enzymes is depicted in Fig. 1.4. The electrons transferred by complex I (NADH:ubiquinone oxidoreductase) come from NADH generated from pyruvate reduction during the citric acid cycle. The stoichiometry of proton pumping and electron transfer in mitochondrial complex I is 2 e^- transferred from NADH for every 4 protons pumped into the IMS. Two protons are also taken up from the matrix by complex I to reduce Q to QH_2 [40, 41].

Complex II is the only membrane bound enzyme of the citric acid cycle and does not pump protons. It catalyses the reduction of succinate to fumarate and electrons are donated to the Q-pool. [42]. The electron transferring flavoprotein (ETF) has a flavin adenine dinucleotide (FAD) molecule that can be reduced by accepting electrons from many dehydrogenases including those involved in fatty acid oxidation. The electrons are transferred to membrane bound ETF-Q oxidoreductase, which reduces quinone (Q) to ubiquinone (QH_2), adding to the QH_2 pool in the mitochondrial inner membrane [43].

The QH_2 pool provides electrons for complex III, the cytochrome bc_1 complex. The Q-cycle is central to the mechanism of complex III, where electrons are transported by the enzyme from the Q-pool to cytochrome *c* coupled to proton pumping and contribution to the PMF. Complex III is shown in Fig. 1.4 reducing Q to QH_2 on one side (Qn), and oxidising $2QH_2$ to Q on the other (Qp). Oxidation QH_2 to Q at the Qp site represents a

bifurcated electron transfer process, where two electrons are passed down different routes in the enzyme [44].

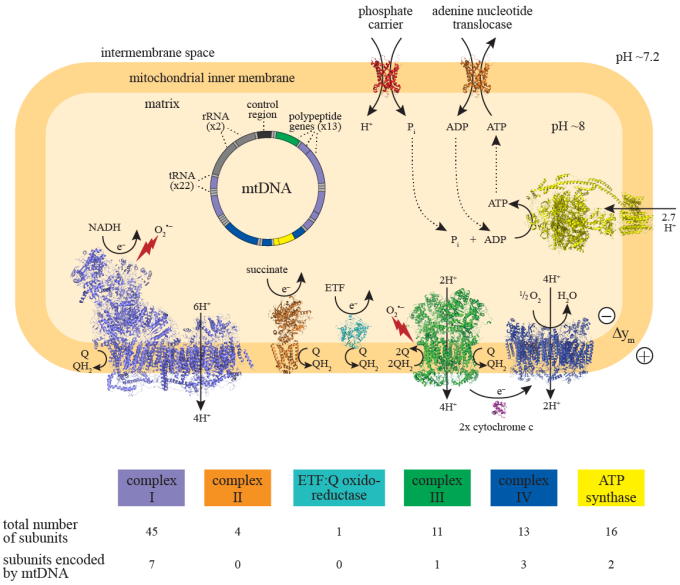

Fig. 1.4 The respiratory chain enzymes and ATP synthase. Complex I, complex II, ETF:Q oxidoreductase, complex III, complex IV and ATP synthase shown in lilac, orange, turquoise, green, dark blue and yellow, respectively. The total number of subunits each respiratory complex contains is presented, including the number of subunits from each enzyme that are encoded on the mitochondrial genome. The adenine nucleotide translocase and phosphate carrier are presented in the upper part of the diagram of the inner mitochondrial membrane, other mitochondrial carriers are not shown. The number of protons required to synthesise one ATP molecule (2.7 protons in ATP synthases with 8 c-subunits) is represented by the solid arrow pointing from the IMS to the matrix. The number of protons translocated by each proton pumping respiratory chain enzyme is denoted by arrows pointing through the respiratory complexes from the matrix to the IMS. Large curly arrows in the matrix represent the reduction of the reducing equivalents NADH, succinate and ETF. Small curly arrows represent the reduction or oxidation of the quinone pool in the IMM. Red lightning bolts show sites of ROS (reactive oxygen species) production in the electron transport chain. Figure supplied by Martin Montgomery, MRC-MBU.

The Q-cycle is central to the mechanism of complex III, where electrons are transported by the enzyme from the Q-pool to cytochrome *c* coupled to proton pumping and contribution to the PMF. Complex III is shown in Fig. 1.4 reducing Q to QH_2 on one side (Qn), and oxidising $2QH_2$ to Q on the other (Qp). Oxidation QH_2 to Q at the Qp site represents a bifurcated electron transfer process, where two electrons are passed down different routes in the enzyme [44]. One electron is transferred to an iron sulphur cluster in the Reiske

protein and then to haem c_1, followed by transfer to cytochrome *c*, resulting in translocation of 2 protons to the intermembrane space (IMS) and the production of semiquinone (SQ) at Qp. The other electron passes from SQ and is delivered to two heme groups in cytochrome b, b_L and b_H. Q binds at Qn near the second heme in cytochrome b and accepts an electron, which results in its reduction to SQ. The first part of the Q-cycle (oxidation of QH_2 to Q) is repeated and provides the electrons to reduce Q to QH_2 at Qn, with 2 protons taken up from the matrix, completing the Q-cycle.

Cytochrome *c* shuttles 4 electrons from the quinone pool to complex IV to reduce one oxygen molecule to two water molecules. A copper centre (Cu_A) is the entry point of electrons, which are then transferred to the nearby haem *a* followed by haem a_3, and finally to another copper centre (Cu_B) which is adjacent to the oxygen binding site. A single oxygen molecule binds in the oxygen binding site, accepts the electrons channelled from the copper and haem centres and two protons are taken up from the matrix via two different channels in complex IV, which provide the protons for reduction of O_2 to $2H_2O$ and also pumps 4 protons from the matrix to the IMS. Complex IV is the terminal enzyme in the electron transport pathway [45].

The fluid mosaic model of membrane proteins suggests that the respiratory chain complexes and ATP synthase would move freely and randomly throughout the IMM. However, there is evidence that complexes I, III and IV can form supercomplexes [46]. The function of supercomplexes is not understood at present, but there are many hypotheses. For example, they may allow generation of a local ΔpH, where protons are utilised directly by ATP synthase, rather than entering the bulk phase and diffusing throughout the IMS and cell cytoplasm [47]. They could also facilitate the efficient transfer of electrons from respiratory complexes to the quinone and cytochrome c pools [48], or to reduce the formation of reactive oxygen species [49]. It has been shown that

supercomplexes exist in the form $CI:CIII_3:CIV_6$ [50] and that these can be either in a "tight" or "loose" conformation, where tight is defined as fully assembled and loose may represent a partially assembled supercomplex [49].

1.5. Mitochondrial diseases

Mitochondria are associated with many pathologies, owing to their involvement in a wide range of processes in the cell (section 1.2). As mitochondria are central to energy metabolism, it is not surprising that many of the diseases with mitochondrial origin display neurological phenotypes. A summary of some of these diseases, the proteins known to be involved and the symptoms are presented in Table 1.1.

Table 1.1 Mitochondrial diseases with both nuclear and mitochondrial origins

Disease	Characteristics
Autosomal dominant optic atrophy [51]	Defects in OPA1, involved in controlling mitochondrial cristae morphology. Results in loss of vision and chromatopsia in the first two decades of life.
Alzheimer's [52, 53]	Possible defects in complex I and ATP synthase. Brains of AD patients show increased oxidative stress, protein oxidation and lipid peroxidation. Results in decreased cognitive function, confusion, difficulty with speech and movement.
Charcot-Marie-Tooth [54]	Mutations in the mitofusin 2 (Mfn2) gene. Mfn2 is involved in mitochondrial fusion. Patients exhibit demyelination of peripheral neuronal axons and present with muscle weakness and/or numbness in extremities and awkward gait.
Freidreich's ataxia [55]	Mutations in the frataxin (Fxn) gene. Fxn is essential for iron-sulphur cluster biogenesis. Patients may suffer from ataxia, hypertrophic cardiomyopathy, diabetes, muscle weakness and skeletal deformation.
GRACILE syndrome [56]	Mutations in the complex III assembly factor BCS1L results in growth retardation, aminoaciduria, cholestasis, iron overload, lactic acidosis and early death.

Disease	Characteristics
Hereditary paraganglioma [57]	Mutations in complex II assembly factor SDHAF1, results in impaired iron-sulphur cluster incorporation into the enzyme. Patients are affected by cancer of the neuroendocrine system.
Leigh syndrome [56, 58, 59]	Mutations in complex I subunits-NDUFS8 and -NDUFA2, complex IV assembly factors SURF-1, COX10, COX15, LPPRC and TACO1, and ATP synthase subunits-a and -A6L. Symptoms include decreased membrane potential and decreased capacity for ATP synthesis. Patients suffer from progressive demyelination of spinal neurons, glial hypertrophy, ataxia, breathing difficulties, optic atrophy, dystonia and often early death.
Leber's hereditary optic neuropathy [51]	Mutations in complex I subunits MT-ND1, MT-ND4 and MT-ND6 result in loss of vision in the second or third decade of life with blurred or cloudy with retinal nerve degeneration.
MELAS [60, 61]	Mutations in complex I subunit ND5 and complex II assembly factor SDHAF2, affecting the capacity of the electron transport chain to generate the membrane potential and decreased ATP synthesis. Patients are affected by strokes, hypertrophic cardiomyopathy, lactic acidosis, seizures and myopathy.
Parkinson's [62]	PINK1 and parkin mutations have been found in PD patients, as well as a decrease in the OSCP-subunit of ATP synthase. Parkin is a mitochondrial E3 ubiquitin ligase recruited by PINK1 to promote autophagy of damaged mitochondria. PD symptoms include progressive loss of dopaminergic neurons in the brain resulting in tremors, slow movement and muscle stiffness.

There are a number of mitochondrial diseases that are thought to arise from mutations in ATP synthase subunits of mitochondrial or nuclear origin, or proteins involved in the assembly of ATP synthase [63]. Mutations affecting ATP synthase are known to affect the a- and A6L- [64, 65], c- [66] and ε-subunits [67], as well as assembly factors for ATP synthase [68]. The severity of the phenotype resulting from the mutation depends on the

mutational load for the a-subunit and A6L-subunit, which are encoded in the mitochondrial genome. Mutational load defines the percentage of the mitochondrial DNA population that carries the mutation. Heteroplasmy is defined by the percentage of mitochondrial DNA nucleoids carrying a mutation in a mixed population of healthy and mutated DNA nucleoids, [69]. Higher mutational load leads to worse prognosis and increased disease severity. Pathological ATP synthase depletion can be linked to mitochondrial mutations involving ATP synthase a- and A6L-subunits in the F_O membrane domain of the enzyme. The point mutation T8993G occurring in the a-subunit gene ATP6 results in neuropathy, ataxia and retinitis pigmentosa (NARP) when 90-95% of DNA nucleoids are mutated, or Leigh syndrome if more than 95% of DNA nucleoids are affected by the mutation [64]. There are numerous other mutations that affect the a-subunit, many of which result in a spectrum of disease phenotypes with varying severity between NARP and Leigh syndrome symptoms, and other diseases that result in seizures, lactic acidosis, or familial bilateral striatal necrosis (FBSN) [63]. The diseases associated with a-subunit mutations share the underlying biochemical origin of proton transport deficiency through ATP synthase, because the physiological role of the a-subunit is to carry protons to and from the c-ring [70]. Mutations in the A6L-subunit have been described and are linked to hypertrophic cardiomyopathy and congestive heart disease [65]. The single mutation T8528C in the ATP6 gene affects both ATP6 and ATP8. ATP8 (A6L) is a supernumerary subunit of ATP synthase and there is evidence that this subunit acts as a strut to improve the coupling of the F_1 domain to F_O via contacts with the b-subunit and the a-subunit [71]. It is reported that mutations in the nuclear encoded ε-subunit are associated with ATP synthase deficiency [67]. The defective protein is incorporated into ATP synthase and ATP synthase is assembled correctly, but ATP synthesis and the amount of ATP synthase are reduced. This mutation results in a cysteine residue replacing Tyr12 in the ε-subunit, and associated

phenotypes of lactic acidosis, 3-methylglutaconic aciduria, mental retardation and delayed onset peripheral neuropathy [67].

Batten disease is a neurodegenerative disease associated with excessive storage of the c-subunit of ATP synthase in lysosomes [72, 73] but there is no difference between c-subunits contained in storage bodies and c-subunits contained in normal mitochondrial ATP synthase including in the trimethylation status of lysine 43 of the c-subunit [72]. The disease affects the paediatric population and results in early death.

A mutation affecting the ATP synthase assembly factor ATP12 in yeast has been reported [74], and results in reduced activity of ATP synthase due to an assembly defect affecting the incorporation of the α- and β-subunits into the F_1 domain of the enzyme. A yeast model of ATP synthase assembly suggests that ATP12 acts as a chaperone to place the α- and β-subunits in the correct orientation and proximity to prevent the monomers from forming insoluble aggregates. The human homologue of ATP12 is ATPAF2. [75].

The ATP synthase may provide the components of the mitochondrial permeability transition pore (mPTP), which is involved in cell death. The damage to heart tissue associated with congestive heart failure and associated reperfusion injury upon treatment are not necessarily caused by inherited defective genes, rather the opening of the (mPTP) [76]. During a heart attack, the blood vessels that supply blood and nutrients to the heart may become blocked by a blood clot, resulting in ischemia. The respiratory complexes cannot transfer electrons due to the lack of the final electron acceptor (O_2), and are in a reduced state when oxygen flow is restored. The restoration of blood flow and infusion of oxygen to the ischemic heart tissue produces reactive oxygen species that damage the respiratory chain enzymes and other mitochondrial residents (proteins, lipids) and results

in the opening of the PTP [77]. Triggers of pore opening include mitochondrial calcium overload, oxidative stress mediated by the increased production of reactive oxygen species (ROS), depleted ATP levels and increased P_i concentration in mitochondria [78, 79]. The accumulation of succinate has been reported in ischemic heart tissue [80], and levels of ROS production are linked to the amount of succinate accumulated at the point of reperfusion, as a result of ROS generation by reverse electron transfer (RET) mediated by complex II. The amount of succinate accumulated in heart tissue during ischemia-reperfusion injury is correlated with PTP-inducing ROS levels [81]. Modulating the amount of succinate *in-vitro* in human cardiomyocytes, and *in-vivo*, mouse heart tissue showed a significantly reduced amount of ROS and the infarct region was much smaller compared to control hearts [81].

1.6. ATP synthase

ATP synthase or F_1F_O-ATP synthase is present in all forms of life, from the inner membrane of mitochondria and chloroplasts [82] to the cell membranes of eubacteria and archaea [83]. ATP synthase is the mitochondrial enzyme responsible for synthesising the ATP generated by oxidative phosphorylation [5]. The human enzyme contains 18 different subunits [82, 84], shown in Fig. 1.5 and Table 1.2, that make up the catalytic F_1 domain and the central stalk, the peripheral stalk and the membrane bound F_O domain which contains the proton channel, the b-subunit and the supernumerary subunits, shown in Fig. 1.5. The subunit compositions of the ATP synthases from cows, sheep, pigs and *S. cerevisiae* and other fungal mitochondrial ATP synthases that have been determined [85, 86].

IF_1 is the natural inhibitor of mitochondrial ATP synthase and prevents ATP hydrolysis in the event of the PMF being insufficient for ATP synthesis, where ATP is hydrolysed in

order to maintain the PMF. IF_1 binds to one of the three catalytic interfaces of the enzyme and the γ-subunit [88, 89].

1.6.1. The structure and mechanism of ATP synthase

ATP synthase consists of three structural domains, which are F_1, F_O and the peripheral stalk. Most of the structural features of mammalian ATP synthase were established in the bovine enzyme.

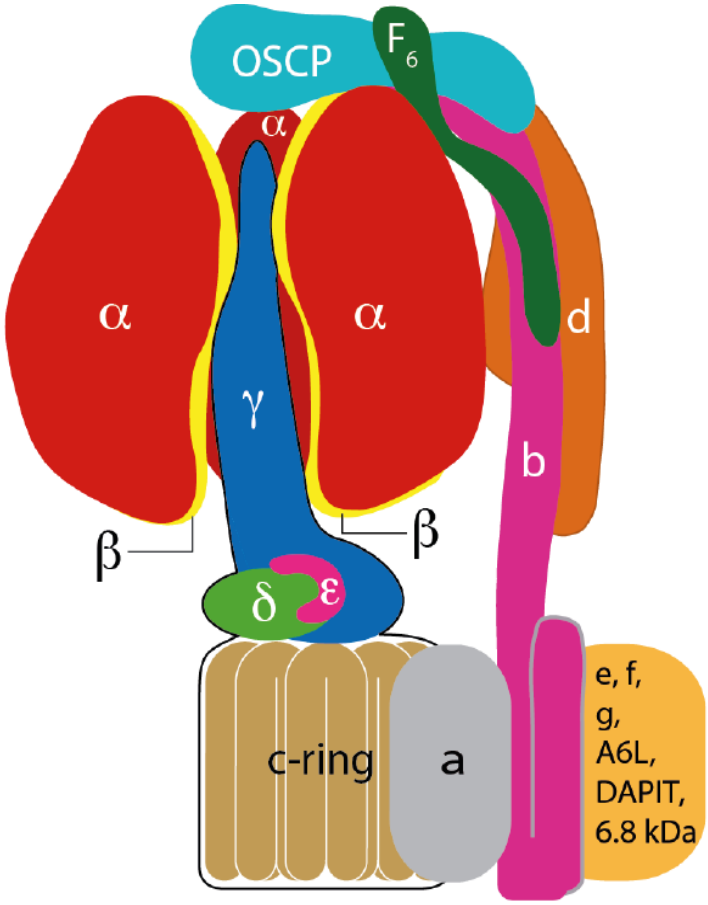

Fig 1.5 Mitochondrial ATP synthase. The stoichiometry of subunits in bovine ATP synthase F_1 is $\alpha_3\beta_3\delta_1\varepsilon_1\gamma_1$. The remaining subunits are present at one copy per enzyme, including the DAPIT- and 6.8 kDa PL subunits, which have been measured by quantitative mass spectrometry to be present in sub-stoichiometric amounts, but are assumed to be present at one copy each subunit per monomeric enzyme [82, 87], [Joe Carroll, unpublished data].

The bovine F_1 domain contains the α-, β-, γ-, δ- and ε- subunits [90]. The F_O domain contains a ring of eight c-subunits, and the a-, A6L-, e-, f-, g-, DAPIT- and 6.8 kDa proteolipid-subunits.

Table 1.2 Genes encoding subunits of ATP synthase in humans, cows, *S. cerevisiae* and *E. coli*.

Subunit	Human	Bovine	Yeast	Bacteria
α	*ATP5A*	*ATP5A*	*ATP1*	*AtpA*
β	*ATP5B*	*ATP5B*	*ATP2*	*AtpD*
γ	*ATP5C1*	*ATP5C1*	*ATP3*	*AtpG*
δ*	*ATP5D*	*ATP5D*	*ATP16*	*AtpC*
ε	*ATP5E*	*ATP5E*	*ATP15*	-
c	*ATP5G1*	*ATP5G1*	*ATP9*	*AtpE*
	ATP5G2	*ATP5G2*		
	ATP5G3	*ATP5G3*		
a	*MT-ATP6*	*MT-ATP6*	*ATP6*	*AtpB*
OSCP**	*ATP5O*	*ATP5O*	*ATP5*	*AtpC*
b	*ATP5F1*	*ATP5F1*	*ATP4*	*AtpF*
d	*ATP5H*	*ATP5H*	*ATP7*	-
F_6***	*ATP5J*	*ATP5J*	*ATP14*	-
i/j	-	-	*ATP18*	-
e	*ATP5I*	*ATP5I*	*TIM11*	-
f	*ATP5J2*	*ATP5J2*	*ATP17*	-
g	*ATP5L*	*ATP5L*	*ATP20*	-

Subunit	Human	Bovine	Yeast	Bacteria
DAPIT	*USMG5*	*USMG5*	-	-
6.8 PL	*MP68*	*MP68*	-	-
A6L	*MT-ATP8*	*MT-ATP8*	*ATP8*	-
IF_1	*$ATPIF_1$*	*$ATPIF_1$*	*INH1*	-

* δ is ε in bacteria, ** OSCP is δ in bacteria, *** F_6 is h in yeast.

The peripheral stalk consists of the OSCP-, F_6-, d- and b-subunits (the b-subunit extends down into the F_O membrane domain via two membrane spanning α helices) and in bacteria, the peripheral stalk consists of the δ-subunit and two b-subunits [91–97]. The A6L- and e-subunits were the first membrane bound supernumerary subunits to be identified [98, 99], followed by the f- and g-subunits [87], then the DAPIT- and 6.8 kDa proteolipid-subunits [100]. The arrangement of the membrane bound nuclear encoded supernumerary subunits are presented in Fig. 1.6, based upon experiments using cross-linking of lysine residues between subunits. Mammalian and probably all metazoan ATP synthases contain eight c-subunits [5, 101]. Non-metazoan species such as bacteria and fungi possess ATP synthase containing between 10 and 15 c-subunits. Common to all species is the symmetry mismatch between the number of catalytic β-subunits and the number of c-subunits in the c-ring. Symmetry mismatch occurs as a result of the number of c-subunits being indivisible by the number of catalytic sites in ATP synthase, and is thought to confer a bioenergetics advantage by preventing the enzyme entering a state where additional energy would be required for rotation of the rotor [102, 103].

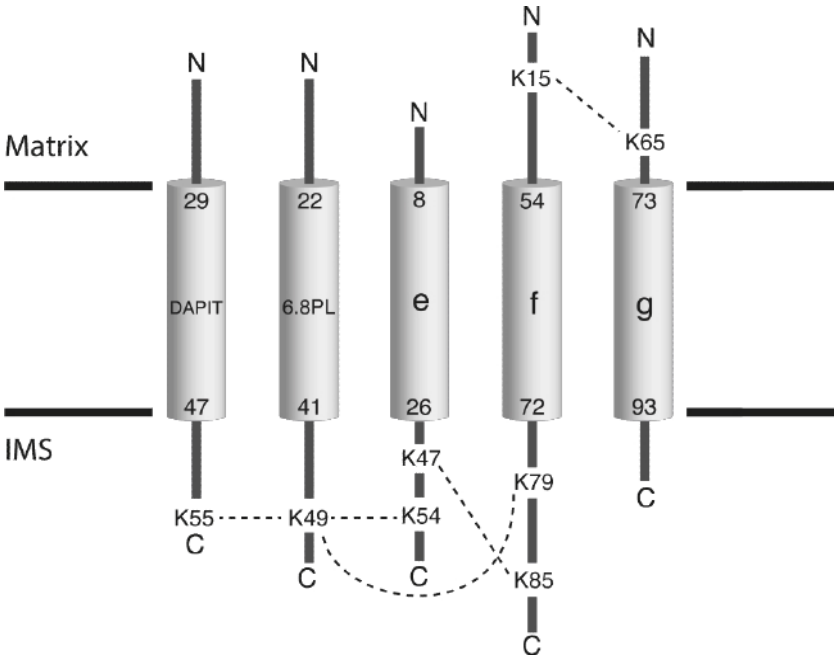

Fig. 1.6 The locations of the nuclear encoded supernumerary subunits e, f, g, DAPIT and 6.8 kDa proteolipid in the inner mitochondrial membrane, as determined by chemical cross-linking of lysine residues. Figure taken from [91].

The structures of the *Pichia angusta*, bovine and *Paracoccus denitrificans* ATP synthase are presented in Fig. 1.7. There are many structural similarities and some differences between ATP synthases from these three organisms. The three enzymes have the same basic structural features. They all contain the globular $\alpha_3\beta_3$ catalytic domain, which is connected by the peripheral stalk OSCP-subunit to all three α-subunits [71, 93]. The peripheral stalks of the ATP synthases extend down into the membrane domain to contact the a-subunit via the b-subunit. The peripheral stalks of some bacterial ATP synthases contain two related but not identical b-subunits, b and b'. The b'-subunit is homologous to the bovine b-subunit but is unrelated in sequence, and extends into the membrane. Bacterial ATP synthase does not possess either the F_6- or d-subunits. All three enzymes contain a bundle of five α-helices in the a-subunit that traverse the membrane tilted at 30°. In the bovine and *Pichia* enzymes, the a-subunit is contacted by the peripheral stalk and A6L, which helps to hold the a-subunit against the c-ring [71]. In the *Paracoccus* enzyme, A6L

is not present. The models of the bovine and *Pichia* ATP synthases possess the A6L- and f-subunits, and the putative locations of these subunits has been added to the fungal enzyme (A in Fig. 1.7). For a comparison of subunits contained in each enzyme, see Table 1.2.

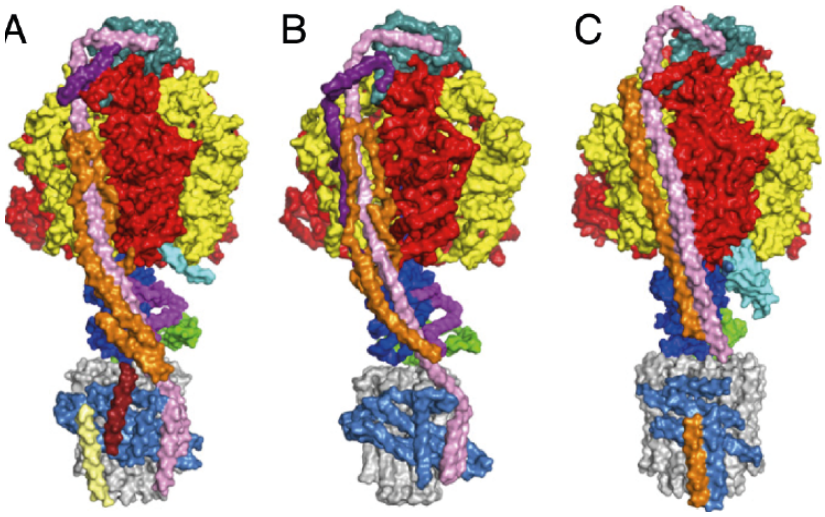

Fig. 1.7 The structures of ATP synthase from *Pichia angusta*, cows and *Paracoccus denitrificans* in A, B and C, respectively. For fungal and cow ATP synthase: α (red), β (yellow), γ (royal blue), δ (green), ε (magenta), OSCP (sea green), F_6 (purple) (h in the fungal enzyme), d (orange), b (pink), c-rings (grey), a (corn flower blue). In panel A, the A6L- and f-subunits are brick red and pale yellow, respectively. In the bacterial enzyme, the b- and b'-subunits are shown in pink and orange, respectively. The bacterial δ-subunit is orthologous to the cow and fungal OSCP-subunit and is in sea-green. The figure was taken from [71], and contains structures from [104] (bovine ATP synthase) and [105] (bacterial *Paracoccus denitrificans*).

The peripheral stalk of ATP synthase is essential for coupling ATP synthesis to the rotation of the c-ring and prevents the catalytic domain of F_1 from rotating along with the γ-subunit and the rotor [106]. The binding interface between the OSCP-subunit and the α-subunit buries hydrophobic residues in the N-terminal domain of subunit-OSCP by interacting with hydrophobic residues in the N-terminal regions of the three α-subunits [93, 107]. The F_1 domain is linked to F_O by OSCP and by the other peripheral stalk subunits F_6, b and d, and also by the central stalk subunits γ, δ and ε [93, 108].

The F_1 domain houses the three catalytic sites of the enzyme, located at the interfaces between the α-subunits and the catalytic β-subunits. The three β-subunits are each in different conformational states at any one time [109, 110]. A number of related high resolution structures of the F_1 domain from bovine or yeast mitochondria have been solved, which have allowed the elucidation of the mechanism of ATP hydrolysis [5, 111–115]. The catalytic states of the enzyme are termed β_E, β_{TP} and β_{DP}, which correspond the to the open, loose and tight states in a binding change mechanism of ATP hydrolysis. The mechanism of ATP hydrolysis requires ATP to bind at the β_E-site, which induces a conformational change in the β-subunit. This results in the active site converting to the β_{DP}-state, during a 120° rotation of the catalytic domain. During ATP hydrolysis, a water molecule is utilised for the nucleophilic attack of the γ-phosphate of ATP, which is accompanied by another 120° rotation and conversion of the β_{DP}-state to the β_{TP}-state. The final 120° rotation is associated with the β_{TP}-state reverting to the β_E-state, and the products of ATP hydrolysis, ADP and P_i, are released. During ATP synthesis, rotation of the catalytic domain is powered by translocation of protons through the ATP synthase from the IMS to the matrix [5]. The mechanism of ATP synthesis is presumed to be a direct reversal of the hydrolytic chemical reaction.

1.6.2. The assembly of ATP synthase

The assembly of the F_1 domain of *S. cerevisiae* ATP synthase is thought to rely on two assembly factors, ATP11 and ATP12 [116]. In yeast, when these two assembly factors are inactivated by mutation, the α- and β-subunits fail to assemble onto the central stalk, but are folded correctly, suggesting an assembly role rather than a chaperone role for ATP11 and ATP12 [116]. The F_6-subunit is presumably assembled after the b-, OSCP- and d-subunits. The peripheral stalk subunits are assembled sequentially in *Saccharomyces*

cerevisiae, with the order b-subunit first, then the OSCP-subunit followed by the d-subunit [117, 118]. The assembly of the F_O domain in yeast involves the activity of the metalloprotease ATP23 which fulfils two known functional roles. ATP23 mediates the processing of the a-subunit to form the mature protein, and also acts as a chaperone with ATP10 to coordinate the association of the a-subunit with the c-ring [119].

The current understanding of the yeast ATP synthase assembly pathway is presented in Fig. 1.8.

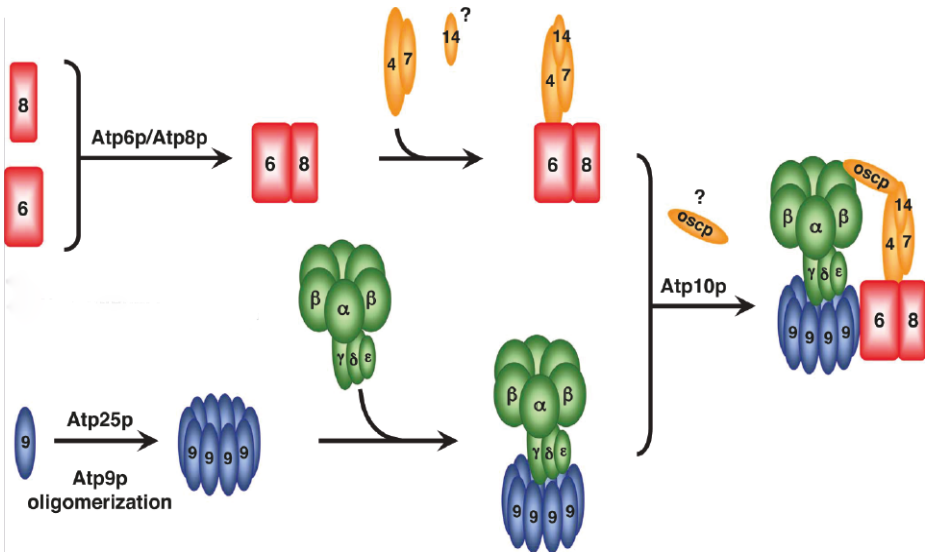

Fig. 1.8. The assembly of yeast ATP synthase via two distinct modular pathways. The figure was taken from [120]. The 8- and 6-subunits are the equivalent of the human A6L- and a-subunits, respectively. The 4- and 7-subunits are the yeast orthologs of the human b- and d-subunits respectively, and subunit-14 is the ortholog of the human F_6-subunit. Human subunit-g is ATP20 in yeast and its incorporation is not shown.

The two yeast assembly factors have orthologs in humans, ATPAF1 and ATPAF2 [68]. There are no known human assembly factors that function in the assembly of the peripheral stalk or F_O membrane domain, nor in the assembly of the central stalk onto the c-ring. The assembly of ATP synthase in human cells must differ from the yeast assembly pathway because subunit-c is encoded on the mitochondrial genome in yeast, unlike in mammals, where it is encoded in the nucleus and requires transport into mitochondria. It has been shown that ATPAF1 and ATPAF2 interact with the α- and β-subunits of human ATP

synthase, respectively, preventing these subunits from forming insoluble aggregates during the assembly of the catalytic domain [68].

It has been proposed that the human ATP synthase F_1 domain is assembled separately from the c-ring, and that the F_1c_8 subcomplex assembles separately from the peripheral stalk [121]. It has also been proposed that the b-, e- and g-subunits form a complex that links the peripheral stalk to F_O, and that the d-subunit is then assembled with the b-subunit. It has been suggested that when the peripheral stalk assembly docks into the IMM via the b-, e- and g-subunits, this sub-complex is recruited to the c-ring in the F_O domain. Next, it is proposed that the OSCP- and F_6-subunits are recruited to the peripheral stalk followed by the remaining supernumerary subunits and finally the a-subunit is assembled [118, 120]. There is evidence suggesting that the a- and A6L-subunits are recruited to the F_O domain after the other F_O subunits because in ρ^0 cells, which lack mitochondrial DNA (and therefore lack the a- and A6L-subunits), the vestigial ATP synthase is assembled [122]. The advantage of assembling the a-subunit onto the c-ring last is to prevent the F_1c_8a subcomplex from hydrolysing ATP [121]. The c-ring is probably the first structure of F_O to form [121], and this may be mediated by the correct folding of the c-subunit without the necessity for additional assembly factors, because in *E. coli*, c-rings can form spontaneously *in-vitro* and without other ATP synthase subunits being present [103]. A mutation in the a-subunit has been shown to affect assembly of ATP synthase, where two sub-complexes of ATP synthase accumulated, one containing the soluble $\alpha_3\beta_3$ F_1 domain and the other containing F_1c_8 [123].

1.7. Aims of this work

The supernumerary subunits e, f, g, DAPIT, A6L and 6.8 kDa proteolipid of human ATP synthase have no well-defined functions in the mitochondrial enzyme [82, 87, 100, 124]. In this work, the roles of subunits e, f, g, DAPIT and 6.8 kDa proteolipid will be investigated by suppression of the individual expression either with siRNA molecules or by gene disruption.

2. Materials and Methods

2.1. Materials and reagents

2.1.1. Chemicals

All the reagents and chemicals used in this work are listed in Appendix I. Solutions were made with Milli-Q water (resistance 18.2 mega Ω/cm^3) supplied by a Millipore Academic water purification system (ThermoFisher Scientific, Hemel Hempstead, UK), or nuclease free water (Qiagen, Manchester, UK). The constituents of buffers are listed in Appendix II.

2.2. Cell culture

2.2.1. Human cell culture

Two human cell lines were used for this work. For siRNA mediated depletion of ATP synthase subunits, 143B osteosarcoma cells were used (American Type Culture Collection, VA, USA). 143B cells are immortal due to transformation during cancer development and lack thymidine kinase. For CRISPR-Cas9 mediated gene deletion, HAP1 chronic myelogenous leukaemia cells were used (Horizon Discovery, Cambridge, UK). HAP1 cells are haploid and immortal due to cancerous transformation and contain a reciprocal translocation of chromosomes 9 and 22. 143B cells were grown in Dulbecco's modified eagle medium (DMEM), supplemented with 10% v/v FBS, 100 U/mL penicillin, 100 μg/mL streptomycin and 45 μg/mL uridine, referred to as complete DMEM throughout the text. HAP1 cells were grown in Iscove's modified Dulbecco's medium (IMDM) supplemented with 10% v/v FBS, 100 U/mL penicillin and 100 μg/mL streptomycin, referred to as complete IMDM throughout the text. Cells were washed with warm Dulbecco's PBS (dPBS) and 0.1% w/v trypsin-EDTA dissociation reagent in Hanks balanced saline solution (HBSS) was used to dissociate adherent cells from cell culture plates. The trypsin was quenched with 10 volumes of growth media, the cells diluted ten-fold and re-plated. Cells were grown at 37°C under 5% CO_2 gas and 95% relative humidity.

2.2.2. siRNA transfection of cells

Cells were dissociated with trypsin-EDTA, plated at 50% or 30% confluence for 143B cells or HAP1 cells, respectively, in 10 cm tissue culture plates and incubated for 2 h at 37°C, 5% CO_2. Plasmids or siRNA oligonucleotides were diluted to achieve a final delivery of either 1 μg or 50-100 nM, respectively to the cells. A list of sequences of siRNA molecules is presented in Table 2.1.

Table 2.1 Oligonucleotide siRNA sequences

Target	siRNA	Sequence 5'-3'
ATP5I	e6 sense	GCAGGUCUCUCCGCUCAUCAA
	e6 antisense	UUGAUGAGCGGAGAGACCUGC
ATP5J2	f7 sense	GGAUCUUGAUGCGGGACUU
	f7 antisense	AAGUCCCGCAUCAAGAUCC
ATP5L	g8 sense	GCCUCGAUUGGCCACAUUU
	g8 antisense	AAAUGUGGCCAAUCGAGGC
USMG5	DAPIT 10 sense	UCCCAUGCCUGGAGAAGCUAA
	DAPIT10 antisense	UUAGCUUCUCCAGGCAUGGGA
C14orf2	6.8k1 sense	AUGCUUCAAAGUAUUAUUAAA
	6.8k1 antisense	UUUAAUAAUACUUUGAAGCAU

Oligonucleotides for siRNA were added to a solution containing Lipofectamine-2000 transfection reagent (12 μL/ mL OptiMEM) and left at room temperature for 20 minutes to allow the formation of liposome complexes containing siRNA. Transfection with pSpCas9(BB)2A-GFP plasmids containing gRNA (guide RNA) is described in section

2.6.6. The transfection solution was applied to the cells ensuring complete coverage of the plate with transfection solution.

2.2.3. Seeding plates with cells for extracellular flux analysis

Cells suspensions were counted using a NucleoCounter NC-3000 (Chemometec, Denmark). Solution 13 (2.5 μL) containing 30 μg/mL acridine orange stain and 100 μg/mL DAPI stain was added to 47.5 μL trypsinised cell suspension. Acridine orange stains both live and dead cells and DAPI stains only dead cells, allowing estimation of cell quantity and viability. The total number of cells minus the number of dead cells gives the number of live cells. Samples (12 μL) were placed onto A8 NC slides (Chemometec) in duplicate. Cells were counted and diluted to 250,000 cells/mL in complete DMEM for 143B cells or complete IMDM for HAP1 cells. Cells (100 μL) were added to 20 wells of an XF^{e}24 Seahorse cell culture plate in a randomised order. Four of the 24 wells were left empty as background controls. The plate was incubated for 2 h at 37°C under 5% CO_2 before a further portion of complete DMEM (150 μL) was added to each well and the plate was incubated at 37°C overnight.

2.2.4. Stable isotope labelling of amino acids in cell culture

Cells were grown in SILAC DMEM or IMDM supplemented with 10% v/v dialysed FBS, 1.737 mM proline, 100 U/mL penicillin, 100 μg/mL streptomycin and 45 μg/mL uridine for 8 days to ensure complete labelling of proteins with heavy isotopic amino acids. Heavy and light isotopic variants of L-lysine and L-arginine were added separately to two separate bottles of media, with concentrations of 0.798 mM and 0.398 mM of L-lysine and L-arginine, respectively. Heavy isotopic variants of L-lysine and L-arginine contained 8 or 10 stable isotopes of ^{13}C and ^{15}N in the amino acids, respectively. Cells were harvested

(section 2.2.5) and protein content estimated (section 2.4.1.1). Cells containing heavy isotopic variants of lysine and arginine were mixed in a 1:1 ratio with cells containing ^{12}C and ^{14}N isotopic forms of lysine and arginine [125]. Samples were analysed by mass spectrometry as described in section 2.5.4.

2.2.5. Harvesting cells

Cells were washed with dPBS (10 mL per 15 cm diameter plate) at 37°C and 2 mL of ice cold PBS containing Complete protease inhibitors was added. Cells were scraped off the plate and transferred to a 50 mL tube on ice. Cells were centrifuged at 100 x *g*, 20°C for 3 min, the supernatant was aspirated and the cells resuspended with the required volume of ice cold PBS with inhibitors and stored on ice before processing.

2.2.6. Freezing cells

Cells which had grown to confluence in a 15 cm tissue culture plate were dissociated with trypsin-EDTA and collected by centrifugation at 100 x *g*, 20°C, 3 min. The supernatant was removed under sterile conditions. Freezing media solution (3 mL) was added to the cells which were resuspended by gently pipetting. 143B cells required 10% v/v DMSO, 30% v/v FBS, 60% v/v DMEM freezing solution and HAP1 cells required 10% v/v DMSO, 50% v/v FBS and 40% v/v IMDM freezing solution. Portions (1 mL) of resuspended cells were added to individual 2 mL cryovials and placed in a cell freezing container surrounded by propan-2-ol and were immediately placed at -80°C.

2.2.7. Extracellular flux analysis to measure oxygen consumption rate (OCR)

The oxygen consumption rate of cells was measured using an XF^{e}24 Seahorse Biosciences extracellular flux analyser (Seahorse Bioscience, MA, USA) [126]. Cells were seeded at a

density of approximately 25,000 cells/well (section 2.2.3). The complete DMEM was removed from wells and replaced with 37°C XF DMEM assay medium (supplemented with 2 mM glucose and 1 mM sodium pyruvate). The cell plate was incubated for 1 h at 37°C, under atmospheric CO_2 to allow the cells to stabilise. The assay measured oxygen consumption rate (OCR) in 3 min bursts followed by a period of re-oxygenation (3 min). This was repeated four times before adding inhibitors and repeating the OCR measurements. Four ports in the assay plate facilitated the separate addition of respiratory inhibitors into each well of the cell culture plate. These were added in the order 2-deoxy-D-glucose, oligomycin A, FCCP, antimycin A/rotenone to achieve final concentrations of 20 mM, 100 nM, 500 nM and 600 nM, respectively. Protein amount was estimated using the SRB assay [127] (section 2.4.1.2).

2.3. Molecular Biology

2.3.1. Quantitative real time PCR

cDNA was produced from mRNA using a proprietary cells-to-CT kit (ThermoFisher Scientific, Hemel Hempstead, UK) and used according to the manufacturer's instructions. Oligonucleotide sequences were used as primers and probes (Table 2.2). 6-carboxyfluoroscein (FAM) and tetramethylrhodamine (TAMRA) were bound to the 5' and 3' ends of the probes, respectively. The relative abundance of specific cDNA targets was estimated by qPCR. The reaction mixture contained 0.75 μM forward and reverse primers, 0.16 μM probe and a proprietary master mix of Taq polymerase and appropriate buffer was used according to the manufacturer's instructions. A 7900 HT Fast Real-Time PCR thermocycler was used to perform the qPCR. The temperature profile was 50°C for 2 min, 95°C for 10 min, 60°C for 1 min, repeated 30 times. The sequences of oligonucleotide qPCR primers and probes are shown in Table 2.2.

Table 2.2 Oligonucleotide sequences of qPCR primers and probes used to quantify the relative amounts of ATP synthase subunit mRNA and β-actin mRNA.

Target	Forward primer 5'-3'	Reverse primer 5'-3'	Probe 5'-3'
e	GCGGAGGTCAGGGACAAGA	GTAGGCCACACCGAGGAACA	CGCTCATCAAGCTCGGCCGC
f	CTGGCATGCTACGTGCTCTTT	CAGAGTGTGTCCTCTTCAGTGGTATT	CTACAAGCATCTCAAGCACGAGCGGC
g	CCGTAACCTTGTGGAGAAGACC	AGCTCAACCTTGGCGTAGTACC	AGTAAGTCACAGCAGCGTTCACCAGCG
DAPIT	GATGCGCAATACCAGTTCACTG	AAGACAATCAATGCAATGCTTCC	TGTGGCCAGTACACAGTTCATTCTACCTGTGA
6.8 kDa PL	CAGATTTGTGGTGCGTTCTGA	GGTAAACTTTGGTGTAGTAGGGCTTC	TGTCCTGCGCCAAGATGCTTCAAAGTATTA
β-actin	CCTGGCACCCAGCACAAT	GCCGATCCACACGGACTACT	ATCAAGATCATTGCTCCTCCTGAGCGC

2.3.2. Agarose gel DNA electrophoresis

Plasmid DNA (15 ng) was mixed with DNA loading buffer (10% v/v glycerol, 20 mM Tris pH 7.4, 5 mM EDTA, 0.01% w/v bromophenol blue and 0.2% w/v SDS) and loaded onto a 1% w/v agarose gel containing 100 ng/mL ethidium bromide made with TBE buffer (90 mM Tris-boric acid, 1 mM EDTA, pH 8.3). DNA was electrophoresed at 40 V for 4 h. Visualisation of DNA bands was carried out by detection of light emitted by ethidium bromide during excitation at 302 nm using a Chemi-Doc XRS$^+$ UV transilluminator (Biorad, Hemel Hempstead, UK).

2.4. Protein biochemistry

2.4.1. Protein estimation

2.4.1.1. Bicinchoninic acid assay

Protein concentrations were estimated using the bicinchoninic acid assay kit [128]. Samples were diluted appropriately and bovine serum albumin (BSA) was used as the reference standard. The 96 well plate assay format was used according to the manufacturer's instructions and absorbance at 562 nm was measured with a Molecular Devices SpectraMax 384 plus spectrophotometer.

2.4.1.2. Sulphorhodamine B assay

Following an extracellular flux assay, the Sulphorhodamine B (SRB) assay was used to estimate cell number [127]. Cells were fixed to the assay plate by adding 9% w/v (final concentration) trichloroacetic acid (TCA) to each well with incubation at 4°C for 1 h. The TCA solution was removed and each well washed with milliQ water (200 μL) three times. The plate was air dried for at 4°C for 48 h. Sulphorhodamine B solution (50 μL/well) was added to each well of the assay plate and left at room temperature for 20 min. The solution was removed and each well washed quickly 3 times with 1% v/v acetic acid (200 μL). The assay plate was air-dried for 1 h at room temperature then 10 mM unbuffered Tris (100 μL) was added to each well of the assay plate and triturated. This solution was diluted 2-fold with 10 mM unbuffered Tris and the absorbance of the solution was measured at 565 nm using a Molecular Devices SpectraMax 384 plus spectrophotometer. A standard curve of A_{565} versus cell number was determined and used to estimate cell numbers in each well of the assay plate.

2.4.2. Mitoplast and mitochondrial membrane preparation

Cells obtained from tissue culture were collected by centrifugation at 2300 x *g* for 5 min at 4°C and the supernatant was removed. Mitoplasts were prepared by the addition of digitonin (to 0.5 mg/mL) in PBS with Complete protease inhibitor solution containing 1 mM EDTA to the cell pellet, to a protein concentration of 5 mg/mL then incubated on ice for 15 min [129]. Mitoplast material was collected by centrifugation at 11200 x *g*, 5 min, 4°C. The supernatant was removed and the pellet washed with PBS solution containing protease inhibitors. Enriched mitochondrial membranes were prepared using the same method, but addition of digitonin was to 2 mg/mL.

2.4.3. Purification of ATP synthase

Mitoplasts were prepared (section 2.4.2) from cell pellets containing 15 mg protein (section 2.4.1.1) and were resuspended to a volume of 500 μL with 0.1 M Tris-HCl pH 8, 0.15 M sodium chloride, 10% v/v glycerol, Complete protease inhibitors without EDTA, 90 μg/mL 1-palmitoyl-2-oleoyl-sn-glycero-3-phosphocholine, 30 μg/mL 1-palmitoyl-2-oleoyl-sn-glycero-3-phosphoethanolamine, 30 μg/mL 1-palmitoyl-2-oleoyl-sn-glycero-3-phosphoglycerol and 2 mM DTT. Digitonin (9 grams of detergent per gram of protein) was added to the samples and they were placed on ice for 15 min, with thorough mixing using a vortex mixer every 3 min. Insoluble material was pelleted by centrifugation at 10500 x *g*, 4°C for 10 min. The supernatant was collected and was clarified by centrifugation through Spin-X micro cellulose filter tubes at 3300 x *g*, 4°C, 15 min. For quantitative mass spectrometry analysis of mitoplasts, a portion (10 μL) of the clarified sample was removed and the proteins reduced and alkylated (section 2.5.1). A slurry of ATP synthase immunocapture resin (100 μL) was added to the remaining material and samples were mixed by rotation overnight at 4°C. The immunocapture resin was pelleted by centrifugation, then the supernatant containing unbound material was removed and stored at -20°C. The beads were washed four times with wash buffer (20 mM Tris-HCl pH 8.0, 0.15 M NaCl, 10% v/v glycerol, 90 μg/mL1-palmitoyl-2-oleoyl-sn-glycero-3-phosphocholine, 30 ug/mL1-palmitoyl-2-oleoyl-sn-glycero-3-phosphoethanolamine, 30 μg/mL1-palmitoyl-2-oleoyl-sn-glycero-3-phosphoglycerol and 0.05% w/v digitonin). The immunocapture slurry was transferred to a micro-spin column using 100 μL of wash buffer. A syringe was used to displace the buffer from the column with air pressure. Wash buffer (200 μL) was added to the beads and displaced with the syringe. Elution of the sample was performed by adding 30 μL 0.2 M glycine-HCl, pH 2.5 containing 0.05% w/v digitonin to the beads. The samples were left at room temperature for 5 min and then centrifugation at

1400 x *g* to elute purified ATP synthase. Unbuffered Tris (1M) was added to the eluted sample at a final concentration of 150 mM to neutralise the pH. The proteins were reduced and alkylated, then the purity of the sample was examined by SDS-PAGE (sections 2.5.1 and 2.4.6), followed by either MALDI mass spectrometry (section 2.5.3) or LC-MS mass spectrometry (section 2.5.4).

2.4.4. Blue native-PAGE

Protein complexes were fractionated by electrophoresis at 75 V, 4°C for 1 h using proprietary electrophoresis buffers (Appendix II). The cathode buffer contained 0.02% w/v Coomassie G250 blue dye (Appendix I) diluted according to the manufacturer's instructions. After 1 h, the cathode buffer was exchanged with a buffer that contained 0.002% w/v Coomassie G250 blue dye. Proteins were then electrophoresed at 150 V, 4°C for 2 h with a X-cell Surelock electrophoresis tank, followed by transfer from the gel onto PVDF membrane using Western blotting (section 2.4.7). Samples were prepared by solubilising mitochondrial membranes (50 μg) with 3 and 6 mg digitonin (separately) per mg of protein in 11.25 μL of 1x Native sample buffer. Samples were incubated on ice for 15 min and centrifuged at 10500 x *g* for 20 min at 4°C. The supernatant (10 μL) was removed and treated for 30 min at room temperature with 150 units of Benzonase to remove DNA. The Benzonase solution contained 1 mM magnesium chloride and 1% w/v digitonin in native sample buffer. Insoluble material was removed by centrifugation (10,500 x *g*, 4°C, 20 min). Samples (approximately 5 μg) were loaded onto a commercial 3-12% acrylamide gradient bis-Tris Native-PAGE gel [130]. Native Mark protein standards and bovine heart mitochondria were used as molecular size markers.

2.4.5. Self-poured 12-22% acrylamide Tris-glycine SDS-PAGE gels

Tris-glycine SDS-PAGE gels with an acrylamide gradient of 12-22% were made in-house using a 10 cm x 10 cm x 0.05 cm format [131]. Gels were composed of stacking and separating gel components. The stacking gel contained 4% acrylamide in 65 mM Tris-HCl pH 6.8, 0.05% w/v SDS, 0.0007% v/v N,N,N',N'-tetramethylethylenediamine (TEMED) and 0.0003% w/v ammonium persulphate and the separating gel contained a 12-22% acrylamide gradient in 375 mM Tris-HCl pH 8.8, 0.1% w/v SDS, 0.0007% v/v TEMED and 0.0003% w/v ammonium persulphate.

2.4.6. SDS-PAGE

Proteins were fractionated using commercial 10-20% w/v or self-poured 12-22% acrylamide gradient Tris-glycine SDS-PAGE gels with Laemmli electrophoresis buffer (Appendix II) [131]. A mix of known protein standards were used to estimate the molecular size of migrating bands. Proteins loaded onto commercial 10-20% acrylamide gradient Tris-glycine gels were electrophoresed at 15 mA for 1 h, then 25 mA for 30 min, or until the dye front reached the bottom of the gel, using a X-cell Surelock electrophoresis tank. Proteins loaded onto self-poured 12-22% acrylamide gradient Tris-glycine gels were electrophoresed at 30 mA for 30 min. Gels containing samples to be analysed by immuno-detection of proteins were equilibrated in carbonate transfer buffer (Appendix II). Gels containing samples to be analysed by mass spectrometry were stained with Coomassie blue gel stain (0.2% w/v Coomassie-R250 blue dye, 50% v/v methanol and 7% v/v acetic acid), and incubated at room temperature for 20 min. The gel was destained with 50% v/v methanol and 7% v/v acetic acid at room temperature with rocking. Silver staining of SDS-PAGE gels containing immunopurified ATP synthase (section 2.4.3) was performed according to [132]. Samples that were to be analysed by Western blotting and immuno-

detection of proteins (section 2.4.7) or prepared into mitoplasts or mitochondrial membranes (section 2.4.2) containing approximately 0.1 mg protein (section 2.4.1) were solubilised on ice for 15 min using 3 mg DDM per 1 mg of protein and 1x native sample buffer (19.5 μL) was used according to the manufacturer's instructions. A centrifugation step at 10500 x *g*, 4°C for 20 min was used to separate insoluble material from solubilised membrane proteins. Proteins in the supernatant (5 μL) were precipitated with 20 volumes of cold ethanol and incubation at -20°C overnight to remove detergent. The sample was centrifuged at 10500 x *g*, 4°C for 10 min and the ethanol was removed and samples left at room temperature for 10 min to allow the residual ethanol to evaporate. Samples were resuspended in SDS-PAGE loading buffer (20% v/v glycerol, 2 mM EDTA, 100 mM Tris pH 6.8, 2% w/v SDS, 50 mM DTT and a trace of bromophenol blue). Samples that were to be electrophoresed by SDS-PAGE and analysed by mass spectrometry were reduced and alkylated as described in section 2.5.1.

2.4.7. Western blotting and immuno-detection of proteins

After electrophoretic separation of proteins, the proteins were transferred to a polyvinylidene difluoride membrane using Western blotting [133]. The SDS-PAGE gel or native-PAGE gel was equilibrated in carbonate transfer buffer (10 mM sodium hydrogen carbonate, 3 mM sodium carbonate and 0.025% w/v SDS, pH 9.9) for 10 min. The SDS was omitted for native gel transfer. Proteins were transferred to a PVDF membrane by electrophoreses with ice-cold carbonate transfer buffer at 300 mA, 60 V for 1 h, using a Biorad Western blotting tank. After transfer, protein binding sites on the PVDF membrane were blocked by incubation for 30 min on a rocker with a solution of Marvel skimmed milk prepared with 5 g milk powder in 50 mL PBS with 0.1% v/v Tween 20. The antibodies used to detect proteins are listed in Table 2.3. Sections of membrane were incubated with

the antibody in milk solution for 1 h, on a roller at room temperature, followed by washes (3 x 5 min) with PBS containing 0.1% v/v Tween-20, then incubation with a secondary antibody for 1 h at room temperature. The proteins on the membrane were visualised by the addition of enhanced chemiluminescence reagent (ECL). The membrane was pre-incubated with the ECL reagent in the dark at room temperature for 5 min, and then signals developed on X-ray film in a dark room using a range of exposure times.

Table 2.3 Antibodies used to detect subunits of ATP synthase and cellular proteins.

Antibody	Dilution	Species	Catalogue number	Source
ATP synthase e-subunit	1:2000	Rabbit	HPA035010	Sigma-Aldrich
ATP synthase f-subunit	1:2000	Chicken	-	In-house
ATP synthase g-subunit	1:10,000	Rabbit	-	In-house
ATP synthase DAPIT-subunit	1:2000	Rabbit	177161AP	ProteinTech Europe
ATP synthase 6.8 kDa PL-subunit	1:2000	Rabbit	147041AP	ProteinTech Europe
ATP synthase β-subunit	1:2000	Rabbit	Sc-33618	Sigma-Aldrich
β-actin	1:20,000	Mouse	A2228	Sigma-Aldrich
Succinate dehydrogenase chain B	1:3000	Rabbit	A002868	Atlas Antibodies
NDUFS1	1:10,000	Rabbit	12444-1-AP	ProteinTech Europe
HRP-conjugated chicken secondary	1:20,000	Rabbit	A9046	Sigma-Aldrich
HRP-conjugated rabbit secondary	1:10,000	Goat	31460	Thermo-Fisher
HRP-conjugated mouse secondary	1:10,000	Sheep	NXA931	GE Healthcare

2.5 Mass spectrometry

2.5.1. Reduction and alkylation of protein samples

Immunopurified ATP synthase and digitonin solubilised mitoplasts (section 2.4.3) were mixed with gel sample buffer (20% v/v glycerol, 2 mM EDTA, 100 mM Tris-HCl pH 8, 2% w/v SDS and a trace of bromophenol blue) and were reduced with 20 mM TCEP at 37°C for 30 min and left at room temperature for 5 min. Alkylation was performed by

adding 15 mM (final concentration) iodoacetamide to the sample and incubation in the dark for 30 min. DTT (final concentration 16 mM) was added to the sample to quench unreacted iodoacetamide. Proteins were separated by SDS-PAGE using 12-22% or 10-20% acrylamide gradient Tris-glycine gels (sections 2.4.5 and 2.4.6). The gel was immediately stained with Coomassie stain (Appendix II) for 30 min and de-stained (Appendix II) for 4 h.

2.5.2. In-gel trypsin digestion of proteins

Individual Coomassie stained protein bands or individual Coomassie stained lanes contained in SDS-PAGE gels were cut out of the gel using a clean razor blade and divided into approximately 4 pieces or 12 equal sized sections, respectively. The 12 gel sections were further divided into approximately 1mm^3 pieces. Gel slices or sections were placed in a clean 1.5 mL tube; 50% v/v methanol was used to clean the tubes. Gel pieces were stored at -20°C until performing in-gel digestion. In-gel trypsin digestion was performed as described by Shevchenko *et al*, 1996 [134] with the following modifications: ammonium bicarbonate was replaced with 20 mM Tris-HCl pH 8.0, iodoacetamide was not added because the proteins had been alkylated before the electrophoresis step (section 2.5.1). Trypsin (12.5 ng/μL) in 20 mM Tris-HCl pH 8.0 and 5 mM calcium chloride was added to cover the gel pieces and digested overnight at 37°C. Peptides were extracted from the gel using a solution of 60% v/v acetonitrile and 4% v/v formic acid (extraction solution) to cover the gel pieces at room temperature for 1 h. The extraction solution was removed and placed into a clean 1.5 mL tube. Tryptic peptide mixtures (0.35 μL) were applied to a MALDI plate and air dried before adding matrix solution (0.35 μL) containing α-cyano-4-hydroxy-trans-cinnamic acid (10 mg/mL) in 60% v/v acetonitrile and 0.1% w/v trifluoroacetic acid to the dried peptide spot. Extraction of peptides was carried out a second

time for peptides that were to be analysed by LC-MS. The extraction solutions were combined and insoluble material removed by a centrifugation step at 10,500 x *g*. 1/3 of the volume was removed and dried in a Thermo Savant SpeedVac SP121P concentrator at 30°C for 30 min. The dried peptides were re-dissolved in 0.1% v/v trifluoroacetic acid and 2% v/v acetonitrile before being separated on a nano-LC column.

2.5.3. MALDI TOF-TOF mass spectrometry for protein identification

MALDI TOF-TOF analysis was performed using an Applied Biosystems 4800 MALDI-TOF mass spectrometer (AB Sciex, Warrington, Cheshire). The mass spectra were calibrated with auto-digested ion products of trypsin (m/z ratios of 2163.057 and 2273.160) and a calcium ion adduct derived from the matrix solution (m/z ratio of 1060.048). Identification of proteins was performed using a Mascot search engine and a UniProt sequence database of human proteins [135].

2.5.4. LC-MS mass spectrometry

Samples containing tryptic peptides that had been labelled by SILAC (section 2.2.4) were separated by reverse phase HPLC using a Thermo/Proxeon Easy-nanoLC on a C18 column (75 μm internal diameter and 100 mm length), using a gradient of 0-40% acetonitrile and 1% formic acid (Nanoseparations, Nieuwkoop, Netherlands). Heavy SILAC labelled tryptic peptides with either a lysine or arginine at their c-termini contain either eight or ten stable isotopes of C^{14} and N^{15}, respectively. The heavy labelling of peptides results in a mass shift of either 10.01 or 8.01 Da for arginine or lysine, respectively, compared to unlabelled or 'light' peptides. Separated peptides were ionised by electrospray and introduced into a Q-Exactive Plus (Thermo Scientific, Hemel Hempstead, UK) Orbitrap mass spectrometer, using a gradient of 5% v/v – 95% v/v aqueous acetonitrile containing

0.1% formic acid. Raw data were analysed by MaxQuant 1.5.0.12 software using a UniProt human protein sequence database and an Andromeda algorithm which uses the MASCOT search engine to identify and quantify peptide SILAC isotopic pairs and proteins [135–137]. The database was modified to include the sequences of the three mature isoforms of IF_1 and the IF_1 precursor protein (Fig. S22 [138]. Perseus version 1.2.0.17 was used to process the MaxQuant output data. The data were filtered to remove exogenous contaminant proteins, proteins identified by a decoy database designed to establish the probability of false positive identification, proteins that were identified using peptide sequences that were not unique to the parent protein, and protein ratios with peptide counts less than or equal to 1. Experiments were performed in duplicate with reciprocal labelling orientations and the ratios from one experiment were inverted and the ratios of both experiments were converted to a Log_2 scale (Fig. 2.1). The median of the two values was calculated and plotted on a bar graph. Statistical significance was calculated with the Benjamini-Hochberg method to quantify statistical outliers. [139].

2.6. CRISPR-Cas9 mediated gene deletion

2.6.1. Preparation of gRNA

Guide RNAs were designed using the CRISPR design tool (http://www.genome-engineering.org/crispr/). Phosphorylation and annealing of guide RNAs (gRNAs) was performed as described by Ran *et al*, 2013 [140]. The reaction mixture contained 5 µM sense and antisense gRNA, 0.5 µL T4 ligation buffer and T4 kinase per 10 µL reaction and 10 mM ATP. The oligonucleotides were phosphorylated at 37°C for 30 min followed by a step of 95°C for 5 min to remove secondary structure and then annealed by cooling to 25°C at a rate of 5°C/min. A list of gRNA sequences is shown in Table 2.6. The gRNA sequences used to transfect HAP1 cells were ATP5J2-1 and ATP5J2-5.

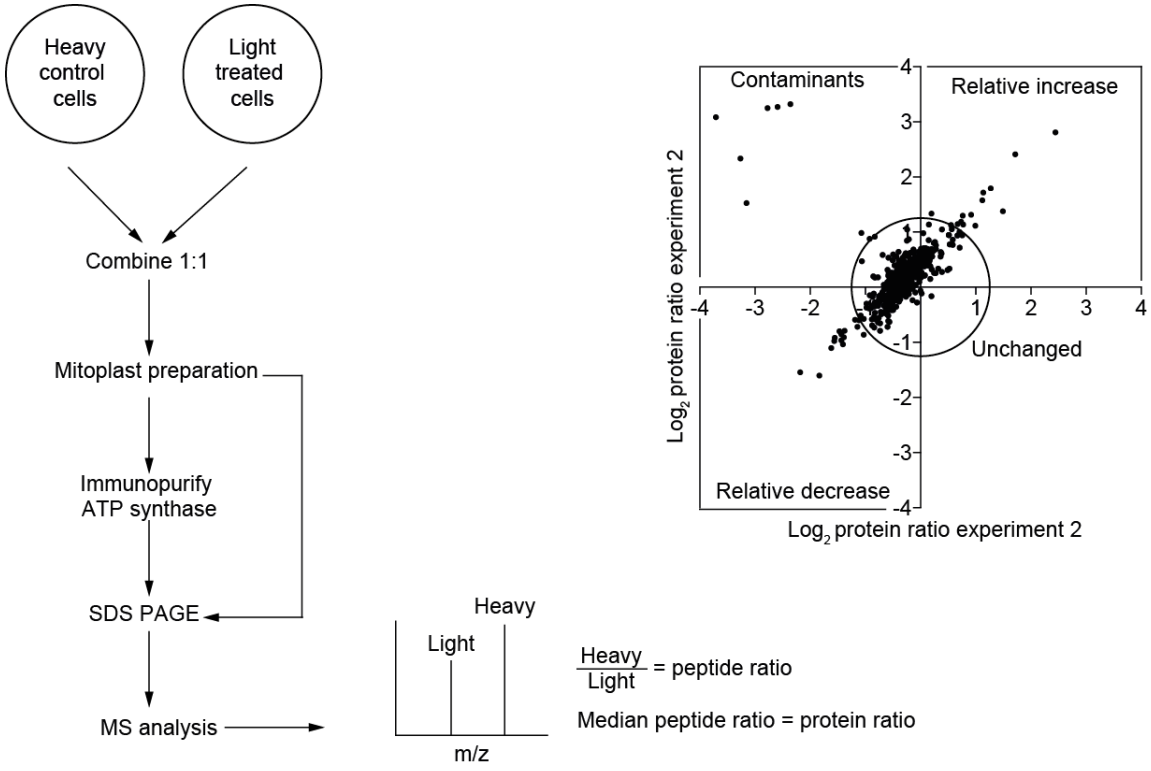

Fig. 2.1 Representation of a SILAC experiment. Cells were reciprocally labelled with 'heavy' or 'light' amino acids and mixed in a 1:1 ratio. Cells from experiment 1 contained heavy control cells and light treated and cells from experiment 2 contained light control cells and heavy treated cells. Treatment refers to siRNA or CRISPR-Cas9 mediated suppression or disruption of the expression of supernumerary subunits of ATP synthase, respectively. After combination of the cells, mitoplasts were prepared and solubilised with digitonin. A portion was analysed by SDS-PAGE, and ATP synthase was immunopurified from the remaining mitoplast material, which was also analysed by SDS-PAGE. Peptides were obtained by trypsin digestion of the proteins, and protein ratios were calculated from the median peptide ratios. Protein ratios from each experiment are represented by each axis on the scatter plot. Proteins that are relatively increased or relatively decreased as a result of treatment with siRNA or CRISPR-Cas9 mediated gene editing are in the top right and bottom left quadrants of the graph, respectively. Contaminants are in the top left and bottom right quadrants. Unchanged proteins are within the circled region.

Table 2.6 Guide RNAs and their sequences.

gRNA	Sequence 5'-3'
ATP5J2-2	CCTCGCGCGGTCCGGCACAG
ATP5J2-5	GTAAGGCTGTTTGGACTCCG
ATP5L-1	TTCCGGCGGGTGACATTCAGCCGGC
ATP5L-2	AGCGCGATGTGAGACCGCCG

2.6.2. Ligation of gRNA into the pSpCas9(BB)-2A-GFP plasmid

Single phosphorylated, duplex gRNA oligonucleotides were ligated into the pSpCas9(BB)-2A-GFP plasmid using T7 DNA ligase. The reaction mixture contained 0.25 pmol gRNA, 26 ng plasmid DNA, 460 Units T7 ligase and 1 µL proprietary ligation buffer per 10 µL reaction. The reaction was left at room temperature over-night. A map of the pSpCas9(BB)-2A-GFP plasmid is shown in Fig. 2.2.

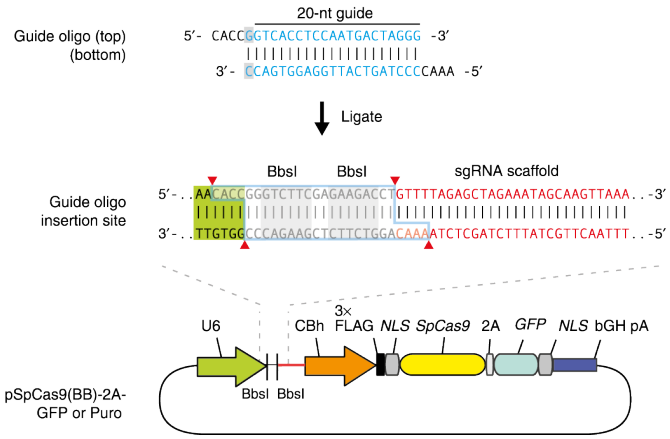

Fig. 2.2. Guide RNA insertion into the pSpCas9(BB)-2A-GFP plasmid. The plasmid contains an sgRNA sequence, which binds Cas9. The gRNA pairs are ligated into the insertion site to guide Cas9 to the DNA sequence to be disrupted. The plasmid contained GFP as a reporter gene. The GFP element assists with FACS (fluorescence activated cell sorting), as cells successfully transfected with the plasmid will also express GFP. The figure is from [140].

2.6.3. Transformation of gRNA plasmids into competent *E. coli* cells

NEB 5-α competent *E. coli* cells were transformed according to the manufacturers heat-shock protocol (C2987). For each gRNA-pSpCas9(BB)-2A-GFP plasmid, 25 µL NEB 5-alpha was thawed at 0 °C for 30 min. A final concentration of 0.37 µM plasmid DNA was added to the thawed cells and mixed gently without pipetting. The mixture was incubated on ice for 30 min, heat-shocked at 42 °C for 30 s, then placed on ice for 5 min before the cells were incubated with shaking for 1 h at 37°C in 100 µL SOC outgrowth medium (0.5%

w/v yeast extract, 2% w/v tryptone, 10 mM NaCl, 2.5 mM potassium chloride, 10 mM magnesium chloride, and 20 mM glucose). The culture was spread onto LB agar with 100 mg/mL ampicillin and incubated over-night at 37°C.

2.6.4. Purification of pSpCas9(BB)-2A-GFP gRNA plasmids

Single colonies of cells were picked and grown overnight in LB media containing 100 mg/mL ampicillin, at 37°C with shaking. DNA was purified from the cells using a Qiagen DNA miniprep kit according to the manufacturer's instructions. Briefly, *E. coli* cells (section 2.6.3) were disrupted with the lysis buffers provided and centrifuged at 10500 x *g* to obtain a supernatant containing DNA. The supernatant was added to an affinity column containing a proprietary silica membrane that binds plasmid DNA. A wash step was used to remove impurities and purified plasmid DNA was eluted in 10 mM Tris-HCl pH 8.5 by centrifugation. All centrifugation steps were carried out at 10500 x *g* and room temperature. The purified plasmid DNA (10 μL) was precipitated with 3 volumes of 100% v/v ethanol, 1 μL Pellet paint co-precipitant and 370 mM sodium acetate. The ethanol was removed after centrifugation at 10500 x *g* for 5 min, and left at room temperature for 10 minutes to allow the residual ethanol to evaporate. The DNA pellet was solubilised in 10 μL nuclease free water.

2.6.5. *In-vitro* assay to confirm the ability of gRNAs to cut f-subunit DNA

Plasmid DNA containing the DNA sequence of ATP synthase f-subunit was digested with gRNA guided Cas9 overnight at 37°C. The reaction contained 1 μL scaffold RNA, 1 μL Cas9 protein and 1 μL substrate plasmid. The samples were electrophoresed (section 2.3.2) to resolve circular undigested DNA from linear digested DNA. The sample (in DNA loading buffer (appendix II) was loaded onto a 1% w/v agarose gel in 90 mM Tris-boric

acid, 1 mM EDTA and 100 ng/mL ethidium bromide, pH8.3 and was electrophoresed at 100 volts for 20 min. Visualisation of DNA bands was performed using UV light at 302 nm.

2.6.6. Transfection of HAP1 cells with pSpCas9(BB)-2A-GFP plasmids

HAP1 cells were seeded to 15% confluence in a tissue culture plate and placed in an incubator over-night at 37°C, under 5% CO_2, and 95% relative humidity. A transfection solution (containing plasmid DNA with gRNAs ATP5J2-1 and ATP5J2-5) was made by combining 750 µL OptiMEM and 22.5 µL Lipofectamine-3000 transfection reagent with 750 µL OptiMEM, 9 µg J2-1-1 plasmid DNA, 9 µg J2-5-2 plasmid DNA and 2 µL/µg DNA p3000 transfection reagent. The solution was left at room temperature for 20 minutes. Cells were washed with sterile warm dPBS and 250 µL transfection solution added to each well. Cells were left for 15 minutes, then OptiMEM (250 µL) was added. The plate was incubated at 37°C for 4 h before the addition of 20% v/v FBS in IMDM (0.5 mL/well) without antibiotics was added.

2.6.7. Cell sorting and seeding single cells for colony growth

Two days after transfection, HAP1 cells were displaced from the plate with trypsin-EDTA dissociation reagent, resuspended in cold IMDM with 10% v/v FBS, 100 U/mL penicillin and 100 µg/mL streptomycin and centrifuged at 100 x *g* for 3 min at room temperature. The supernatant was removed, cells resuspended in IMDM (1 mL) with FBS and antibiotics, transferred to a sterile vial and placed on ice. Flow cytometry was performed with a BD Influx cell sorter using FACS software. Cells were counted and sorted based on the intensity of the fluorescence signal from GFP in the cells then single cells were seeded into 96 well sterile tissue culture plates. Plates were incubated at 37°C, 5% CO_2 with

complete IMDM. The medium was changed once each week and cells from single colonies were dissociated from the plate, diluted 3-fold and transferred into single wells of a 24 well plate. Clonal cells were grown to 70% confluence, dissociated from the plate with trypsin-EDTA dissociation reagent and seeded in triplicate in 24 well plates and incubated until they reached 70% confluence. Wells in two of the three replicate plates were washed with 0.4 mL PBS and the plates stored at -20°C immediately. Wells in the remaining plate were trypsinised with 0.1 mL of the dissociation reagent and then 0.1 mL cold freezing solution was added (20% v/v DMSO, 50% v/v FBS, 30% v/v IMDM), followed by addition of 0.1 mL 10% v/v DMSO, 50% v/v FBS, 40% v/v IMDM. Cell plates were wrapped in two layers of tissue and were placed on dry ice for ~30 min until the media was frozen, followed by storage at -80°C.

2.6.8. Characterisation of the gene deletion status of clonal cell populations

Clonal cells in 24 well plates that had been washed with PBS were lysed with 100 μL buffer (10 mM Tris HCl, pH 7.4, 0.2% w/v SDS, Roche protease inhibitor (1 tablet/50 mL) and 0.5 units of Benzonase). SDS-PAGE loading buffer (section 2.4.6), was added to the lysed cell solution and 10 μL of each sample was resolved by SDS-PAGE. Proteins were transferred to a PVDF membrane by electrophoresis and detected with antibodies raised against the f- and g-subunits and β-actin was used as a loading control (section 2.4.7). The presence of the truncated f-subunit or g-subunit genes were assessed by amplifying the f-subunit or g-subunit genes by PCR and analysing the DNA products using agarose gel electrophoresis. Genomic DNA was purified from clonal HAP1 cells grown in 24 well plates. Protein was removed by incubation with 0.4 mg/mL of Proteinase K at 50°C for 2 h in 0.2% w/v SDS, 75 mM sodium chloride and 20 mM EDTA. The DNA was transferred to a 1.5 mL tube and an equal volume of propan-2-ol was added. Samples were kept at 4°C

overnight then centrifuged at 10500 *g* at 4°C for 20 min to pellet DNA. The propan-2-ol was removed and the DNA was washed with 200 µL absolute ethanol followed by a second centrifugation. The ethanol was removed, samples air-dried and the DNA was re-dissolved in buffer EB (10 mM Tris pH 8.5). DNA was amplified by PCR using 2.5 µL 10x Hot Start reaction buffer/25 µL reaction, 1.5 mM magnesium sulphate, 0.2 mM dNTPs, 10% v/v DMSO, 0.4 µM forward and reverse primers, 0.75 units of Hot Start DNA polymerase and 2 µL genomic DNA template/25 µL reaction. The temperature profile was 94°C for 3 min then 35 cycles of 94°C for 20 s, 59°C for 20 s and 68°C for 40 s followed by a final step of 72°C for 5 min. Agarose gel electrophoresis was used to separate f- or g-subunit DNA PCR products (section 2.3.2). The primers for generating the f- and g-subunit PCR products are presented in Table 2.7.

Table 2.7 Primer sequences for the f- and g-subunit used to amplify the f- and g-genes from HAP1 genomic DNA. ATP5J2 forward and ATP5J2 reverse are the f-subunit primers and ATP5L forward and ATP5L reverse are the g-subunit primers.

Primer	Sequence (5'-3')
ATP5J2 forward	CTGCAGGACCCTCGGATTTT
ATP5J2 reverse	TTCACCCTCCACGCCTAAC
ATP5L forward	GGTTTTCCGGACCTCTACGA
ATP5L reverse	ATCTGCAGGTCAGACGAGTG

3. Results

3.1. Investigation of the functions of the supernumerary subunits of human ATP synthase

The supernumerary subunits e, f, g, DAPIT, A6L and 6.8 kDa proteolipid of human ATP synthase have no known functions in mitochondria [82, 87, 100, 124]. Human 143B cells were treated separately for 96 h with siRNAs to deplete the e-, f-, g-, DAPIT- and 6.8 kDa proteolipid-subunits. The roles of the f- and g-subunits were also investigated by the disruption of the corresponding genes in human HAP1 cells.

3.2. Structures of the genes for the nuclear encoded supernumerary f- and g-subunits of ATP synthase

The chromosome locations of the genes encoding the f- and g-subunits and their structures are summarised in Table 3.1 and Fig. 3.1. The diagrams were constructed with gene and mRNA sequences from the 'genome reference consortium human build 38' (patch release 7, GRCh38.p7) [141]. The gene for the f-subunit contains an alternative 5' donor site at position 73, which allows the synthesis of the f-2 isoform in addition to the f-1 isoform. Isoform f-1 has six additional amino acids (GECPAP) near to its N-terminus (Fig. 3.3B.

Table 3.1 Chromosome locations of supernumerary subunits f and g of human ATP synthase.

Subunit	Gene	Chromosome, location
f	ATP5J2	7, 7q22.1
g	ATP5L	11, 11q23.3

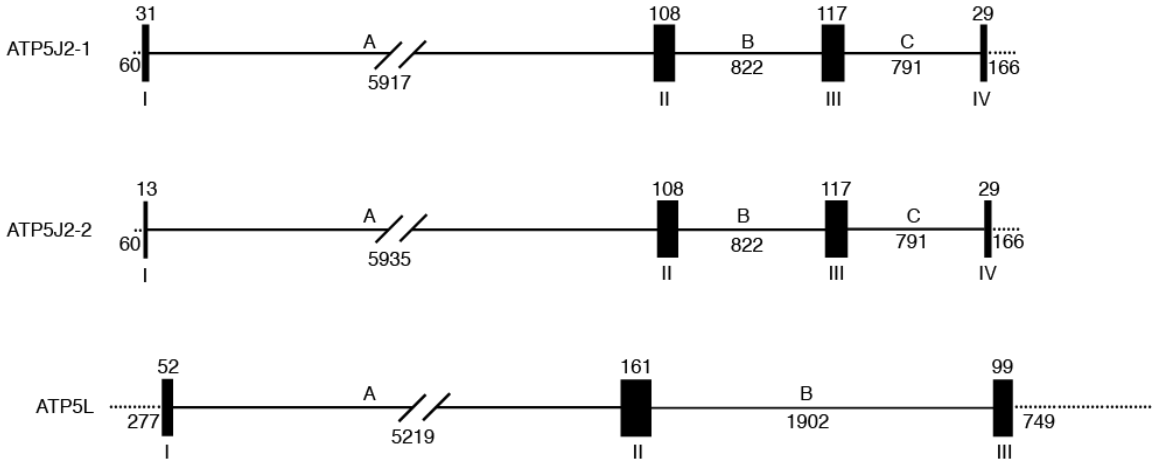

Fig. 3.1 Structures of genes encoding supernumerary subunits f and g of ATP synthase. Dashed lines at the beginning and end of the genes represent the 5' and 3' UTRs, respectively, and solid lines and black boxes are introns and exons, respectively. The numbers below and above each box or line correspond to the number of base pairs in the introns and exons, respectively.

3.2.1. The efficacy of the gRNAs ability to cut DNA

In order to disrupt the f- and g-subunit genes, the CRISPR-Cas9 system was used. To demonstrate that the Cas9 nuclease could cut the f-subunit gene, a plasmid containing the f-gene was incubated with RNA guided Cas9 and four gRNA molecules (Fig. 3.2A). Nicked, linear and supercoiled forms of the plasmid DNA, shown at the top, middle and bottom of the gel, were produced. The gRNAs in lanes 2 and 4 were the most effective at generating linear DNA, as the majority of the product DNA was present as the linearised form. Guides 1 and 3 were less efficient, as some supercoiled DNA remained, plus more nicked DNA was produced than in lanes 2 and 4. Therefore, guides 2 and 4 were chosen to transfect HAP1 cells; they correspond to gRNAs ATP5J2-2 and ATP5J2-5 in Table 2.6. The ATP5L1 and ATP5L2 gRNAs were confirmed by Dr. Jiuya He (MRC-MBU) to cut the ATP5L gene efficiently, and the HAP1 cells were also transfected by Dr. Jiuya He. Once the cells had been transfected and clonal populations grown from single cells, the gene disruption was demonstrated by amplifying the f- and g-genes from genomic DNA from the clonal populations by PCR followed by analysis of the product by agarose gel

electrophoresis (Fig. 3.2B and C, respectively). The PCR product from the control f-gene was 384 bp long, and the PCR product containing the Δf-gene deletion was 315 bp (Fig. 3.2B). The PCR product from the control g-gene was 415 bp long and the Δg-gene was 344 bp long (Fig. 3.2C). Both DNA products were analysed by Sanger sequencing (Fig. 3.3A and 3.4A).

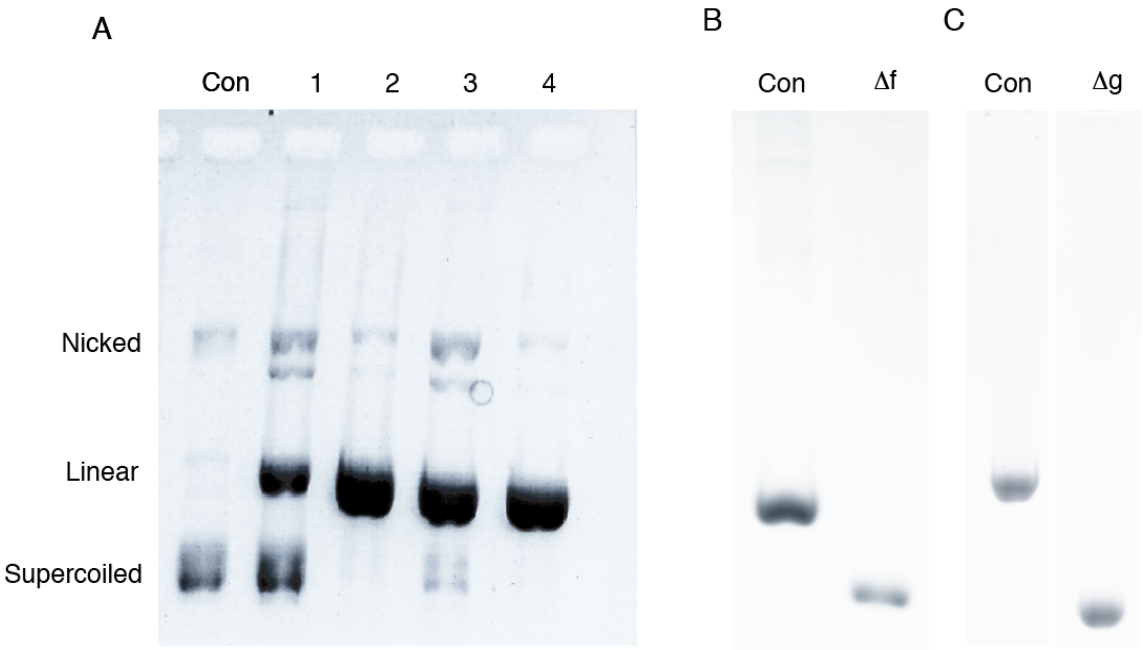

Fig. 3.2 Disruption of the f-gene. In panel A, validation of gRNAs for disruption of the f-gene in HAP1 cells. The control contained Cas9 and the plasmid containing the f-gene, but no gRNAs. Lanes 1-4 correspond to four gRNAs added to the plasmid containing the f-gene with Cas9. Panels B and C, the PCR products from control and Δf-HAP1 cells and Δg-HAP1 cells, respectively. Their sequences were determined.

3.2.2. Disruption of the genes for the f- and g-subunits

The Cas9 nuclease was guided to specific sequences in the f- and g-genes by pairs of guide RNA molecules with PAM (protospacer adjacent motif) sequences. For the f-subunit gene, the 5'-3' and 3'-5' PAMS are CCT and GCC, respectively and for the g-subunit gene the 5'-3' PAMS are CGG and CCG, respectively. The deletions resulted in 69 and 71 base pairs (bp) of DNA being removed from the f- and g-subunit genes, respectively. Within the

deleted regions, the 5' cap of the corresponding mRNA and translational initiator methionine codon were removed from both the f- and g-subunit genes. In the f-subunit gene, the entire sequence of exon I was removed, and 17 bp were removed from intron A (Figs. 3.1 and 3.3A). For the g-subunit gene, 33 bp upstream of exon I were removed and 32 out of 51 bp were removed from the start site of exon I, resulting in a frame shift mutation. The effects on the DNA and protein sequences are shown in Figs. 3.3 and 3.4, respectively. The f-subunit gene deletion occurred across an intron-exon boundary, between exon I and intron A (Fig. 3.1 and 3.3A), which introduced a frame-shift mutation upstream of intron A. If the ribosome was able to bind to a start site ATG codon upstream of the f- or g-subunit gene deletions and transcribed the corresponding mRNA, the frame-shift mutation would probably result in proteins with amino acid sequences did not resemble those of the WT f- and g-subunit proteins. The predicted theoretically translated protein sequences after the f- and g-subunits were disrupted are in Fig. 3.3B and 3.4B, respectively.

A

```
WT    GTGCATTCCCTACCCAGCAGCCCTCGCGCGGTCCGGCACAGCGGACACCAGGACTCCAAA
Δf    GTGCATTCCCTACCCAGCAGCCCTCGCGCGGTCCGGCA----------------------

WT    ATGGCGTCAGTTGGTGAGTGTCCGGCCCCAGGTAAGGCTGTTTGGACTCCGTGGTGGAAG
Δf    [------------------------------]----------------TCCGTGGTGGAAG
```

B

Isoform 1

```
WT    MASVGECPAPVPVKDKKLLEVKLGELPSWILMRDFSPSGIFGAFQRGYYRYYNKYINVKK
Δf    ----------------KLLEVKLGELPSWILMRDFSPSGIFGAFQRGYYRYYNKYINVKK

WT    GSISGITMVLACYVLFSYSFSYKHLKHERLRKYH
Δf    GSISGITMVLACYVLFSYSFSYKHLKHERLRKYH
```

Isoform 2

```
WT    MASVVPVKDKKLLEVKLGELPSWILMRDFSPSGIFGAFQRGYYRYYNKYINVKKGSISGI
Δf    ----------KLLEVKLGELPSWILMRDFSPSGIFGAFQRGYYRYYNKYINVKKGSISGI

WT    TMVLACYVLFSYSFSYKHLKHERLRKYH
Δf    TMVLACYVLFSYSFSYKHLKHERLRKYH
```

Fig. 3.3 The effect of gene editing on the f-gene and protein. A, A 69 bp deletion in the gene removed the sequence encoding part of the 5' cap of the corresponding mRNA, the ATG initiator codon (shown in yellow) and the following 9 codons from exon I and one base pair from intron A (Fig. 3.2). The binding sites of the gRNAs are grey and the coding region of exon I is surrounded by square brackets. **B,** The gene disruption deleted 10 and 6 amino acids from the N-terminus of isoforms 1 and 2, respectively. WT, wildtype; Δf, deletion strain Δf-HAP1. There is no evidence that the truncated f-subunit protein is translated or that there is a transcript.

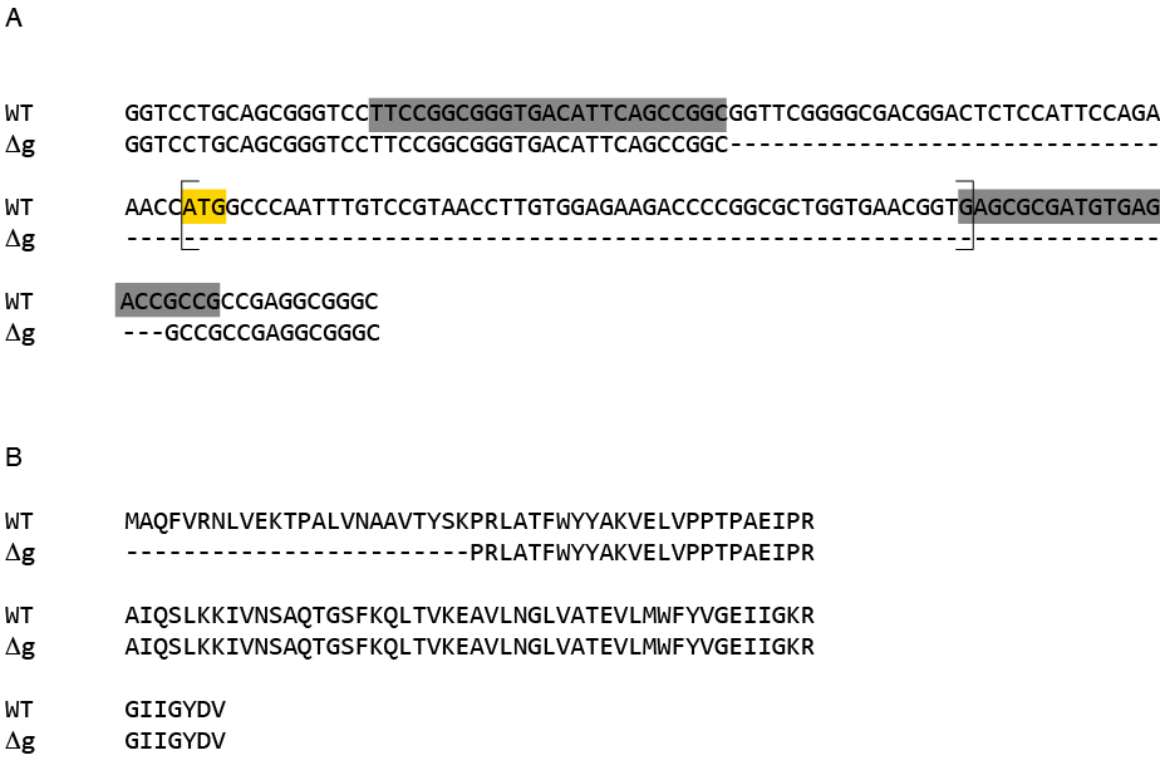

Fig. 3.4 The effect of gene editing on the gene and protein of the g-subunit. A, A 71 bp deletion in the gene removed the ribosome binding site, the initiator codon (yellow) an additional 35 bp corresponding to 11 codons and 2 bp in exon I. The binding sites for gRNAs are grey. The coding region of exon I is marked between square brackets. **B,** The gene disruption deleted 13 amino acids at the N-terminus of subunit-g. WT, wildtype; Δg, deletion strain Δg-HAP1. There is no evidence that the truncated gene is transcribed or the protein translated.

3.3. Suppression of the expression of the e-subunit

The role of the e-subunit of ATP synthase was investigated by suppressing its expression using siRNA, followed by biochemical characterisation of the enzyme. The subunit composition of immunopurified ATP synthase depleted of the e-subunit was examined by SDS PAGE and mass mapping (Fig. 3.5A and B, and Appendix III Table S1). The identification of subunits was based on peptide mass mapping of a previous sample of control ATP synthase.

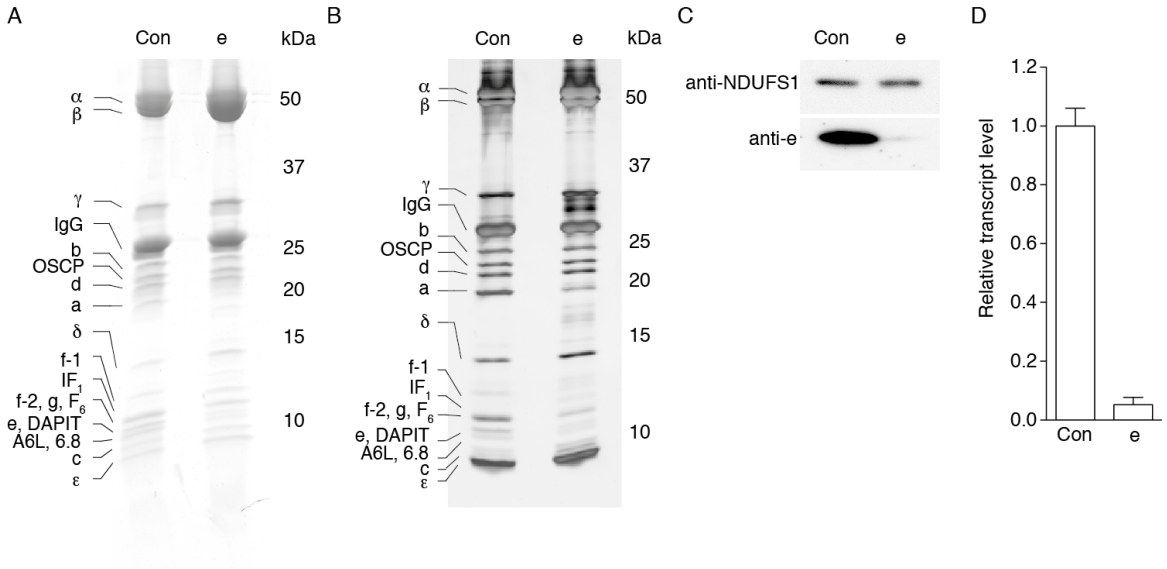

Fig. 3.5 Analysis by SDS-PAGE of residual ATP synthase complexes from 143B cells where the expression of the e-subunit had been suppressed with RNAi molecules. Cells were treated with 90 nM siRNA for 96 h and then mitoplasts were prepared, followed by solubilisation of membrane proteins with digitonin (13.4g/g protein) and immunopurification of ATP synthase. Proteins were detected with either Coomassie blue dye in panel A, or by silver staining in panel B. The identities of subunits of the enzyme identified by peptide mass mapping are indicated on the left-hand side of the gels. The labels f-1 and f-2 are the two isoforms of the f-subunit. The efficiency of suppression of the e-subunit protein after 96 h is in panel C, where the complex I subunit NDUFS1 was used as a loading control. The e-subunit transcript level after treatment with siRNA for 48 h panel D and was normalised to cellular transcript levels of β-actin.

ATP synthase from the control cells contained all eighteen subunits of the enzyme. Compared to the control, the residual ATP synthase complex from cells with suppression of the e-subunit contained similar levels of all five subunits from the F_1-catalytic domain of the enzyme (α, β, γ, δ and ε), plus the peripheral stalk subunits OSCP, F_6, b and d, and the c-subunit of the enzyme's rotor from the membrane domain. The level of the F_O domain a-subunit had also decreased. The amount of the natural inhibitor of ATP synthase, IF_1, was increased compared to the control. In e-subunit depleted ATP synthase, depletion of f-isoform 1 (f-1), f- isoform 2 (f-2), g-, F_6-, DAPIT-, A6L- and 6.8 kDa proteolipid-subunits is also apparent. The level of suppression of the e-subunit protein and transcript are presented in Fig. 3.5C and D, respectively.

To analyse the relative quantity of ATP synthase subunits in the residual ATP synthase complex with suppression of the e-subunit, SILAC with mass spectrometry was performed (Fig. 3.6A and B).

The data are presented in scatter plots showing proteins with increased association, decreased association or unchanged association with ATP synthase, and are represented in the upper right quadrant, lower left quadrant and middle of the scatter plots, respectively. See Fig. 2.1 for an explanation of the interpretation of these scatter plots. Proteins contained in both immunopurifed ATP synthase and mitoplasts were analysed to investigate the possibility of protein degradation or increased association of proteins with ATP synthase. As a result of depletion of the e-subunit, the majority of the subunits in the F_O domain of ATP synthase dissociated from the enzyme. The subunits with a four-fold relative decrease in association with ATP synthase were the a-subunit, the two isoforms of the f-subunit (f-1 and f-2), the g-subunit, and the DAPIT- and 6.8 kDa proteolipid-subunits. The A6L-subunit displayed a three-fold relative decrease in association with ATP synthase. In contrast, there was a three-fold relative increase of IF_1-M1, which corresponds to one of the mature forms of the IF_1 protein (Appendix V, Fig. S22), indicating a relative increase in association of IF_1 with ATP synthase compared to the control. IF_1-M1 contains an N-terminal Phe-25 residue. The relative abundances of subunits of the F_1 domain and the peripheral stalk were unchanged. The mitochondrial

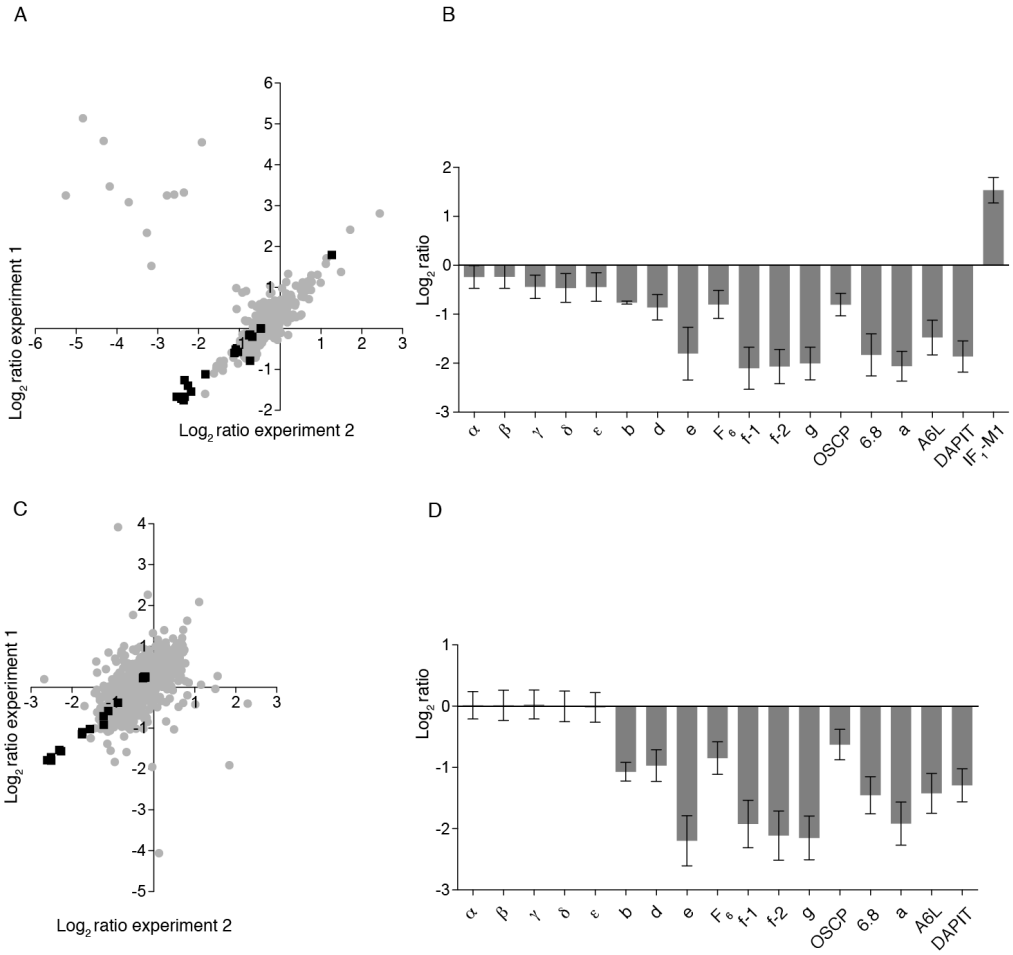

Fig 3.6 Relative quantitative mass spectrometric analysis of ATP synthase in e-subunit depleted ATP synthase from mitoplasts. Mitoplasts were prepared from 143B cells which had been labelled with SILAC and treated for 96 h with 90 nM siRNA. In panel A, ATP synthase was immunopurified from mitoplasts solubilised with digitonin (13.4g/g protein). Proteins were separated by SDS-PAGE, individual bands were Coomassie stained, then in-gel digested with trypsin and analysed by quantitative mass spectrometry. Black squares and grey circles represent ATP synthase subunits and all other proteins identified in the sample, respectively. Each axis represents data points from experiments 1 and 2. The data points are relative protein ratios derived from peptide pair ratios calculated using MaxQuant. In panel B, the data points for ATP synthase in panel A are summarised. The bars represent the median relative ratios from both experiments and the error bars represent the range of the ratios. In panel C, proteins from a portion of solubilised mitoplast material was analysed. The portion was ethanol precipitated, and analysed by SDS PAGE as in panel A. In panel D, the data points for ATP synthase in panel C are summarised. IF_1 was not identified in the mitoplast experiment.

proteome was also investigated by analysing mitoplasts (Fig. 3.6C and D). Subunits that were relatively decreased in the immunopurified ATP synthase (Fig. 3.6A and B) were also decreased to a similar extent in mitoplasts, indicating that these subunits are degraded when

they are lost from the enzyme in e-subunit depleted cells. The evidence that these subunits are degraded is that these subunits do not remain unchanged in mitoplasts. No protein ratios were obtained for IF_1 in mitoplasts. Protein ratios for the data points are included in Appendix IV, Tables S4 and S5.

In order to assess the respiratory capacity of cells with suppression of the e-subunit, the oxygen consumption rate (OCR) of cells was measured (Fig. 3.7A). The respiratory states measured were basal respiration, (respiration before the addition of respiratory modulators), respiration after inhibition of glycolysis with 2-deoxy-D-glucose (2DG), respiration after inhibition of the catalytic activity of ATP synthase with oligomycin A (oligo) and accelerated respiration induced by the respiratory uncoupler FCCP. The cellular OCR during glycolysis inhibited respiration was significantly lower in e-subunit depleted cells compared to the control cells. Also, ATP-linked respiration (the difference between glycolysis inhibited respiration and oligomycin sensitive respiration) was also significantly lower in e-subunit suppressed cells, suggesting that the respiratory chain in subunit-e depleted mitochondria cannot pump more protons due to the lack of proton transport through ATP synthase. The mitochondrial OCR (Fig. 3.7B) was calculated by subtracting non-mitochondrial respiration (measured after the joint addition of antimycin A and rotenone) from basal, oligomycin sensitive and accelerated respiration. Basal and accelerated mitochondrial respiration were significantly decreased in cells with e-subunit depletion. ATP synthase depleted of the e-subunit did not display a significant difference in oligomycin sensitivity compared to the control, as indicated by the cellular and mitochondrial OCR after addition of oligomycin. Once the mitochondrial respiration was calculated, significant differences in the basal and accelerated respiration were observed.

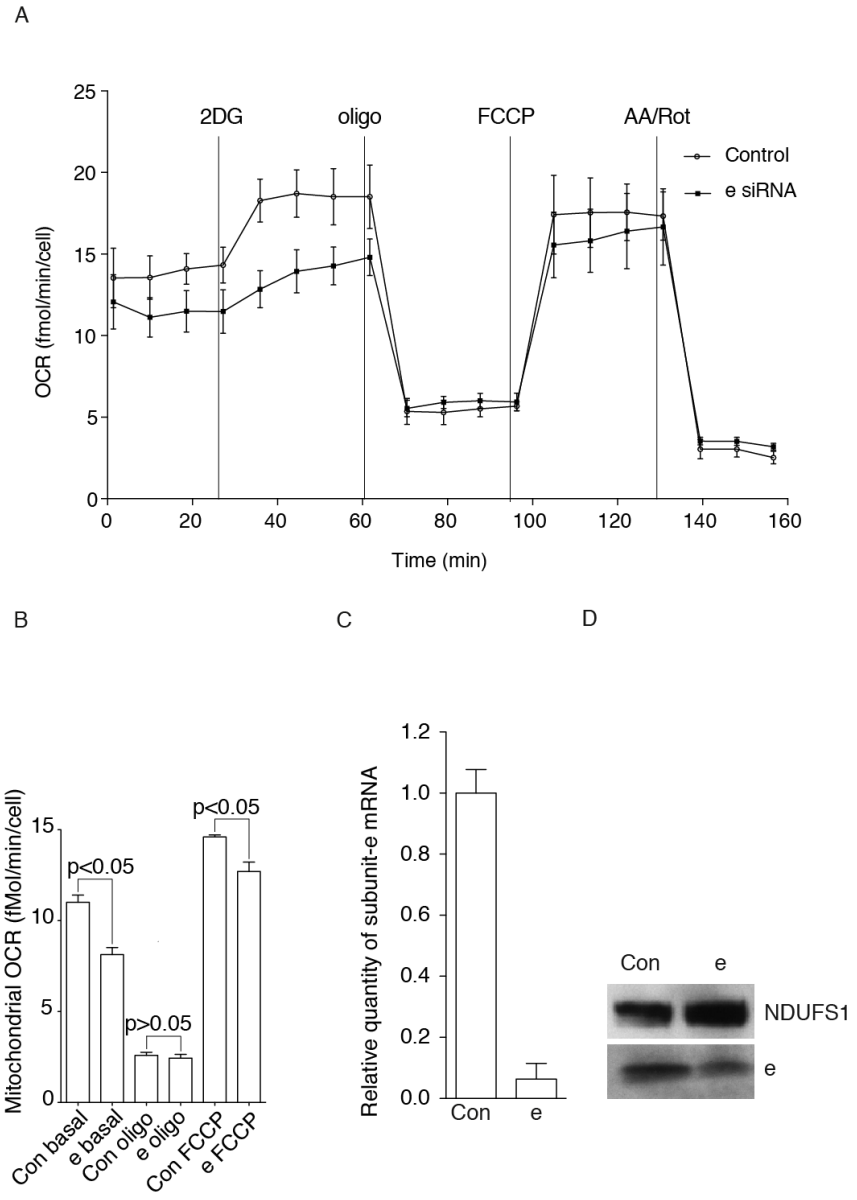

Fig. 3.7 The OCR of 143B cells depleted of the e-subunit of ATP synthase. 143B cells were analysed 96 h after transfection of the cells with 90 nM siRNA using a Seahorse XF^{e}24 instrument. In panel A, the cellular OCR is measured after the additions of the respiratory modulators 2-deoxy-D-glucose (2-DG), which inhibits glycolysis, oligomycin A (oligo), which inhibits ATP synthase, FCCP, a protonophore which accelerates respiration, and antimycin A with rotenone (AA/Rot), which are complex III and complex I inhibitors, respectively. The concentrations of each modulator added to the cells was 20 mM, 1 μM, 0.5 μM and 0.6 μM each, respectively. Each data point represents the mean (n=5) +/- the standard deviation. In panel B, the mitochondrial OCR (the measurement with the AA/Rot residual rate subtracted) is displayed during basal, ATP synthase inhibited (oligo) and accelerated (FCCP) respiration. The bars represent the mean mitochondrial OCR of the four time points during each measurement period. A paired Students' t-test was used to show statistical significance between control and siRNA treated groups. The efficiency of the siRNA mediated suppression of the e-subunit transcript level and protein are in panels C and D, respectively. The e-subunit mRNA level was normalised to transcript levels of cellular β-actin.

This may be due to the level of e-subunit depletion, where if the e-subunit had been depleted more than was observed, the significant differences may have also been observed in Fig.

3.7 A. The level of suppression of the transcript and e-subunit protein in this experiment are presented in Fig. 3.7C and D, respectively.

The effect of suppressing the e-subunit on the oligomerisation state of ATP synthase was examined by blue native (BN)-PAGE (Fig. 3.8A). Mitochondrial membranes were treated with digitonin (6 g/g protein) to solubilise native protein complexes, which were separated by BN-PAGE, followed by Western transfer and antibody detection of protein complexes containing the β-subunit of ATP synthase. Oligomeric ATP synthase and the ATP synthase dimer were significantly depleted in subunit-e depleted mitochondrial membranes, and sub-complexes e-S1 and e-S2 accumulated. Oligomers (O) represent two forms of multimers containing the ATP synthase dimer. The level of the suppression of the e-subunit protein in this experiment is presented (Fig. 3.8B).

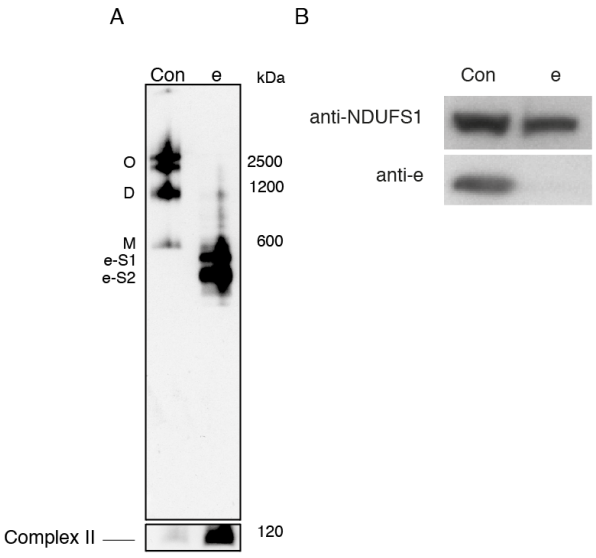

Fig. 3.8 Analysis of the native state of ATP synthase after depletion of the e-subunit using siRNA. Mitochondrial membranes were prepared from 143B cells within 3 h of harvesting and membrane proteins were solubilised with digitonin (6g/g protein). Native protein complexes were separated by BN-PAGE followed by immunoblotting and detection of ATP synthase complexes with a β-subunit antibody. O refers to oligomeric forms of ATP synthase, D is dimeric ATP synthase, M is monomeric ATP synthase, e-S1 and e-S2 are subcomplexes of ATP synthase in order of decreasing size. The SDHA subunit of complex II was used as a loading control. The efficiency of the siRNA to suppress the expression of the e-subunit is in panel B.

3.4. Suppression and disruption of the expression of the f-subunit

The subunit composition of ATP synthase was examined, in 143B cells where the expression of the f-subunit had been suppressed by siRNA, and in Δf-HAP1 cells (Fig. 3.9A and B and Fig. 3.9E and F, respectively). ATP synthase was immunopurified from mitoplasts, analysed by SDS-PAGE and subunits were identified by peptide mass mapping (Appendix III, Tables S1 and S2). When the expression of the f-subunit was suppressed, the subunits that remained unchanged compared to the control were those in the F_1 domain, the peripheral stalk and the c-subunit. The a-subunit was depleted compared to the control, and the band containing IF_1 was more intense than in the control. Depletion of subunits was seen in the band containing the f-subunit isoform 1, and there was a slight decrease in the band containing the f-subunit isoform 2, g- and F_6-subunits, which co-migrate. The band containing the A6L- and 6.8 kDa proteolipid-subunits was depleted, as well as the band containing the e- and DAPIT-subunits. The level of suppression of the f-subunit protein and transcript are presented in Fig. 3.9C and D. The changes in ATP synthase where the f-subunit had been suppressed with siRNA oligonucleotides (Fig. 3.9A and B) were reflected, but more severely, in Δf-HAP1 ATP synthase (Fig. 3.9E and F). When a protein is depleted with siRNA, the changes in the level of that protein are only transient and the protein is not lost completely. In contrast, the disruption of a gene results in sustained, indefinite loss of the protein, and so the effects of the loss of that protein are usually amplified, as in the case of Δf-HAP1 ATP synthase. In Δf-HAP1 ATP synthase, the loss of the A6L-, 6.8 kDa proteolipid-, DAPIT- and a-subunits is apparent. The band containing the DAPIT- and e-subunits from Δf-HAP1 ATP synthase stains less intensely than the equivalent band in the control. The DAPIT-subunit was not automatically identified by mass spectrometry peptide mass mapping, suggesting that the majority of the protein contained in this band in Δf-HAP1 ATP synthase is the e-subunit. The band containing IF_1

stains more intensely than the control in Δf-HAP1 ATP synthase. The F_1 and peripheral stalk subunits were unchanged. In the F_O domain, the g-, and ε-subunits were unchanged. The level of the f-subunit compared to the control in Δf-HAP1 mitoplasts is presented in Fig. 3.9G.

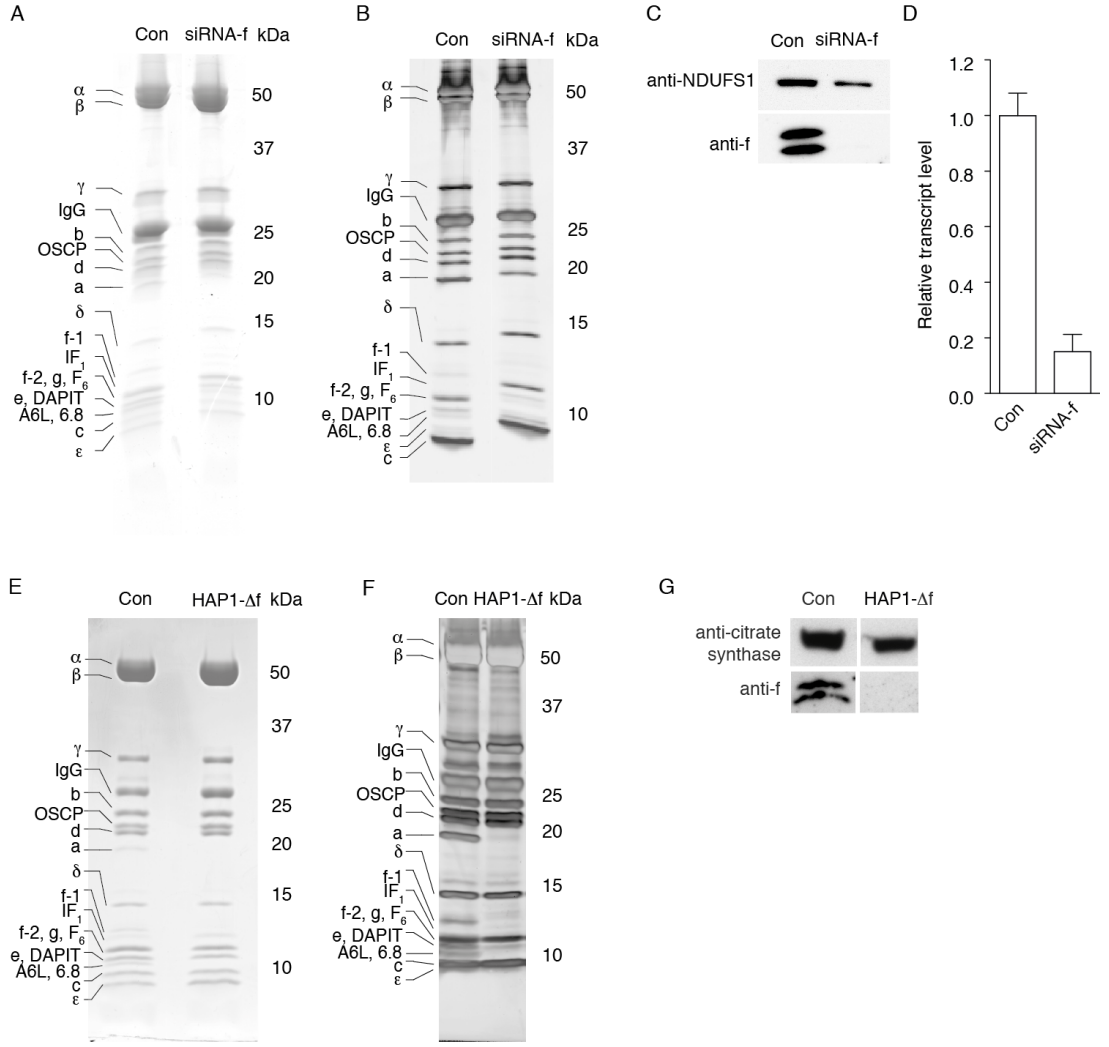

Fig. 3.9 Analysis of residual ATP synthase complexes from 143B cells where the expression of the f-subunit had been suppressed with RNAi molecules, or from Δf-HAP1 cells. Mitoplasts from cells transfected with 90 nM siRNA for 96 h (panels A and B), or mitoplasts from Δf-HAP1 cells (panels E and F) were solubilised with digitonin (13.4g/g mitoplast protein) and ATP synthase was immunopurified. Proteins were separated by SDS-PAGE and visualised with either Coomassie blue dye in panels A and E, or by silver staining in panels B or F. The ATP synthase subunits identified by mass mapping are shown to the left of the gels. The extent of the suppression of the f-subunit protein is in panel C, the complex I subunit NDUFS1 was used as a loading control. The level of the f-subunit transcript after the cells were exposed to the siRNA for 48 h is in panel D, and was normalised to transcript levels of cellular β-actin. The absence of the subunit-f protein in mitoplasts from Δf-HAP1 cells is in panel G.

To quantify the relative changes in ATP synthase subunits after the suppression or disruption of the expression of the f-subunit, ATP synthase was immunopurified from f-subunit depleted or Δf-HAP1 mitoplasts, respectively. SILAC labelling and mass spectrometry were used for relative quantification of the proteins. The pattern of depleted subunits in Fig. 3.9 was reflected in the analysis of subunit-f depleted ATP synthase after siRNA treatment, or in Δf-HAP1 ATP synthase (Fig. 3.10A and B and Fig. 3.11A and B, respectively).

After the expression of the f-subunit was suppressed by siRNA, both isoforms of the f-subunit showed a four-fold relative depletion in immunopurified ATP synthase. Subunits with a similar level of depletion were the DAPIT-, 6.8 kDa proteolipid-, a- and A6L-subunits. The e- and g-subunits remained unchanged, along with the peripheral stalk subunits and F_1 domain subunits. The IF_1-M1 isoform displayed a two-fold increase in association with immunopurified ATP synthase. In mitoplasts from cells where the f-subunit had been suppressed, the 6.8 kDa proteolipid-, a- and A6L-subunits were also depleted, and so was the DAPIT-subunit, to a lesser extent. (Fig. 3.10C and D), indicating that these subunits apart from DAPIT are turned over either before or after incorporation into ATP synthase with f-subunit-suppression. The IF_1-M1 protein (Appendix V, Fig. S22) was unchanged in mitoplasts, suggesting that suppressing the f-subunit does not result an apparent increase in the expression of IF_1 in mitochondria. The observed increase in association of IF_1 with ATP synthase therefore reflects a specific increase in its interaction with the complex. A list of the protein ratios used to create Figs. 3.10 and 3.11 is in Appendix IV Tables S6-S10. Peptide ratios used to calculate the γ-, δ-, and ε-subunits manually are in Appendix IV Table S22.

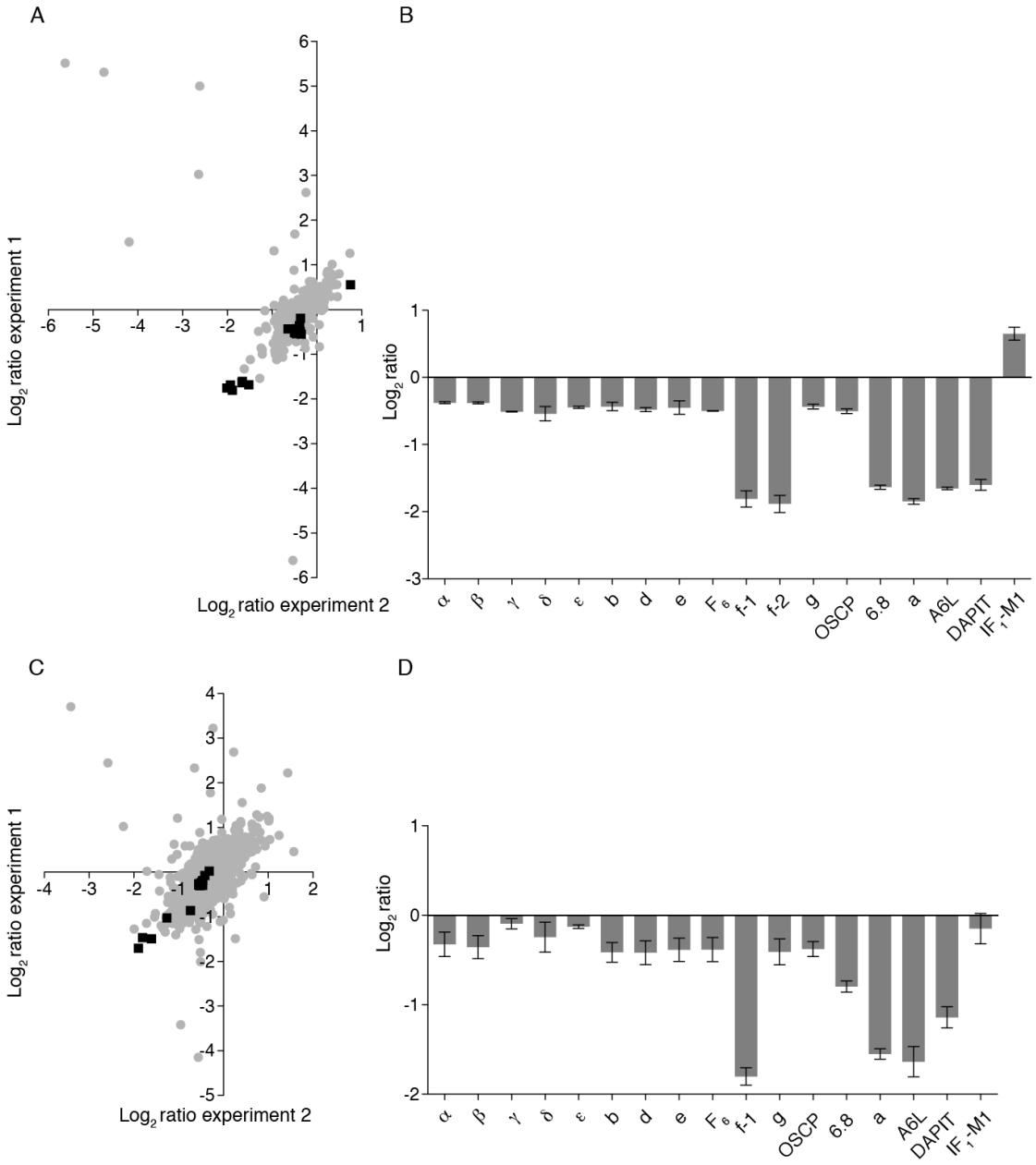

Fig. 3.10 Relative quantitative mass spectrometric analysis of ATP synthase with f-subunit suppression. Proteins were labelled by SILAC in f-subunit depleted cells. Mitoplasts were prepared and solubilised with digitonin (13.4g/g mitoplast protein). In panel A**,** immunopurified ATP synthase was analysed by SDS-PAGE and relative quantitation of proteins was performed by quantitative mass spectrometry. In panel B**,** the ATP synthase subunits in panel A are summarised. Bars represent median ratios from two experiments and the error bars show the range of the ratios. In panel C, the solubilised mitoplast material was ethanol precipitated, and analysed as in panel A. In panel D, the data points for ATP synthase in panel C are summarised.

The gene encoding the f-subunit was disrupted (Fig. 3.2), and immunopurified ATP synthase from Δf-HAP1 mitoplasts was analysed by mass spectrometry with SILAC (Fig.

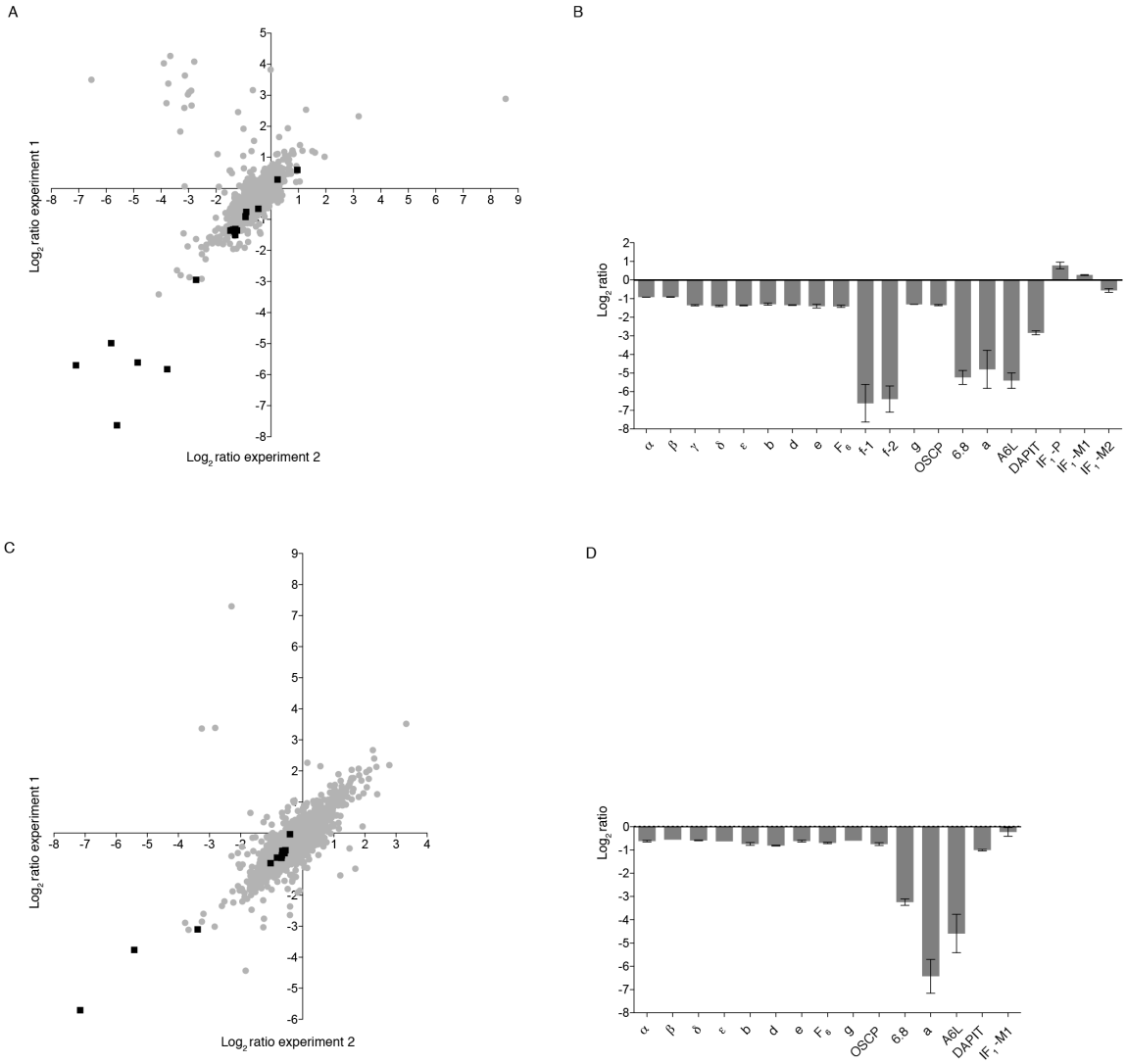

Fig. 3.11 Characterisation of ATP synthase from Δf-HAP1 cells. Δf-HAP1 cells were labelled with SILAC, mitoplasts were prepared and solubilised with digitonin (9g/g mitoplast protein). In panel A, ATP synthase was immunopurified from mitoplasts and relative quantification of subunits was obtained by mass spectrometry. In panel B, a summary of ATP synthase subunit ratios in panel A is presented. In panels C and D, Δf-HAP1 mitoplasts that had been solubilised with digitonin and ethanol precipitated were analysed by mass spectrometry as in panels A and B. The γ- and ε-subunits were calculated manually from peptide ratios where less than two unique peptides were identified in one or both experiments.

3.11A and B). This experiment should not provide a protein ratio for the f-subunit as the proteins should only be present in the wildtype sample. However, both isoforms of the f-subunit were identified, and were depleted approximately $\log_2$ 7-fold (a 128-fold

depletion). The peptide data for the f-subunit in Δf immunopurified ATP synthase samples can be explained by incomplete labelling of the wildtype (WT) sample in experiment 1, where the WT cells were labelled with heavy isotopes of arginine and lysine, but in experiment 2, where the WT cells were unlabelled or 'light', the identification of the 'heavy' f-subunit suggests that the Δf-HAP1 sample contained some residual f-subunit protein. This may have arisen by cross contamination, which could have occurred from the adjacent lane in the gel on which the samples were loaded. When Δf-HAP1 mitoplasts were analysed (Fig. 3.11C and D), there was no evidence of the two isoforms of the f-subunit.

In Δf-HAP1 ATP synthase, the subunits that displayed a 32-fold relative decrease were the a-, A6L- and 6.8 kDa proteolipid subunits. The DAPIT-subunit displayed an 8-fold relative decrease. The IF_1 precursor protein was identified in immunopurified Δf-HAP1 ATP synthase, as well as the IF_1-M1 and IF_1-M2 isoforms. The IF_1 precursor was elevated 2-fold, however, the IF_1-M1 and IF_1-M2 isoforms remained unchanged. In Δf-HAP1 mitoplasts, the relative changes observed in immunopurified ATP synthase were approximately reflected. The 6.8 kDa proteolipid-, a- and A6L-subunits were decreased 8-, 90- and 22-fold, respectively, but the DAPIT-subunit was unchanged. Only the IF_1-M1 isoform was identified in mitoplasts, and was unchanged.

The effect on the OCR of cells after the suppression or disruption of the expression of the f-subunit was examined in 143B cells or HAP1 cells, and is shown in Figs. 3.12 and 3.13, respectively. The cellular OCR of cells with suppression of the f-subunit was significantly lower than the control during basal and glycolysis inhibited respiration (fig. 3.12A). There was a small but statistically significant decrease in the cellular OCR after the second measurement following FCCP addition. The oligomycin sensitive OCR of f-subunit suppressed cells and the mitochondrial OCR was also decreased to a small but statistically

significant extent (Fig. 3.12A and B). ATP-linked respiration (the difference between basal respiration and oligomycin sensitive respiration) was significantly lower in cells with f-subunit suppression. There was no significant difference in cellular OCR of control cells or cells with f-subunit suppression during accelerated respiration, indicating that the suppression of the f-subunit did not affect the activity of the respiratory complexes. The mitochondrial OCR in 143B cells depleted of the f-subunit (Fig. 3.12B) was significantly decreased during basal and accelerated respiration. The degree of suppression of the expression of the f-subunit protein and transcript is shown in Fig. 3.12C and D, respectively.

In contrast to 143B cells with f-subunit suppression, in Δf-HAP1 cells, the cellular OCR was significantly decreased during basal, glycolysis inhibited, oligomycin sensitive and accelerated respiration (Fig. 3.13A). This suggests ATP synthesis and respiration in Δf-HAP1 cells are severely disrupted. Δf-HAP1 ATP synthase did not display sensitivity to oligomycin as indicated by the observation that the OCR did not significantly decrease after the addition of oligomycin. Also, the respiratory capacity of the electron transport chain may be decreased, indicated by the significantly lower OCR during accelerated respiration. When the mitochondrial OCR was calculated (Fig. 3.13B), the significant differences in cellular OCR were reflected.

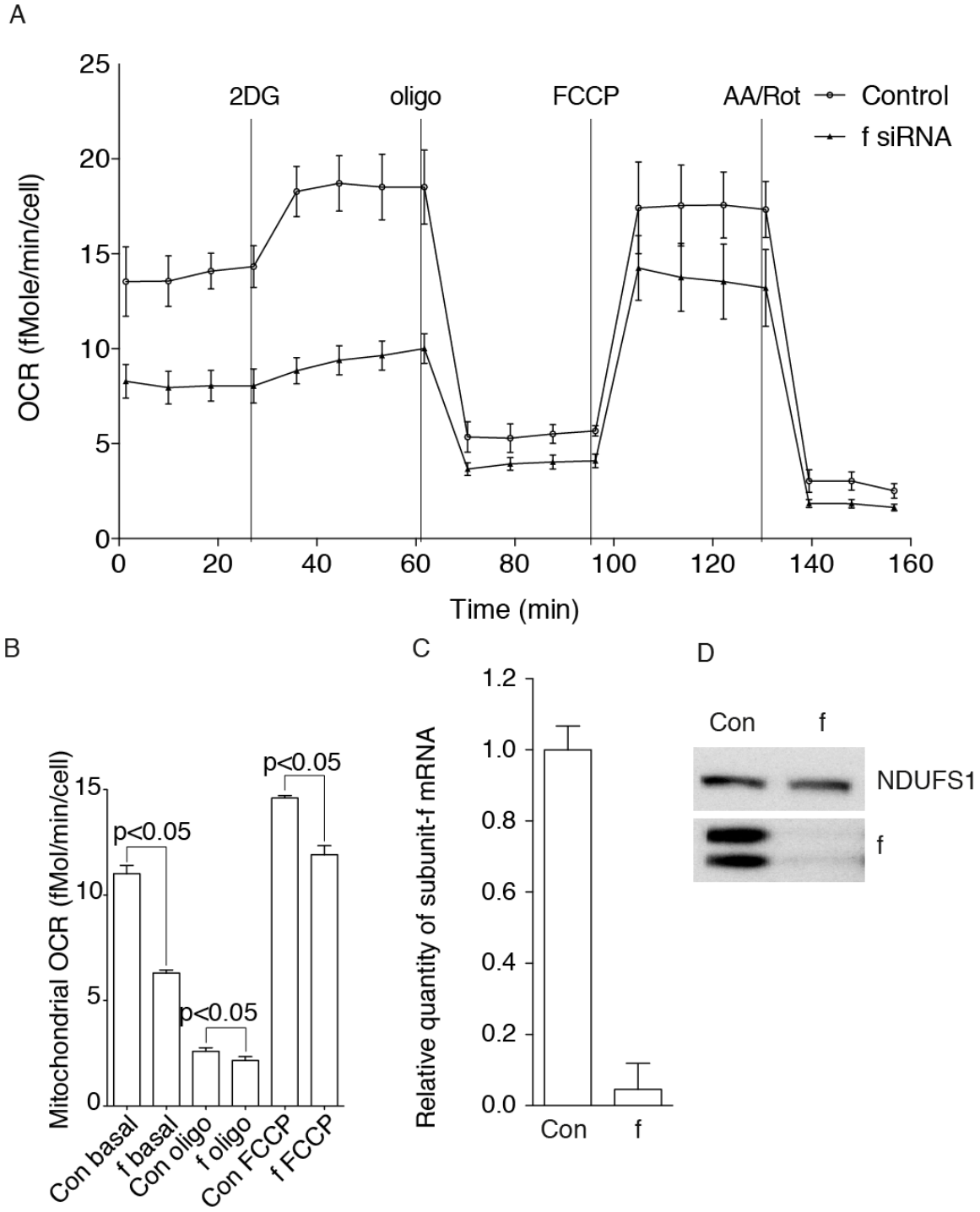

Fig. 3.12 The cellular and mitochondrial OCR in 143B cells depleted of the f-subunit of ATP synthase. In panel A, the cellular OCR of cells was measured 96 h after transfection of the cells with 90 nM siRNA. Each data point is the mean of measurements taken from five different wells, error bars are the standard deviations. In panel B, mitochondrial OCR was calculated during basal, oligomycin sensitive and accelerated respiration. The non-mitochondrial respiration (after addition ofAA/Rot) was subtracted from these data points. Details of the assay are described in the Figure legend of Fig. 3.7. The extent of the suppression of the f-subunit transcript is in panel B, normalised to cellular β-actin mRNA. Panel C shows the extent of the f-subunit protein suppression, where the complex I subunit NDUFS1 was used as a loading control.

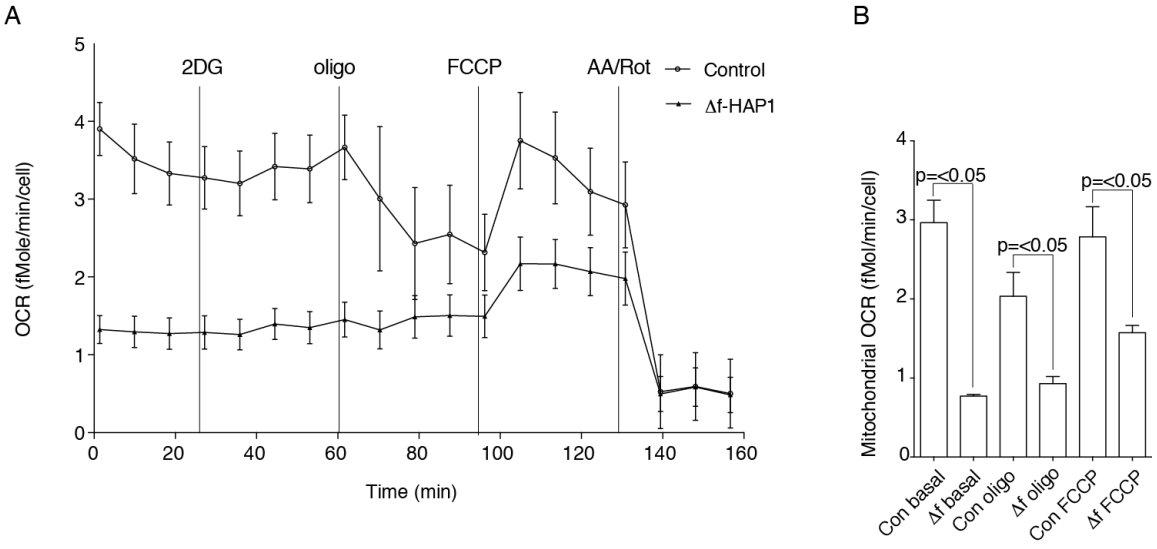

Fig. 3.13 The cellular and mitochondrial OCR in Δf-HAP1 cells. The cellular OCR of Δf-HAP1 cells is shown compared to control HAP1 cells is in panel A**.** The data points represent the mean values (n=10) +/- the standard deviation, measured at each time point. In panel B, the mitochondrial OCR was calculated by subtracting the non-mitochondrial OCR from each of the data points in panel A. Bars represent the mean of the four values in panel A that represent basal, oligomycin inhibited and accelerated and the error bars show the standard deviation. Details of the assay are described in the Figure legend of Fig. 3.7 Fig. 3.9G shows the protein level of the f-subunit in control HAP1 cells and in Δf-HAP1 cells.

BN-PAGE was used to examine the effect of suppressing or disrupting the expression of the f-subunit on the formation of native protein complexes of ATP synthase. The native state of ATP synthase in mitochondrial membranes from 143B cells treated with siRNA to deplete the f-subunit is in Fig. 3.14A. The oligomers (O) and the ATP synthase dimer (D) were diminished. Two subcomplexes accumulated, a predominant f-S1 subcomplex was observed, and also a less prevalent f-S2 subcomplex was detected. In mitochondrial membranes and mitoplasts from Δf-HAP1 cells, severe depletion of oligomers and the ATP synthase dimer was observed (Fig. 3.15A and B) and the Δf-S1 and Δf-S2 subcomplexes accumulated.

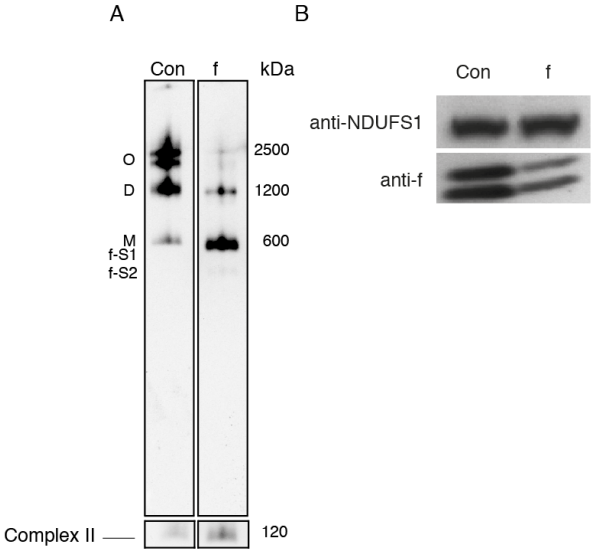

Fig. 3.14 Analysis of the native state of ATP synthase after depletion of the f-subunit. The f-subunit was depleted in 143B cells using siRNA, then mitochondrial membranes were prepared from 143B cells and were solubilised with digitonin (6g/g protein). Native protein complexes were separated by BN-PAGE and ATP synthase complexes were detected using immunoblotting with an antibody that detects the β-subunit. The f-S1 and f-S2 are subcomplexes of ATP synthase in order of decreasing size. The SDHA subunit of complex II was used as a loading control. The level of depletion of the f-subunit is in panel B, where the complex I subunit NDUFS1 was used to control for loading.

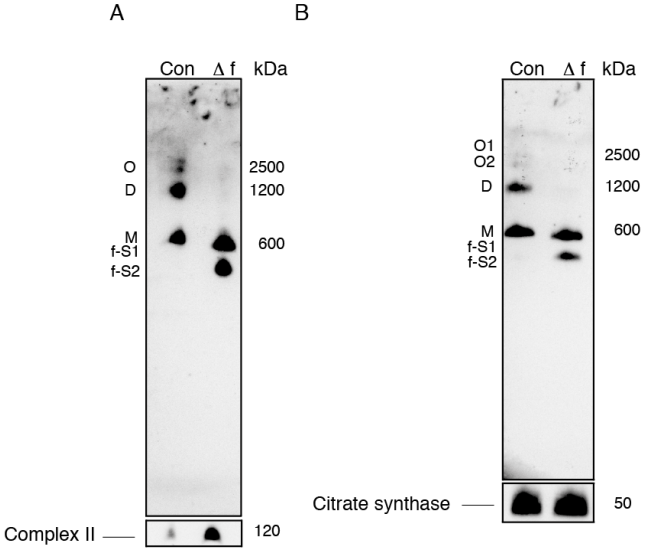

Fig. 3.15 Effect on the native state of ATP synthase from Δf-HAP1 cells. Mitochondrial membranes (A) or mitoplasts (B) were prepared and proteins solubilised with digitonin (6g/g or 9 g/g protein, respectively). Native protein complexes were separated by BN-PAGE and ATP synthase complexes were detected using immunoblotting with an antibody raised against the β-subunit. Subcomplexes of ATP synthase are labelled Δf-HAP1-S1 and Δf-HAP1-S2. An antibody that recognises citrate synthase was used as a loading control. The protein level of the f-subunit is in Fig. 3.9G.

3.5. Suppression and disruption of the expression of the g-subunit

To assess the effect of disruption of the expression of the g-subunit on the subunit composition of ATP synthase, mitoplasts were prepared from Δg-HAP1 cells and ATP synthase was immunopurified. Peptide mass mapping was used to identify the subunits (Appendix III, Table S3). All subunits were identified in the control, except IF_1. The ATP synthase from Δg-HAP1 cells lacked the band containing the g-, f- and F_6 subunits, and also all of the bands between the f-1 isoform of the f-subunit down to the band containing the ε- and c-subunits (Fig. 3.16A and B). The missing bands correspond to the bands in the control that contain the f-1 and f-2 isoforms of the f-subunit, and the g-, F_6-, e-, DAPIT-, A6L- and 6.8 kDa proteolipid-subunits. The Δg-HAP1 ATP synthase did not appear to have IF_1 associated with it. The amount of Δg-HAP1 ATP synthase was reduced compared to the control, as judged by the intensity of the bands containing the F_1 domain subunits. The peripheral stalk subunits b, OSCP, d and F_6 were also reduced, with the F_6-subunit most severely depleted. The Δg-HAP1 ATP synthase in Fig. 3.16A displayed two bands that were absent in the control and in Δg-HAP1 ATP synthase that was silver stained (Fig. 3.16B). The band that migrated to the position of the f-2-, g- and F_6-subunits in the control contained the ε-subunit (*). No ATP synthase subunits were identified in the other lower band (**), only bovine trypsin, which was used to digest proteins prior to peptide mass mapping. The protein in the band labelled ** may not contain any lysine or arginine residues that would allow mass spectrometric identification of tryptic peptides, and may represent a contaminant because approximately 30x more sample was loaded onto the gel in Fig. 3.16A than in Fig. 3.16B, where the bands were not visible.

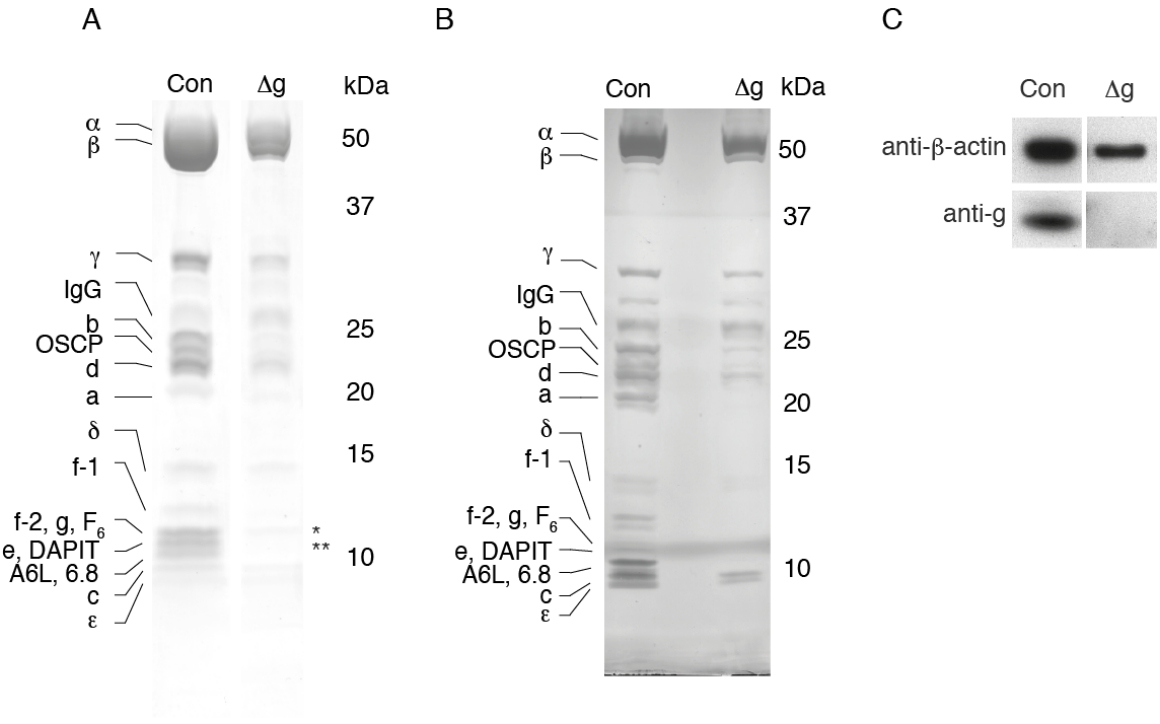

Fig. 3.16. Analysis by SDS-PAGE of residual ATP synthase complexes from Δg-HAP1 cells. Mitoplasts were prepared and solubilised with digitonin (13.4g/g protein), followed by immunopurification of ATP synthase. Proteins were stained with either Coomassie blue dye in panel A, or by silver staining in panel B. Subunits of the ATP synthase identified by peptide mass mapping are designated on the left-hand side of the gels. The efficiency of disruption of expression of the g-subunit protein is in panel C, where citrate synthase was used as a loading control. The bands marked * and ** in the residual Δg-HAP1 ATP synthase complex contained the δ-subunit and bovine trypsin, respectively. The c-subunit and ε-subunit were not identified automatically with the MASCOT search engine.

The subunit composition of immunopurified ATP synthase with suppression and disruption of expression of the g-subunit was also investigated by SILAC labelling and quantitative mass spectrometry. After depletion of the g-subunit with 90 nM siRNA for 96 h, a three-fold relative depletion in the g-subunit was obtained. Other subunits which were decreased by a similar level were the e-subunit and both isoforms of the f-subunit (Fig. 3.17A and B). Proteins that displayed a two-fold relative decrease in association with ATP synthase were the DAPIT-, 6.8 kDa proteolipid-, and a-subunits. The A6L-subunit was 1.5-fold decreased. IF1-M1 and IF1-M2 (Appendix V, Fig. S22) increased their association with ATP synthase by four and three-fold, respectively. The IF_1-M1 and IF_1-M2 mature forms,

correspond to the IF_1 protein with N-termini of Phe25 or Gly26, respectively. In an equivalent experiment, which analyses the mitochondrial proteome, the F_1 domain subunits (α, β, γ, and δ) were unchanged, except the ε-subunit, which decreased by 1.5-fold (Fig. 3.17C and D). The protein ratios used to create Figs. 3.17 and 3.18 are in Appendix IV, Tables S11-S15. The peptide data used to manually calculate the IF_1-M1 and IF_1-M2 protein ratios is in Appendix IV Table S23.

The peripheral stalk subunits b, d, and F_6 displayed a decrease in association with ATP synthase. The f-1 isoform of the f-subunit was three-fold decreased. The a-subunit was decreased to a similar extent in mitoplasts as in immunopurified ATP synthase, indicating that it was turned over in g-subunit depleted ATP synthase. Both IF_1-M1 and IF_1-M2 remained unchanged in mitoplasts, suggesting that the total amount of IF_1 in mitochondria did not increase when IF_1 bound to ATP synthase in g-subunit depleted ATP synthase.

The subunit composition of ATP synthase from Δg-HAP1 cells (Fig. 3.18A and B) was analysed as described for the siRNA mediated suppression of the expression of the g-subunit (Fig. 3.17). In immunopurified ATP synthase, the g-subunit was identified, despite evidence that the gene encoding the g-subunit had been disrupted to the extent of losing part of the DNA encoding for the 5' cap of the mRNA, the initiator methionine codon and twelve amino acids at the N-terminus (Fig. 3.4). The g-subunit displayed a relative decrease of approximately 5-fold. Immunopurified Δg-HAP1 ATP synthase displayed a 90-fold depletion in the f-1 isoform of the f-subunit. The F_1 subunits were 3-fold depleted, the peripheral stalk subunits were 6-fold depleted and the a-, A6L- and DAPIT-subunits were depleted by 5.5-fold. The e- subunit was not significantly changed, with a 4-fold decrease, but ranging between 1.5 to -22.6. The IF_1-M1 isoform was unchanged.

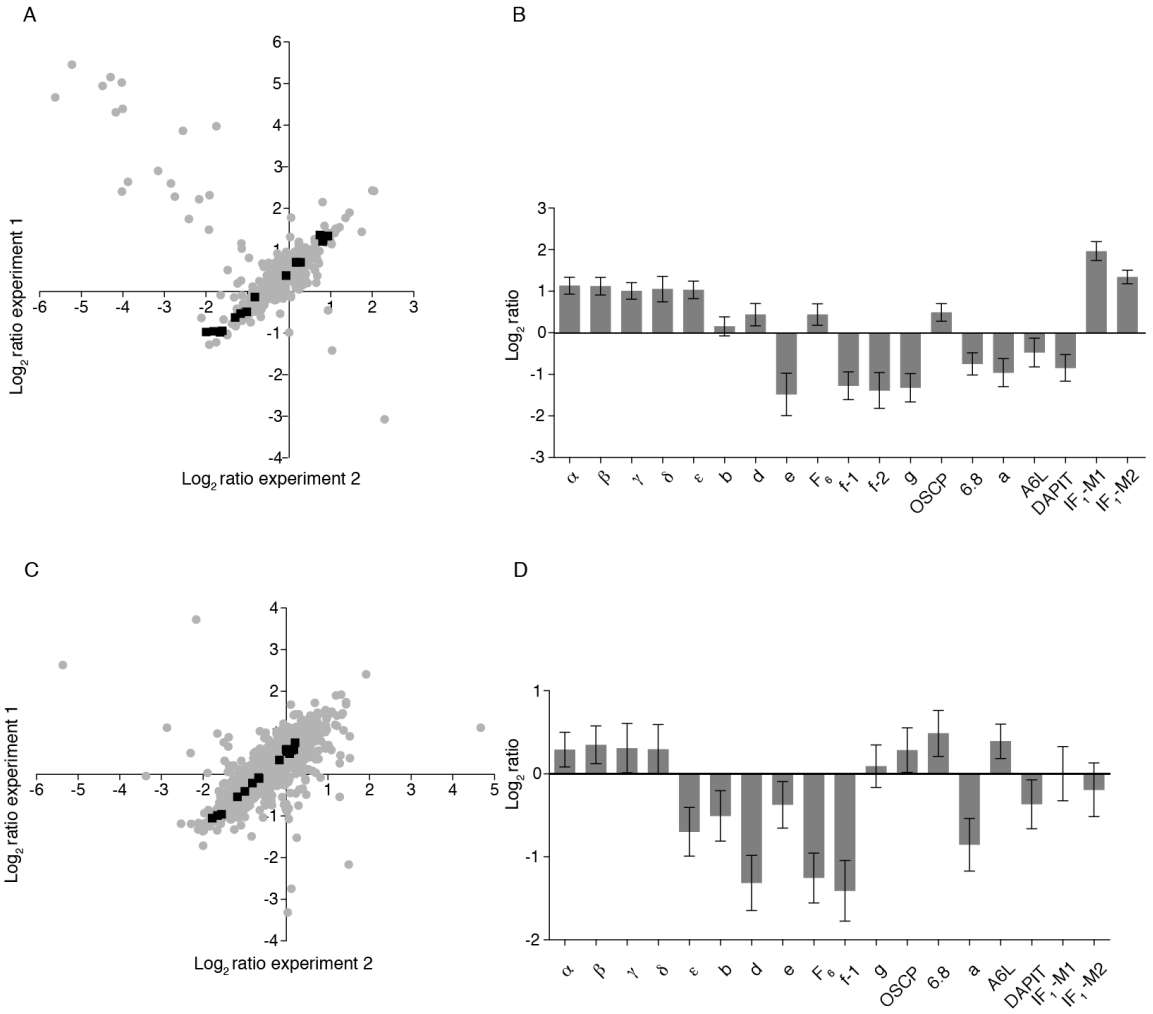

Fig 3.17 Relative quantitative mass spectrometric analysis of ATP synthase in g-subunit depleted cells. Mitoplasts were prepared and solubilised with digitonin (13.4g/g mitoplast protein). In panel A, ATP synthase was immunopurified and subunits separated by SDS-PAGE followed by quantitative mass spectrometry. In panel B, a summary of the ratios for ATP synthase subunits in panel A is presented. In panel C, mitoplast material was analysed as described in panel A. In panel D, a summary of the data points for ATP synthase in panel C is shown. The IF_1-M1 and IF_1-M2 isoforms were not identified automatically in neither immunopurified ATP synthase or mitoplast material because there were two or less unique peptide ratios present in one or both experiments. The protein ratios for the two IF_1 isoforms were calculated manually from the peptide ratios calculated by MaxQuant.

In Δg-HAP1 mitoplasts (Fig. 3.18C and D), the g-subunit was decreased 16-fold, and the f-subunit isoform 1, 6.8 kDa proteolipid- and a-subunits were decreased 45-, 16- and 11-fold, respectively. The e- and DAPIT-subunits were both decreased 5.5-fold. The F_1 subunits and peripheral stalk subunits were decreased by approximately 3- and 8-fold. The IF_1-M1 isoform was decreased by approximately 1.5-fold. The changes in the F_1 domain subunits were statistically insignificant, as was the change in IF_1-M1 in mitoplasts.

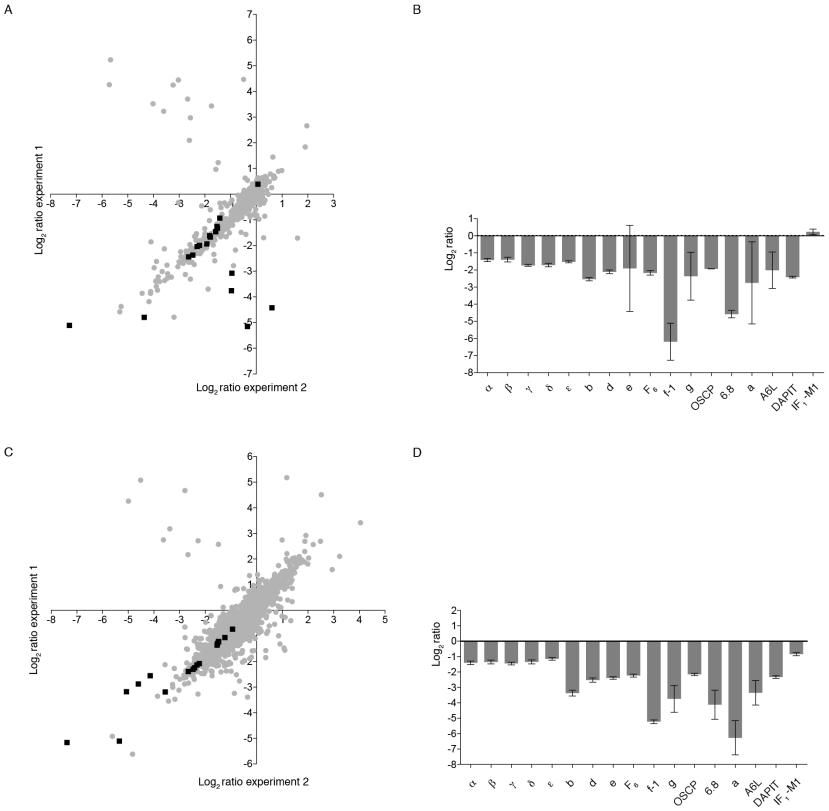

Fig. 3.18. Relative quantitative mass spectrometric analysis of ATP synthase subunits from Δg-HAP1 mitoplasts. Panels A and B show relative quantification of proteins from immunopurified ATP synthase from mitoplasts solubilised with digitonin (13.4g/g protein). In panel C, solubilised mitoplasts that had been ethanol precipitated were analysed, and the ATP synthase protein ratios are summarised in panel D. Appendix IV Tables S14 and S15 contain the protein ratios of all identified subunits used in this Figure.

To assess the effect on the respiratory capacity of Δg-HAP1 cells, the cellular OCR was measured after the addition of respiratory modulators 2DG, oligomycin A, FCCP, antimycin A with rotenone (Fig 3.19A). A significant decrease in the cellular OCR was

observed in Δg-HAP1 cells throughout the assay (during basal, glycolysis inhibited, oligomycin sensitive, and accelerated respiration) albeit with the oligomycin sensitive OCR exhibiting a smaller, but significant decrease compared to the larger differences at the other points during the assay. There appeared to be no ATP-linked respiration in Δg-HAP1 cells, as there was no difference between the basal OCR and the OCR after oligomycin was added.

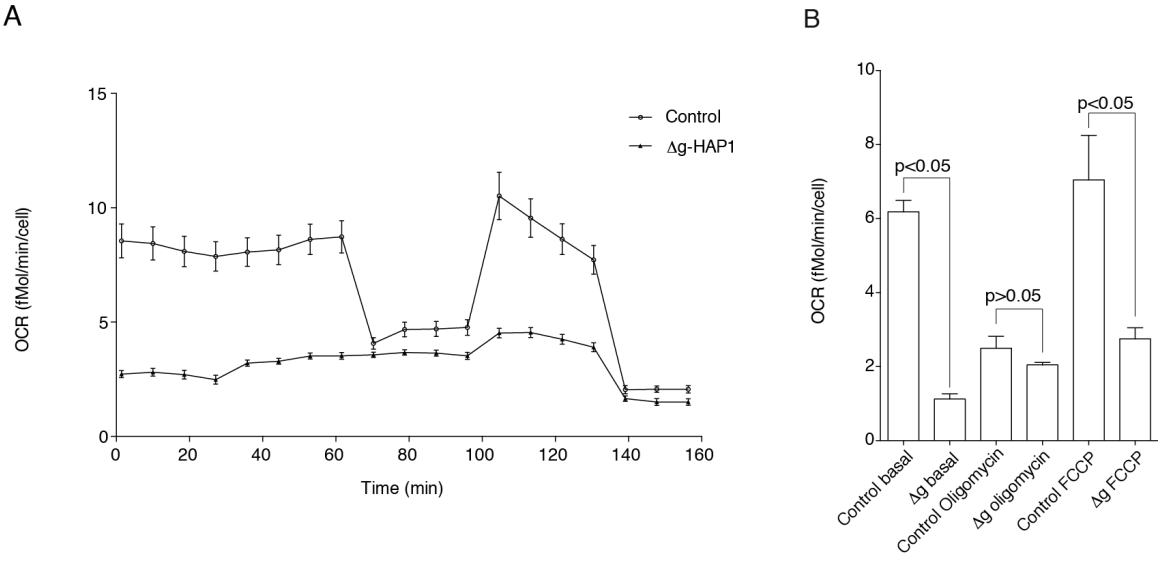

Fig. 3.19 The OCR of HAP1 cells with disruption of the gene encoding the g-subunit. The OCR of Δg-HAP1 cells, which lack the g-subunit is compared to control cells. In panel A, the cellular OCR was measured after the additions of respiratory modulators. Data points represent the mean values (n=10) +/- the standard deviations. In panel B, the mitochondrial OCR is displayed as bars showing the mean of the four data points in panel A that represent basal, ATP synthase inhibited (oligo) and accelerated (FCCP) respiration. The error bars show the standard deviations of the four data points used to generate the bars. Significance values were calculated with a paired Student's t-test. The disruption of expression of the g-subunit is in Fig. 3.16C. Full details of the assay are in the Figure legend of Fig. 3.7.

The mitochondrial OCR (Fig. 3.19B) was calculated by subtracting the average non-mitochondrial OCR from each of the data points in Fig. 3.19A. The mitochondrial OCR of Δg-HAP1 cells was significantly lower than the mitochondrial OCR of control cells during basal, oligomycin sensitive and accelerated respiration, suggesting that ATP synthase from Δg-HAP1 cells is not active and that there is also a respiratory chain defect, because the

mitochondria did not display an increase in their OCR after the protonophore FCCP was added.

The oligomerisation state of the ATP synthase with suppression or disruption of the expression of the g-subunit was investigated by BN-PAGE. In siRNA treated mitochondrial membranes, oligomers (O) and the ATP synthase dimer were depleted and subcomplexes g-S1 and g-S2 accumulated (Fig. 3.20A). Monomeric ATP synthase was not significantly affected.

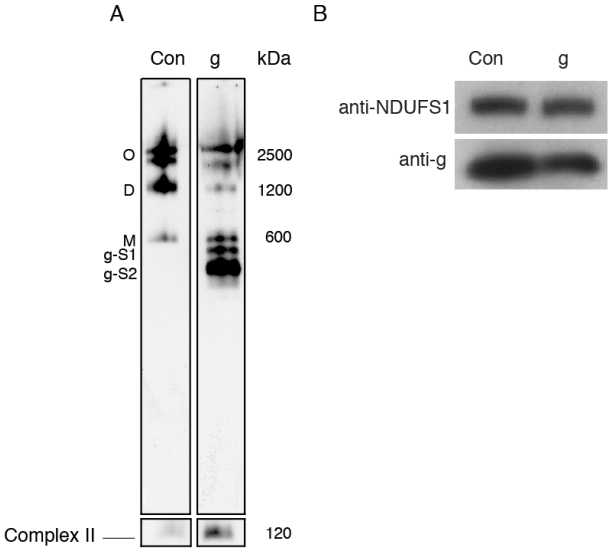

Fig. 3.20 Analysis of the native state of ATP synthase after depletion of the g-subunit. Mitochondrial membranes were solubilised with digitonin (6g/g). Subcomplexes of ATP synthase are labelled g-S1 and g-S2 in order of decreasing size. The SDHA subunit of complex II was used as a loading control. The extent of the depletion of the g-subunit is in panel B, and the NDUFS1 subunit of complex I was used to control for loading.

However, when the gene encoding the g-subunit was disrupted, ATP synthase oligomers, dimers the monomer were not detected in mitochondrial membranes, and two sub-complexes were observed, denoted Δg-HAP1-S1 and Δg-HAP1-S2 in Fig. 3.21A. However, when mitoplasts were prepared from the same batch of cells, only one subcomplex was observed (Δg-HAP1-S1(mp). There were also no signs of ATP synthase

oligomers or dimers as was the case in Fig. 3.21A, but there was a small amount of ATP synthase complex detected at the same position as the control ATP synthase monomer.

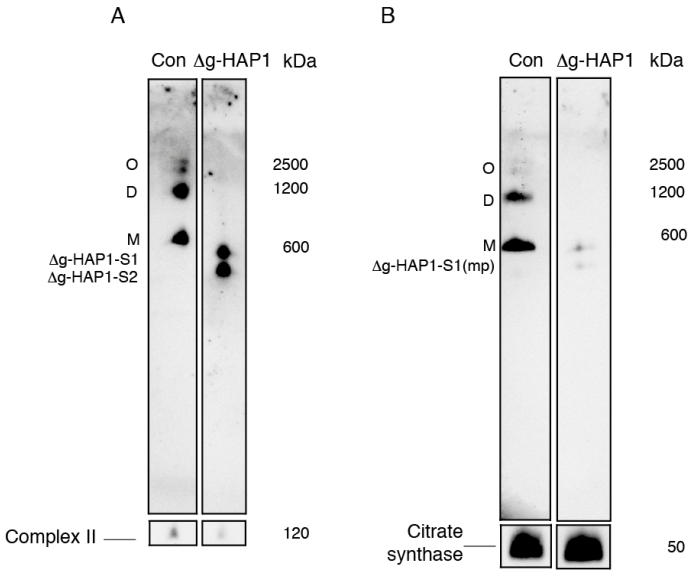

Fig. 3.21 The effect on the native state of ATP synthase in Δg-HAP1 cells. Mitochondrial membranes (A) or mitoplasts (B) were prepared from Δg-HAP1 cells and proteins were solubilised with digitonin (6g/g or 9 g/g protein, respectively). Native protein complexes were analysed by BN-PAGE and immunoblotting to detect the β-subunit of ATP synthase. Subcomplexes of ATP synthase are labelled Δg-HAP1-S1 and Δg-HAP1-S2. The level of the g-subunit protein is in 3.16C.

3.6. Suppression of the expression of the DAPIT-subunit

The subunit composition of residual ATP synthase after suppressing the DAPIT-subunit with siRNA was investigated. In DAPIT-subunit depleted ATP synthase, the profile of all ATP synthase subunits was identical to the control, apart from the band which contains the DAPIT-subunit, which stained less intensely, (Fig. 3.22A and B). The extent of suppression of the DAPIT-subunit protein and transcript is in Fig. 3.22C and D, respectively. Peptide mass mapping was used to identify the subunits labelled in Fig. 3.22A and B, and the peptide data is in Appendix III, Table S1.

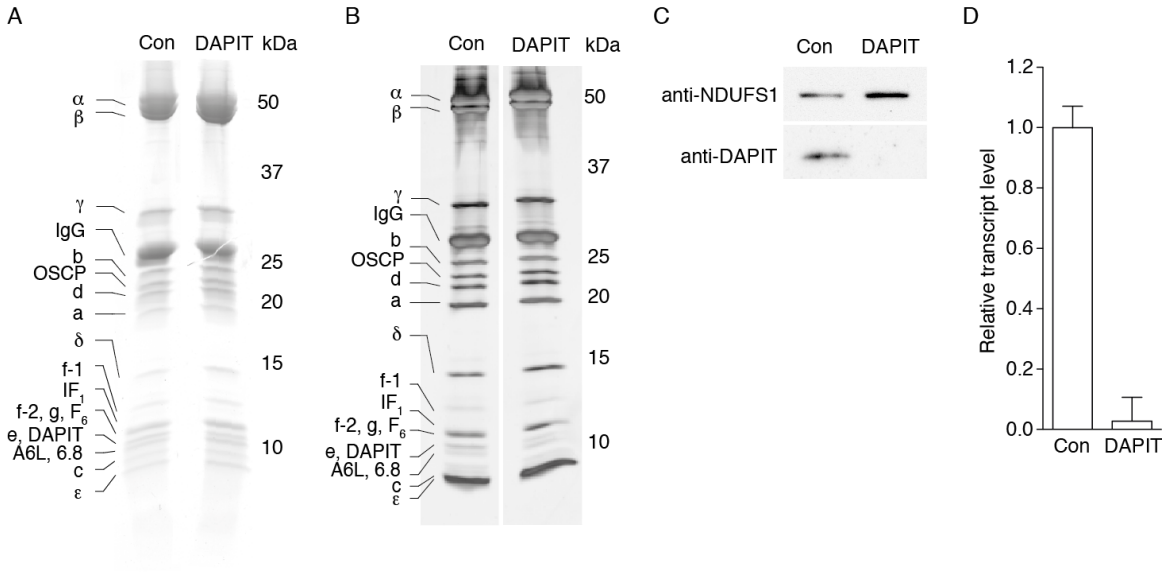

Fig. 3.22 Analysis by SDS-PAGE of residual ATP synthase complexes from 143B cells where the expression of the DAPIT-subunit had been suppressed with RNAi molecules. Cells were treated with 90 nM siRNA for 96 h and then mitoplasts were prepared, and solubilised with digitonin (13.4g/g) followed by immunopurification of ATP synthase. Proteins were visualised with either Coomassie blue dye in panel A, or by silver staining in panel B. ATP synthase subunits were identified by peptide mass mapping and are indicated to the left of the gels. The degree of the suppression of the DAPIT-subunit protein is in panel C, where the loading control was the complex I subunit NDUFS1. The DAPIT-subunit transcript level was normalised to cellular β-actin transcripts after treatment with siRNA for 48 h is shown in panel D.

The quantitative mass spectrometry data in Fig.3.23A and B is consistent with the profile of immunopurified ATP synthase in Fig. 3.22A and B. The DAPIT-subunit was three-fold decreased ($-\text{Log}_2$ 1.5=3), and the effect on the ATP synthase complex was negligible. All of the subunits of ATP synthase remained unchanged after the DAPIT-subunit was depleted, and IF_1 did not display any change in association with the enzyme. This result was reflected in the mitochondrial proteome, which is shown in Fig. 3.23C and D, where again, the only subunit of ATP synthase that was changed was the DAPIT-subunit. However, the IF_1-M1 protein increased four-fold in mitoplasts, and IF_1-M2 was 1.5-fold increased. However, the protein ratios from mitoplast IF_1-M1 and IF_1-M2 isoforms (for their sequences, see Appendix V, Fig. S22) were calculated manually from the available peptide ratios. There were less than two unique peptides in one or both experiments, the

protein ratios could not be automatically calculated. This may have increased the median range as less peptide ratios were used to calculate these ratios than the minimum number of peptides required by the MaxQuant algorithm used to identify peptide pairs and calculate protein ratios. The protein ratios of the proteins identified in Fig. 3.23 are listed in Appendix IV, Tables S16 and S17.

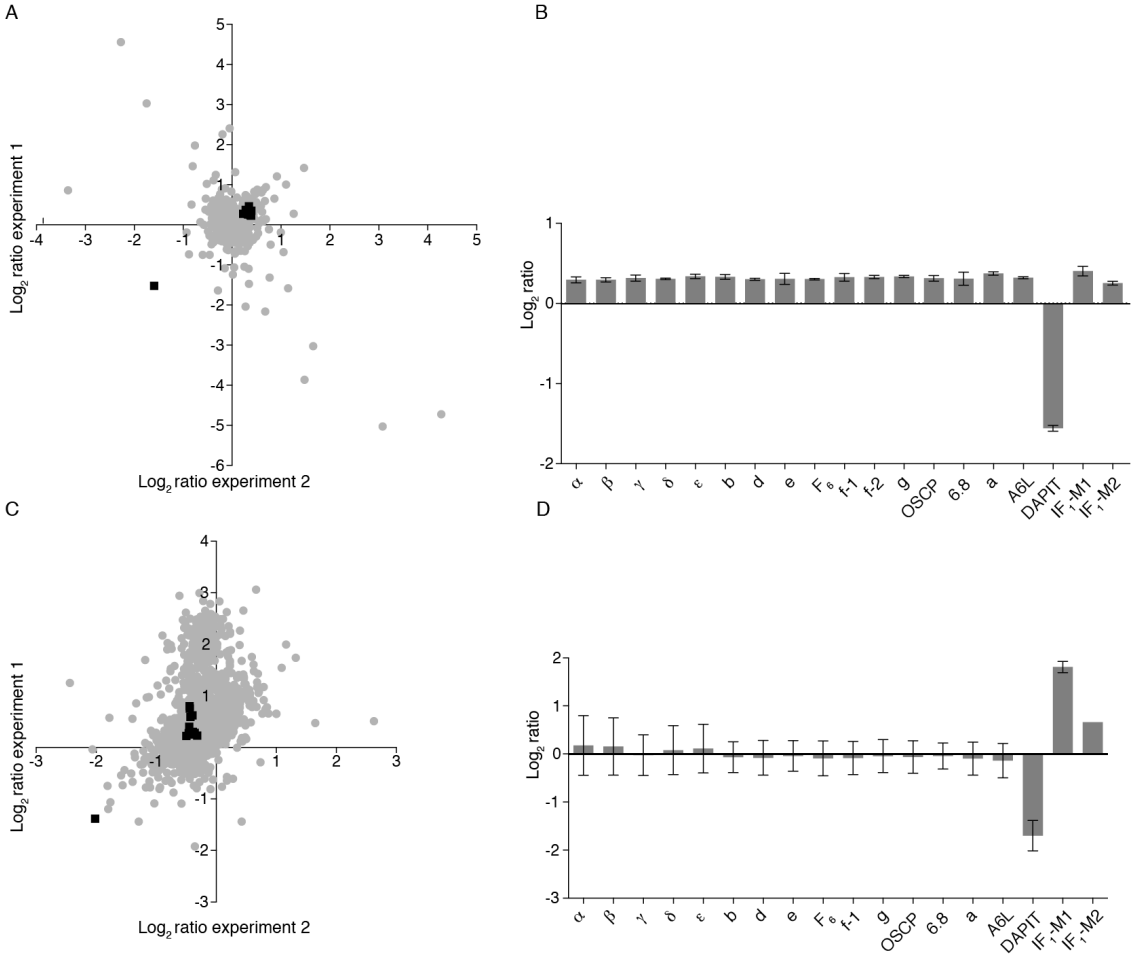

Fig 3.23 Relative quantitative mass spectrometric analysis of ATP synthase with suppression of the DAPIT-subunit with siRNA. Proteins were labelled by SILAC in 143B cells. Mitoplasts were prepared and solubilised with digitonin (13.4g/g protein). In panel A, the subunits of immunopurified ATP synthase subunits were separated by SDS-PAGE followed by quantitative mass spectrometry. In panel B, the data points for ATP synthase in panel A are summarised. In panel C, the mitoplast proteome was analysed as in panel A. In panel D, the data points for ATP synthase in panel C are summarised. The bars show the median relative ratios from both experiments and the error bars represent the range of the ratios.

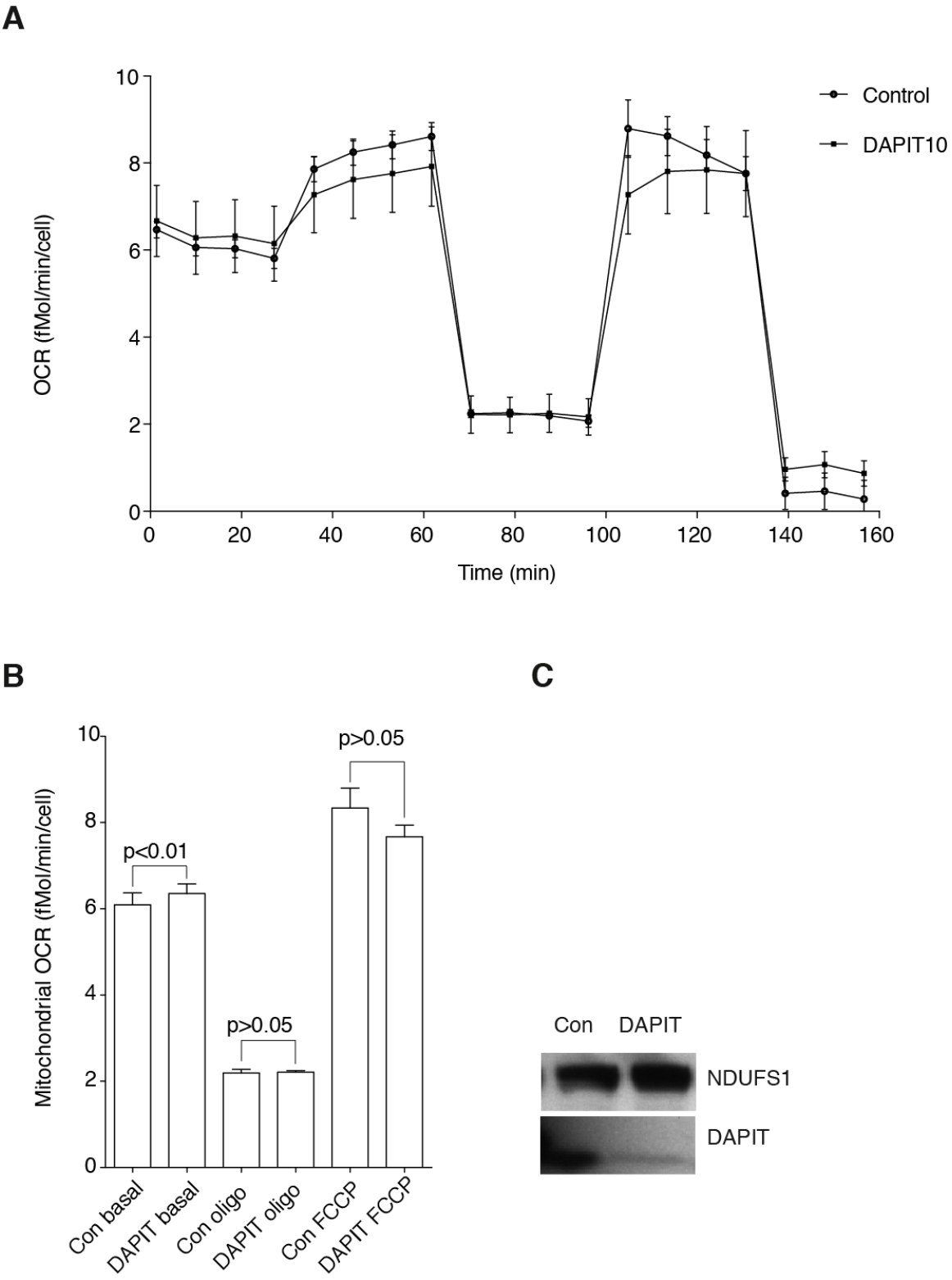

Fig. 3.24 The mitochondrial OCR of 143B cells depleted of the DAPIT-subunit was measured. The OCR of 143B cells was measured 96 h after transfection of the cells with 90 nM siRNA and is displayed in panel A. The mitochondrial OCR is in panel B and was calculated by subtracting non-mitochondrial respiration from the data points in panel A, then the mean of these four data points that represent each respiratory state was used to generate the bars. The error bars are the standard deviations between the four data points. A paired Students' t-test was used to calculate statistical significance. The level of suppression of the DAPIT-subunit protein is in panel B. NDUSF1 was used as a loading control. Details of the assay are described in the Figure legend of Fig. 3.7.

The cellular OCR of 143B cells where the expression of the DAPIT-subunit had been suppressed (Fig. 3.24A) was investigated. The suppression of the DAPIT-subunit does not result in any significant defects in cellular OCR during basal respiration, glycolysis inhibited respiration, oligomycin inhibited respiration, nor during FCCP mediated accelerated respiration (Fig. 3.24A). The mitochondrial OCR of DAPIT-depleted cells (Fig. 3.24B) was calculated and the result showed no significant decrease during basal and oligomycin sensitive respiration, however, a small but statistically significant difference was reported during accelerated respiration. The extent of the suppression of the DAPIT-subunit protein is presented in Fig. 3.24C.

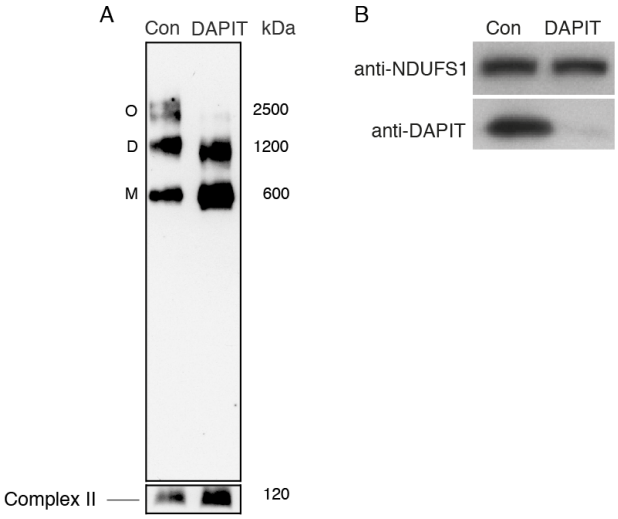

Fig. 3.25 Analysis of the native state of ATP synthase after depletion of the DAPIT-subunit using siRNA molecules. Mitochondrial membranes solubilised with digitonin (6g/g protein) were analysed by BN-PAGE to investigate the oligomeric state of ATP synthase. Native ATP synthase complexes were detected using an antibody that detects the β-subunit of ATP synthase. SDHA was used as a loading control. The efficiency of the siRNA to suppress the expression of the DAPIT-subunit protein is in panel B. The complex I subunit NDUFS1 was used as a loading control.

The effect of suppressing the DAPIT-subunit on the native ATP synthase complex was investigated by BN-PAGE (Fig. 3.25A). Oligomers of ATP synthase (O) were reduced in subunit-DAPIT depleted mitochondrial membranes.

A band near to the control ATP synthase dimer migrated further in the DAPIT-depleted sample and the band containing monomeric ATP synthase appeared unchanged, when loading was controlled for.

3.7. Suppression of expression of the 6.8 kDa proteolipid-subunit

The role of the 6.8 kDa proteolipid-subunit in maintaining the subunit composition of the ATP synthase was investigated by siRNA (Fig. 3.26A and B).

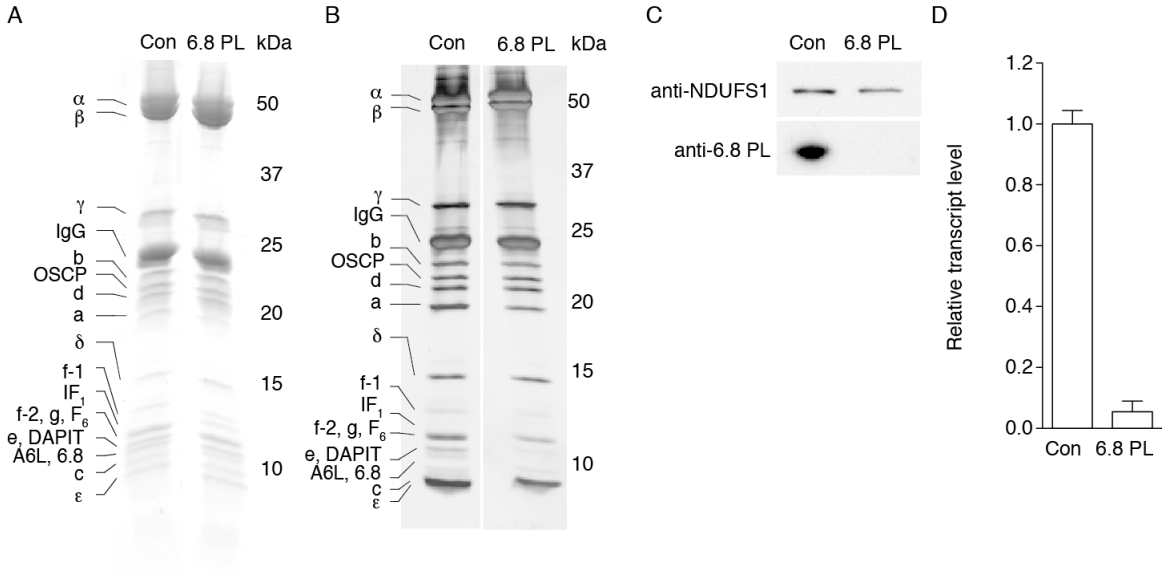

Fig. 3.26 Analysis by SDS-PAGE of residual ATP synthase complexes from 143B cells where the expression of the 6.8 kDa proteolipid-subunit had been suppressed using siRNA. Cells were treated with 90 nM siRNA for 96 h and then mitoplasts were prepared, followed by immunopurification of ATP synthase. Immunopurified proteins were detected with either Coomassie blue dye in panel A, or by silver staining in panel B. The identities of immunopurified proteins were identified by peptide mass mapping are shown to the left of the gels. The level of suppression of the expression of the 6.8 kDa proteolipid-subunit protein is in panel C, where the complex I subunit NDUFS1 was used as a loading control. The 6.8 kDa proteolipid-subunit transcript level 48 h after transfection, and normalised to cellular β-actin mRNA is in panel D.

The subunits that remained unchanged in immunopurified ATP synthase from 6.8 kDa proteolipid-subunit depleted cells were the F_1 domain subunits, the peripheral stalk subunits and all of the F_O subunits, except for bands containing the a-, A6L- and 6.8 kDa proteolipid-subunits, which co-migrate (Fig. 3.26A and B). The extent of the suppression of the expression of the 6.8 kDa proteolipid subunit protein and transcript is presented in Fig. 3.26C and D, respectively. Proteins were identified by peptide mass mapping (Appendix III, Table S1).

In order to determine the relative abundance of ATP synthase subunits in cells depleted of the 6.8 kDa proteolipid-subunit, SILAC assisted mass spectrometry was performed with immunopurified ATP synthase (Fig. 3.27A and B). A two-fold depletion of the 6.8 kDa proteolipid-subunit was achieved. The other subunits that were also decreased by approximately two-fold were the a- A6L- and DAPIT-subunits. The A6L-subunit was only identified in experiment 2 and was depleted two-fold. IF_1-M1 showed a two-fold increase in association with ATP synthase. The F_1 domain and the b-, d- and F_6-subunits were relatively unchanged. These changes were reflected when the mitochondrial proteome was investigated, with the exception of IF_1-M1, which displayed a 1.5-fold increase in mitoplasts (Fig. 3.27C and D). In immunopurified ATP synthase, the protein ratios for 6.8 kDa proteolipid and A6L were not identified automatically, and were instead calculated manually from the available peptide ratios. See Appendix V Fig. S22 for the sequences of the IF_1 isoforms and Appendix IV Tables S24 and S25 for protein ratios that were calculated from peptide evidence. Additionally, in mitoplasts the protein ratios for the ε-subunit were obtained in experiment 2 only. The protein ratio for the IF_1-M1 and IF_1-M2 isoforms, and the A6L-subunit were manually calculated from peptide ratios. IF_1-M2 was

relatively unchanged in mitoplasts, suggesting that the total amount of IF_1-M2 in mitochondria did not change when the expression of the 6.8 kDa proteolipid-subunit was

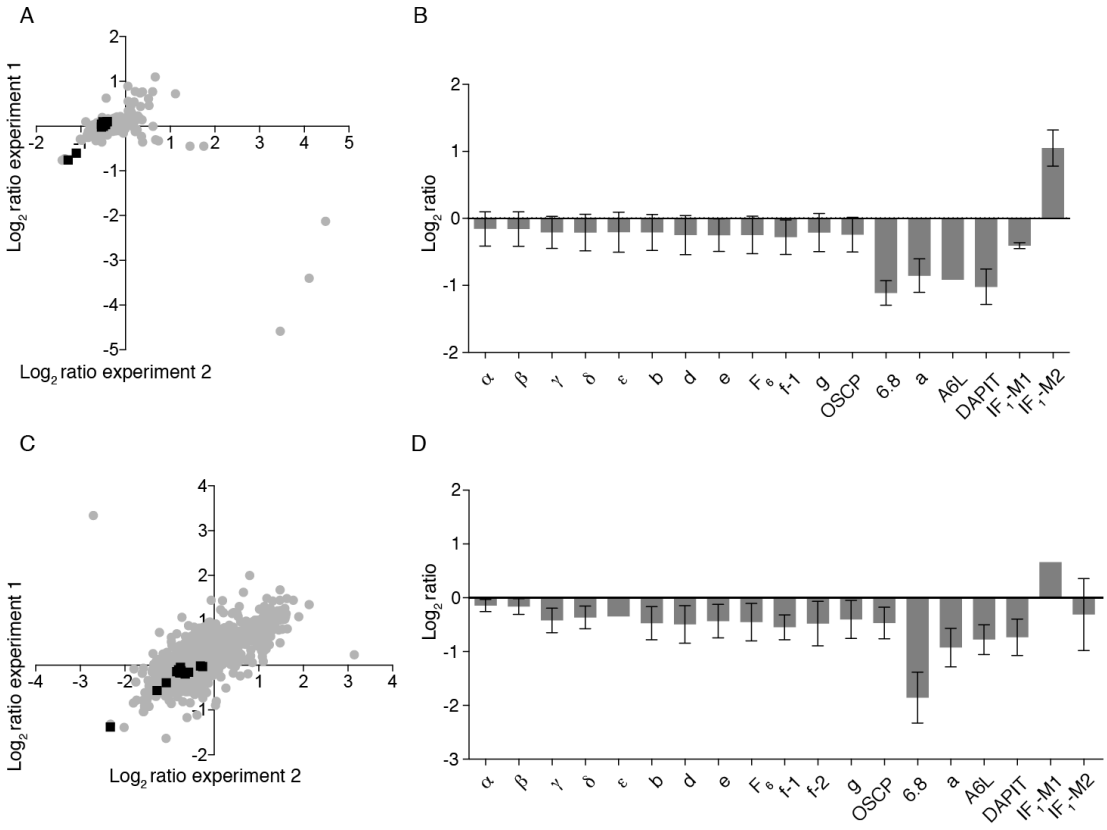

Fig 3.27 Relative quantitative mass spectrometric analysis of ATP synthase subunit composition from cells with suppression of the 6.8 kDa proteolipid subunit. Subunits were labelled by SILAC in control cells and in cells where the 6.8 kDa proteolipid-subunit had been depleted from ATP synthase. Mitoplasts were solubilised with digitonin (13.4g/g protein). In panel A**,** ATP synthase was immunopurified and the subunits were separated by SDS-PAGE followed by quantitative mass spectrometry. In panel B**,** the data points for ATP synthase in panel A are summarised. In panel C**,** solubilised mitoplast material was ethanol precipitated, proteins separated by SDS-PAGE and analysed as in panel A. In panel D**,** the protein ratios for ATP synthase shown in panel C are summarised.

suppressed. The proteins identified in this experiment and their ratios are listed in Appendix IV, Tables S18-S21.

The cellular OCR of 143B cells with suppression of 6.8 kDa proteolipid-subunit was measured (Fig. 3.28A). There were no significant differences in the cellular OCR of cells

depleted of the 6.8 kDa proteolipid subunit during basal, glycolysis inhibited, oligomycin sensitive or accelerated respiration. However, when the mitochondrial OCR was calculated

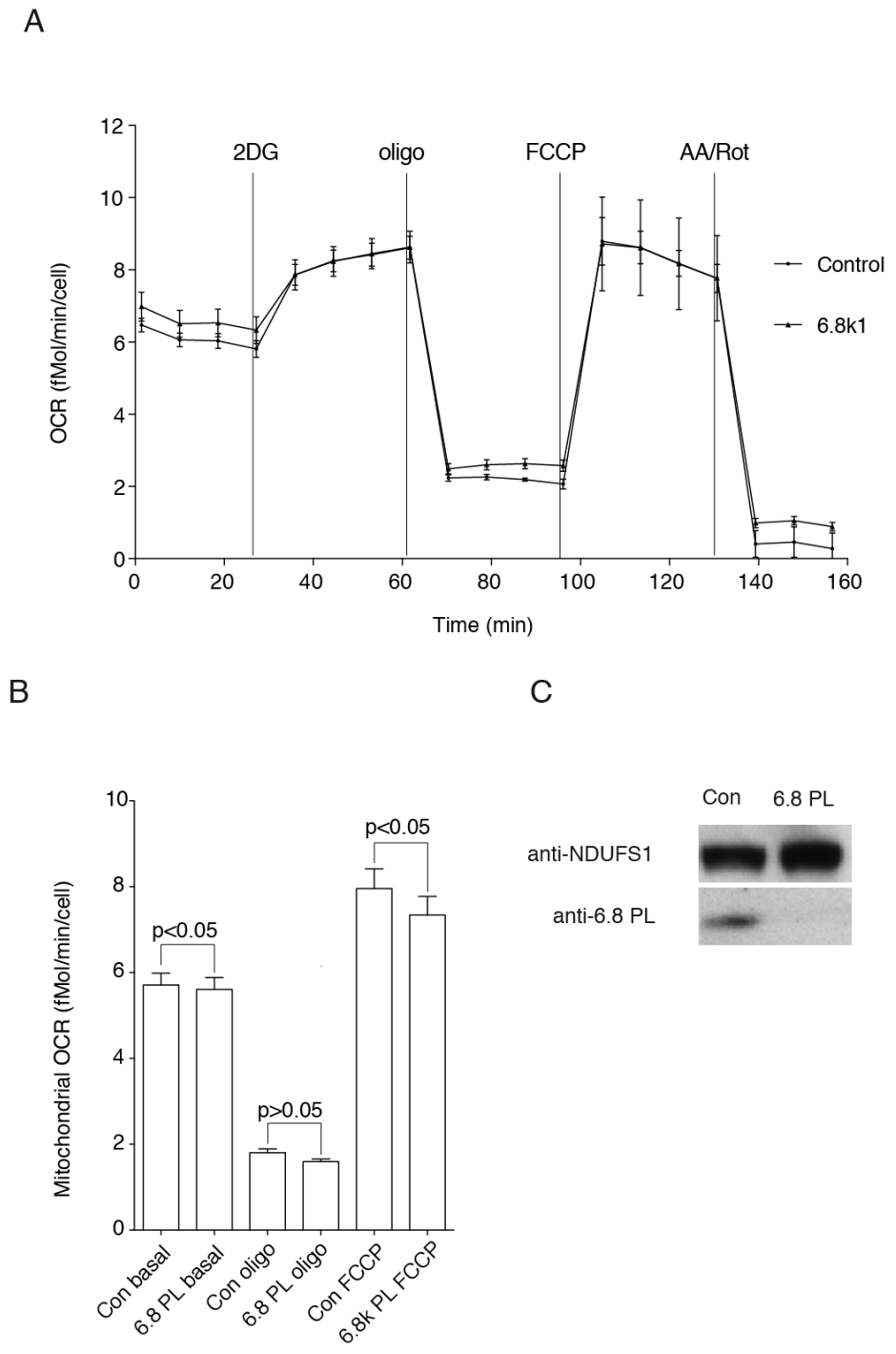

Fig. 3.28 The mitochondrial oxygen consumption of 143B cells depleted of the 6.8 kDa proteolipid-subunit of ATP synthase. In panel A, OCR of cells was measured 96 h after transfection of the cells with 90 nM siRNA. Points are the mean values of measurements taken from ten different wells at different time points and error bars represent the standard deviations of the values. In panel B, the mitochondrial OCR was calculated by subtracting the non-mitochondrial OCR from the data points displayed in panel A. The efficiency of the siRNA mediated suppression of the 6.8 kDa proteolipid-subunit protein is in panel C. Details of the assay are described in the Figure legend of Fig. 3.7.

(Fig. 3.28B), a small but statistically significant decrease was observed during basal and accelerated respiration. A difference in ATP-linked respiration was not observed between the control cells and the 6.8 kDa proteolipid-subunit depleted cells, suggesting no defect in the activity of ATP synthase with suppression of this subunit. The extent of the depletion of the 6.8 kDa proteolipid-subunit protein in this experiment is in Fig. 3.28C.

The effect on oligomerisation of ATP synthase was investigated by BN-PAGE after depletion of the 6.8 kDa proteolipid subunit with siRNA (Fig. 3.29A). Oligomers (O) were diminished in 6.8 kDa proteolipid-subunit depleted cells. There was also less dimeric ATP synthase (D) than in the control, and the 6.8-S1 and 6.8-S2 subcomplexes accumulated. The level of 6.8 kDa proteolipid depletion is presented in Fig. 3.29B.

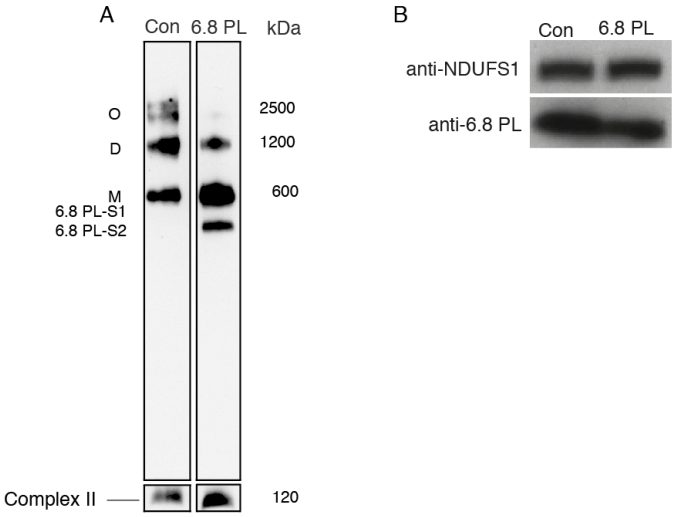

Fig. 3.29 Analysis of the native state of ATP synthase after depletion of the 6.8 kDa proteolipid-subunit using RNAi. Mitochondrial membranes were prepared from 143B cells treated with 90 nM siRNA for 96 h to suppress the expression of the 6.8 kDa proteolipid subunit. Native protein complexes were solubilised with digitonin (6g/g protein) and separated by BN-PAGE. ATP synthase complexes were detected using an antibody that detects the β-subunit. The SDHA subunit of complex II was used as a loading control. The efficiency of the siRNA to suppress the expression of the 6.8 kDa proteolipid-subunit is in panel B and the complex I subunit NDUFS1 was used as a loading control.

4. Discussion

4.1. The pathways of assembly of mitochondrial ATP synthases

A proposed pathway for the assembly of yeast mitochondrial ATP synthase is shown in Fig. 4.1. In yeast, the F_1 catalytic domain, consisting of the α- and catalytic β-subunits, is assembled via a pathway involving the assembly factors Atp11p and Atp12p [75]. These assembly factors have homologues in humans (ATPAF1 and ATPAF2), which function analogously [68]. The α- and β-subunits associate with the central stalk (the γ-, δ- and ε-subunits), and this sub-assembly is thought to induce the expression of the mitochondrially encoded ATP6 and ATP8 (the a- and A6L-subunits in mammalian ATP synthases, respectively) [120]. There is no known assembly factor for the incorporation of the central stalk into the $\alpha_3\beta_3$ assembly in yeast or humans. In yeast, the assembly factor Atp25p assists in the formation of the c_{10}-ring, and the F_1 subassembly ($\alpha_3\beta_3\gamma\delta\varepsilon$) docks onto this ring [142], but there is no known assembly factor for the c_8-ring of human ATP synthase. The A6L-subunit is then incorporated, followed by the pre-assembled peripheral stalk (subunits OSCP, b, d and F_6) [120, 143, 144]. The a-subunit is incorporated by the assembly factors Atp10p and Atp23p, followed by the dimerisation specific subunits e, g and k [144]. There is currently no information available about the requirement of assembly factors for, or order of the insertion of, the supernumerary e-, f-, g-, k-, or j-subunits. Yeast ATP synthase lacks the DAPIT- and 6.8 kDa proteolipid-subunits [145]. In yeast, the INA complex (INAC) has been identified as an assembly factor for the assembly of the peripheral stalk, linking F_1 with F_O [146, 147], but evidence for the INAC in humans has not yet been found. It has been suggested that the INAC interacts directly with subunits-b, -OSCP and -d of ATP synthase. The loss of the INAC results in the uncoupling of F_1 from F_O and subsequent futile ATP hydrolysis [146]. The c-subunit in yeast is encoded on the mitochondrial genome, and assembles into a ring with ten subunits [102], whereas in mammals, the c-subunit is encoded on the nuclear genome, requiring import into the IMM, where it forms

the c_8-ring [5]. These differences point to an intrinsic distinction in the assembly pathways of mammalian and yeast ATP synthases.

The metazoan c-subunit has a fully trimethylated Lys43 residue, the function of which is currently unknown [148]. In contrast, the yeast c-subunit contains the conserved lys43 residue, but it is not trimethylated. The c-subunit of yeast is not imported into the mitochondrion from the cytoplasm because it is encoded on the mitochondrial genome, unlike the metazoan counterpart, which is encoded in the nucleus. This might point to the function of the trimethylated Lysine 43 of the c-subunit being important for the assembly of the c-ring and/or import of c-subunits into the mitochondria from the cytoplasm in metazoan species.

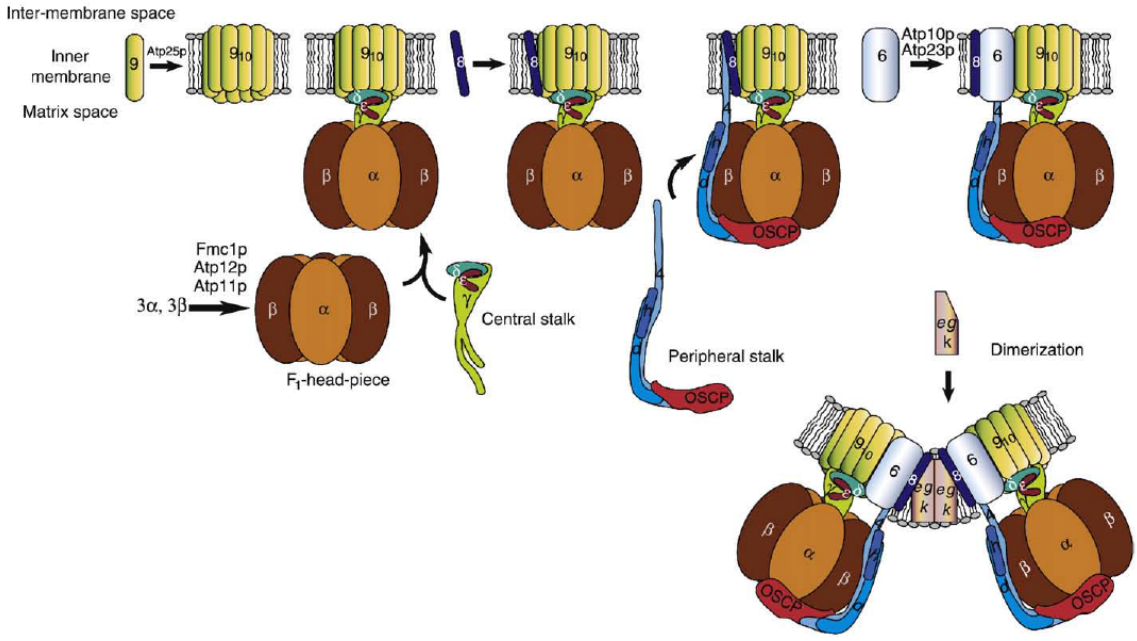

Fig. 4.1 The assembly model of mitochondrial ATP synthase in yeast. The ring of 10 c-subunits (subunit 9) assembles first, followed by the F_1 domain subunits and ATP8. The peripheral stalk is then assembled, followed by ATP6 and e, g and k, which aid the dimerisation of ATP synthase. The Figure was taken from [144].

The order of the assembly of the human ATP synthase complex including the supernumerary subunits was defined in a recent PhD thesis [138] and is also confirmed and further delineated in this work (Fig. 4.2). This ATP synthase assembly model [138] states that the F_1 domain (α_3, β_3, γ, δ and ε) assembles with the help of ATPAF1 and ATPAF2, and the natural inhibitor of ATP synthase, IF_1, binds to assembly intermediates lacking the a-subunit. The c-ring assembles either with the F_1 domain alone, or after the peripheral stalk. The e-, f- and g-subunits of both of these assembly intermediates associate with the F_O domain, and are bound by IF_1 [138]. The binding of IF_1 to these assembly intermediates is supported by evidence from this work, which shows that IF_1 exhibits an increased association with ATP synthase that had undergone suppression or disruption of the expression of the e-, f-, g- and 6.8 kDa proteolipid-subunits (Figs 3.6, 3.10, 3.11, 3.17, 3.18 and 3.27). But IF_1 does not associate with ATP synthase when the expression of the DAPIT-subunit alone was suppressed (Fig. 3.23), which resulted in the formation of a completely assembled ATP synthase complex.

The assembly model for ATP synthase [138], is modified by the findings presented in this thesis. The difference is the addition of a delineation step in the assembly of the e- and g-subunits of the F_O domain. In the assembly model proposed by Ford [138], F_1 domain is assembled then the e- and g-subunits are the first supernumerary subunits to assemble concurrently with the peripheral stalk subunits, followed by the f-subunit, then the 6.8 kDa proteolipid-subunit (which is dependent on the assembly of the a- and A6L-subunits), followed finally by the DAPIT-subunit. All Figures referred to from the Ford thesis [138], are in Appendix V.

In yeast mitochondrial ATP synthase, Δe and Δg mutants resulted in the loss of dimeric ATP synthase. The loss of the yeast e-subunit resulted in a loss of the g-subunit, but the loss of the g-subunit did not result in the loss of the e-subunit [37]. Relative quantitative

mass spectrometry of the subunit abundances of Δg-HAP1 ATP synthase (Fig. 3.18A and B) indicated that the e-subunit was unchanged in experiment one. In ATP synthase with suppression of the e-subunit with siRNA, the g-subunit was depleted four-fold (Figs. 3.5 and 3.6A and B). These observations should, however be interpreted with caution, as the experiment in Fig. 3.18 was flawed in that it appears that the g-subunit was present but it is possibly the result of contamination of control g-subunit protein from adjacent lanes on the gel. It is also difficult to reconcile the differences in the e-subunit protein ratios in Fig. 3.18A and B and it should be said that the data in this experiment are inconclusive due to the persistence of the g-subunit. However, even if there was a small amount of the g-subunit protein translated, the level of protein depletion observed was comparable to the level observed when siRNA was used to deplete the g-subunit (Fig. 3.17A and B). In that case, the data from these experiments suggest that the e-subunit is assembled first, followed by the g-subunit because the suppression of the e-subunit resulted in a more consistent depletion of supernumerary subunits between experiments than in the Δg-HAP1 ATP synthase. It must also be noted that this comparison is drawn from experiments with different experimental designs. The proposition that the e-subunit is the first supernumerary subunit to assemble is based on observations from experiments performed using siRNA to deplete the e-subunit, and comparing these findings with results from the disruption of the expression of the g-subunit, which should result in complete removal of the protein. These results point to the suggested assembly of the e- and g-subunits one after the other, but further work is needed to clarify the assembly pathway because of the experimental anomalies found in this work. A more informative comparison could be drawn if the experiments to investigate the functions of the e- and g-subunits were repeated (and with Δe-HAP1 cells, rather than siRNA).

The next subunit to assemble after the e- and g-subunits is the f-subunit, based on the finding that the f-S1 and f-S2 subcomplexes of ATP synthase form (Figs. 3.14 and 3.15) and the complex consists of the ATP synthase monomer lacking the a-, A6L-, DAPIT- and 6.8 kDa proteolipid-subunits (Figs 3.10 and 3.11). It is possible that the larger of the subcomplexes that accumulate are the result of disruption of the ATP synthase complex by the BN-PAGE protocol. This claim is supported by evidence from DAPIT-suppressed ATP synthase, where no effect on the subunit composition of the enzyme is observed (Figs. 3.22 and 3.23A and B).

After the f-subunit, the 6.8 kDa proteolipid-subunit assembles, based on evidence from BN-PAGE analysis after suppression of the expression of the 6.8 kDa proteolipid subunit which resulted in the formation of the 6.8-S1 and 6.8-S2 subcomplexes (Fig. 3.29). The ATP synthase subcomplex in 6.8 kDa proteolipid depleted ATP synthase probably consisted of ATP synthase lacking the a-, A6L- and DAPIT-subunits (Fig. 3.27A and B). Interestingly, cells where the expression of the 6.8 kDa proteolipid subunit had been suppressed with siRNA did not display a significant change in cellular or mitochondrial OCR (Fig. 3.28), despite the a-, A6L- and DAPIT-subunits being lost from the enzyme. This observation may cloud interpretation of the results, because the loss of the a-, A6L- and DAPIT-subunits from 6.8 kDa proteolipid-depleted cells may be the result of the solubilisation of the mitoplasts or mitochondrial membranes with digitonin (Figs. 3.26, 3.27 and 3.29). This claim could be supported by evidence where the OCR was measured in whole cells (Fig. 3.28), where membranes are not disrupted with detergent. If the a-, A6L- and DAPIT-subunits were really lost from the enzyme, the loss of the a-subunit alone should result in defects in the OCR because ATP synthase becomes uncoupled from respiration and hydrolyses ATP, and in ρ^0 cells, which lack the a- and A6L-subunits, ATP is hydrolysed by ATP synthase to contribute to the membrane potential [149, 150].

The lack of any drastic effect on the subunit composition of ATP synthase with suppression of the DAPIT-subunit (Figs. 3.22 and 3.23A and B), suggests that it is the last of the supernumerary subunits to assemble, as stated in the assembly model by Ford [138]. The suppression of the DAPIT-subunit of ATP synthase also did not result in any significant changes in the OCR of 143B cells (Fig. 3.24), which is consistent with the observation of the lack of change in the subunit composition of ATP synthase (Figs. 3.22 and 3.23A and B), and also the lack of observable subcomplexes of ATP synthase (Fig. 3.25). In summary, the additional steps in the assembly pathway of human ATP synthase identified by the work in this thesis is the delineation of the assembly of the e- and g-subunits, which do not assemble concurrently, but instead the tentative conclusion is drawn that e-subunit assembles first, followed by the g-subunit.

The experiments performed to assess the assembly pathways of ATP synthase were performed with mitoplast material or mitochondrial membranes that had not been frozen before solubilisation and were kept on ice during sample preparation and fractionated by BN-PAGE at 4°C. This experimental set-up reduces experimentally derived artefacts which may cause structural degradation of the enzyme, allowing the identification of true assembly intermediates of ATP synthase. However, it is possible that all S-1 subcomplexes were the breakdown products of ATP synthase complexes due to the BN-PAGE protocol, because the S-1 subcomplexes showed variability in their levels across experiments done with cells with f-subunit suppression or disruption (Figs. 3.14 and 3.15).

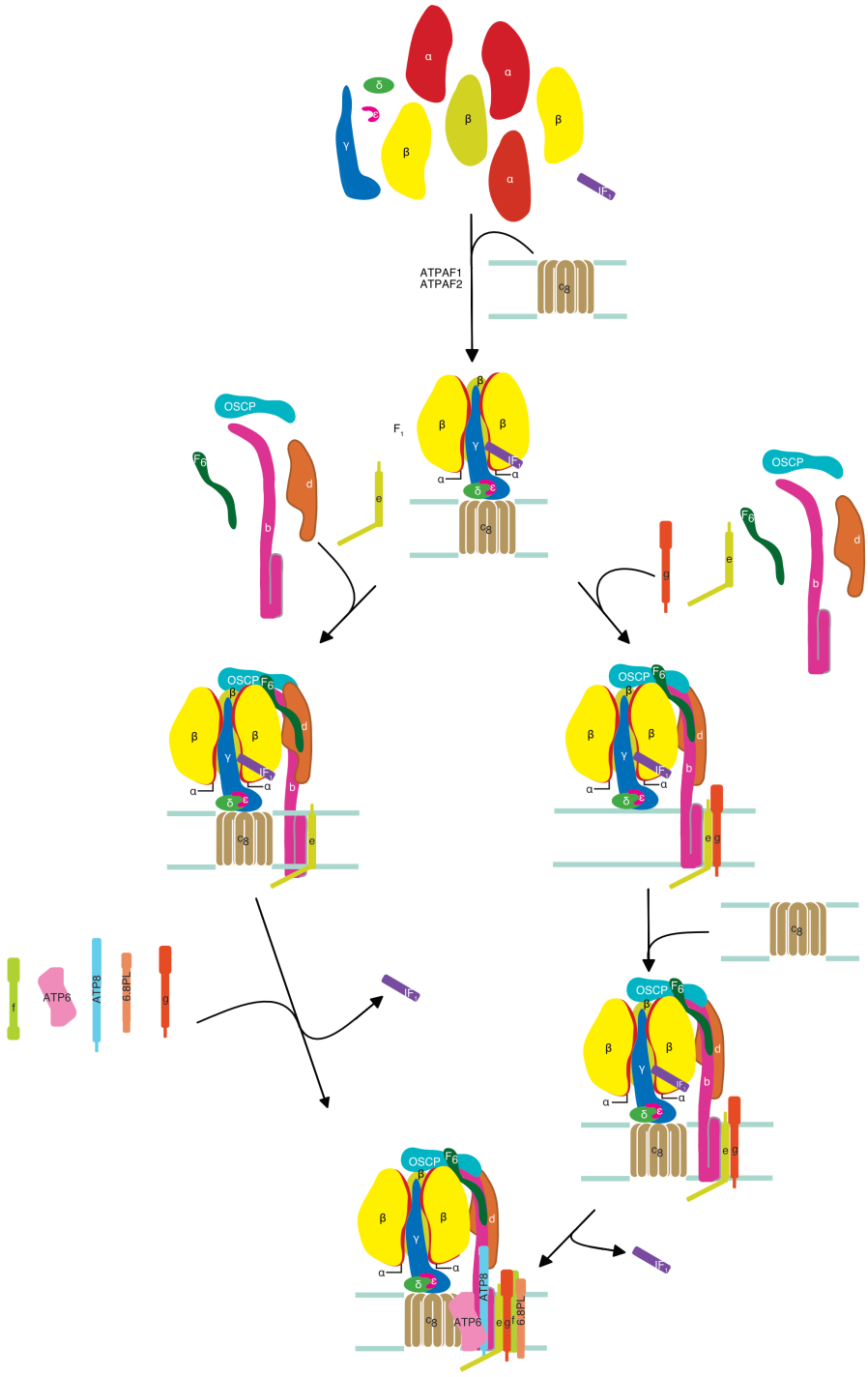

Fig. 4.2 The pathway of assembly of monomeric human mitochondrial ATP synthase. The F_1 domain subunits and the c-ring assemble first. The F_1 domain requires the ATPAF1 and ATPAF2 assembly factors and IF_1 binds to prevent ATP hydrolysis. F_1 then associates with the assembled c-ring. On the left, the peripheral stalk subunits and the e-subunit assemble next, followed by the g- then the f-, ATP8- (A6L), 6.8 kDa proteolipid- and ATP6- (a)-subunits and IF_1 is released. On the right, the peripheral stalk and e- and g-subunits can assemble before the addition of the c-ring, followed by the addition of the f, A6L-, 6.8PL and a-subunits, and release of IF_1. The Figure was adapted from Fig. S25 [138].

The suppression of the e-subunit with siRNA resulted in the depletion of the entire complement of supernumerary subunits and the a-subunit. There is a similarity in the results seen in Fig. S23 [138], and this work Fig. 3.8, where two subcomplexes (e-S1 and e-S2) accumulated when the e-subunit was depleted in mitoplasts or mitochondrial membranes.

In ATP synthase with depletion of the g-subunit with siRNA, the e-, f-, 6.8 kDa proteolipid-, A6L- and DAPIT-supernumerary subunits dissociate from ATP synthase as well as the a-subunit. In Δg-HAP1 mitochondrial membranes, the ATP synthase was predominantly in the form of the Δg-S1 and Δg-S2 subcomplexes (Fig. 3.19). These subcomplexes also accumulated in mitochondrial membranes with suppression of the expression of the g-subunit (Fig. 3.20). The effects of the suppression of the g-subunit with siRNA on the native state of ATP synthase are consistent between this work and the results presented in Fig. S23[138] where bands representing monomeric ATP synthase and the two g-subcomplexes are present in both sets of results, although the g-S2 subcomplex accumulated to a greater degree in this work (Fig. 3.21). However, in Δg-HAP1 mitochondrial membranes and mitoplasts, monomeric ATP synthase is not observed, and/or was severely depleted, respectively, suggesting that the g-subunit plays a role in the stability of the entire ATP synthase complex.

The suppression or disruption of the expression of the f-subunit both resulted in the depletion of the 6.8 kDa proteolipid-, a-, A6L- and DAPIT-subunits from ATP synthase, suggesting that the f-subunit is assembled after the e- and g-subunits, but before the 6.8 kDa proteolipid subunit. This interpretation is drawn because when 6.8 kDa proteolipid expression was suppressed with siRNA, the relative levels of the f-subunit were unchanged (Fig. 3.26 and Fig. 3.27A and B). The results of suppression or disruption of the expression of the f-subunit on the subunit composition of ATP synthase were consistent, and mass spectrometric analysis of ATP synthase from both f-subunit suppressed and Δf-HAP1 cells

revealed that the Δf-S2 subcomplex (Figs. 3.14 and 3.15) consisted of F_1c_8 + peripheral stalk + e and g. The results of native analyses of subunit-f depleted ATP synthase complexes presented by Ford (Fig. S23) [138] are consistent with BN-PAGE analyses of ATP synthase with suppression of the f-subunit Figs. 3.14. The IF_1 precursor protein (see Appendix V for the sequence) was increased in association with Δf-ATP synthase, and it has been suggested that in ρ^0 cells, IF_1-P binds preferentially to monomeric ATP synthase [138].

In BN-PAGE experiments, the a-, A6L- and DAPIT-subunits were probably not associated with ATP synthase when the 6.8 kDa proteolipid-subunit was suppressed with siRNA (Fig. 3.28A and B) suggesting that the incorporation of the a- and A6L-subunits into the enzyme depends on the presence of the 6.8 kDa proteolipid subunit. Two subcomplexes of ATP synthase formed when the 6.8 kDa proteolipid-subunit was suppressed with siRNA in experimental conditions involving digitonin solubilisation of membrane proteins Fig. S23 [138], but only one subcomplex was observed in Fig. 3.29. However, as mentioned, the loss of these subunits may be an experimental artefact. The solubilisation of 6.8 kDa proteolipid depleted mitochondria with digitonin may also result in the loss of subunits from ATP synthase where there is a possibility that no such effect would be observed in ATP synthase depleted of the 6.8 kDa proteolipid-subunit before solubilisation. The OCR of cells depleted of the 6.8 kDa proteolipid-subunit was unchanged (Fig. 3.28), suggesting that 6.8 kDa proteolipid-subunit may play a role in stabilising the a-, A6L- and DAPIT-subunits when ATP synthase is solubilised with digitonin.

The depletion of the DAPIT-subunit was inconsequential for the subunit composition of ATP synthase, as no changes in any of the subunits of ATP synthase were observed when immunopurified ATP synthase was investigated (Figs. 3.22 and 3.23A and B, respectively). There was however, a discrepancy between the results of the native analysis of ATP

synthase with suppression of the DAPIT-subunit presented in Fig. S23 [138] and in this work (Fig. 3.25), where a large amount of D-S1 subcomplex and also a small amount of D-S2 subcomplex accumulated, but in this work (Fig. 3.25), the monomeric ATP synthase band was unchanged compared to the control and the DS-2 subcomplex was not observed in this work. ATP synthase lacking DAPIT may be less stable under the experimental conditions used to analyse the native state of the enzyme. However, in DAPIT-depleted cells that were not treated with digitonin, ATP synthase may be as structurally stable as the control ATP synthase. DAPIT is the last of the supernumerary subunits to be incorporated into the F_O domain, based on the evidence in this work, and also the evidence reported in [138].

A notable observation from analysis of the subunit composition of ATP synthase where the expression of the e-, f-, g- and 6.8 kDa proteolipid-subunits had been depleted or disrupted, is that the a- and A6L-subunits were significantly depleted from the enzyme in each case. This suggests that the e-, f-, g- and 6.8 kDa proteolipid-subunits stabilise the association of the a- and A6L-subunits in the ATP synthase complex.

4.2. Structural roles of the supernumerary subunits

Out of all the supernumerary subunits investigated in this work, the depletion of the g-subunit resulted in the highest degree of loss of subunits from ATP synthase (Figs. 3.16 and 3.18A and B), and also resulted in a substantial loss of monomeric and dimeric ATP synthase (Fig. 3.21). However, to get a clearer picture of the severity of the impact on the subunit composition of the enzyme, each subunit investigated in this thesis, should be investigated by disruption of their genes. The data in this thesis suggests that the g-subunit plays a significant role in stabilising the association of subunits with each other in the F_O

domain within the membrane domain. However, the stability of the c-ring is not dependent on any of the supernumerary subunits investigated (Figs. 3.5, 3.9, 3.16 3.22 and 3.26).

The structural role of the e-subunit may be similar to that of the g-subunit, due to the similar profile of the subunit composition of ATP synthase when the expression of either the e- or g-subunits was suppressed or disrupted, but the effect observed when the e-subunit was suppressed was less severe than when the g-subunit was disrupted (Figs. 3.5 and 3.16, respectively).

A proposed theoretical structural role of the f-subunit, based on the experiments in this work, is to stabilise a module of subunits in the F_O domain that contain the a-, A6L-, 6.8 kDa proteolipid- and DAPIT-subunits (Figs. 3.10A and B and 3.11A and B). This suggestion is based upon the finding that suppression or disruption of the expression of the f-subunit resulted in the subsequent depletion of these subunits and that the OCR of cells with disruption or suppression of the f-subunit was significantly decreased. The f-subunit is thought to be in close proximity with the a- and A6L-subunits in the *Pichia angusta* enzyme [71], and the experimental evidence in this thesis points to the f-, A6L- and a-subunits being in a similar arrangement in human ATP synthase.

The structural role of the DAPIT-subunit appears to be minimal for maintaining the structural integrity and subunit composition of the monomeric enzyme, as indicated in Figs. 3.22 and 3.23A and B, where no other ATP synthase subunits were depleted when the expression of the DAPIT-subunit was suppressed. This result is reflected in an experiment where the expression of the DAPIT-subunit was suppressed (Fig. S24) [138]). There are, however, some differences in the outcomes of the experiments performed to assess native protein complexes of ATP synthase with suppression of DAPIT (Fig. S23 [138]). In Fig. S23, suppression of the DAPIT-subunit resulted in accumulation of the D-S2 subcomplex, but this was not detected in Fig. 3.25. As there was a lack of evidence for the depletion of

any subunits of ATP synthase lacking the DAPIT-subunit (Figs. 3.22 and 3.23A and B), the D-S1 and DS2 subcomplexes in Fig. S23 may represent artefactual evidence.

The 6.8 kDa proteolipid-subunit appeared to exert a similar stabilising force on the a-, A6L- and DAPIT-subunits, as the suppression of this subunit resulted in the depletion of these three subunits from the enzyme (Fig. 3.28A and B). It is unclear why there is such a discrepancy between ATP synthase lacking 6.8 kDa proteolipid in cells without added digitonin, compared to ATP synthase lacking 6.8 kDa proteolipid in ATP synthase that had been solubilised with digitonin.

Structural information [71] indicates that the A6L-subunit functions as a strut to brace the a-subunit against the c-ring.

The mitochondrial OCR of cells with suppression or disruption of the expression of the e-, f- and g-subunits exhibited significant defects in basal respiration and accelerated respiration (Figs. 3.7, 3.12, 3.13 and 3.19), but this phenotype was not reflected in cells where the DAPIT- or 6.8 kDa proteolipid-subunits had been suppressed (Figs. 3.24 and 3.28, respectively). This finding may indicate, that the e-, f- and g-subunits act together or separately to stabilise the association of the a-subunit with A6L and the c-ring because the disruption or suppression of these subunits resulted in significant decreases in the OCR of 143B cells. Also, the depletion of the e-, f- and g-subunits all resulted in the loss of the a- and A6L-subunits.

4.3. The roles of the supernumerary subunits in the oligomerisation of ATP synthase

All of the supernumerary subunits investigated in this work are involved in the stabilisation of oligomeric forms of ATP synthase, because dimeric and oligomeric forms of the enzyme were depleted when the expression of each of the supernumerary subunits was suppressed or disrupted individually. Also, DAPIT is primarily involved in the stabilisation of

oligomeric forms of ATP synthase, as there was little effect on the dimerization of ATP synthase lacking DAPIT. The proposed model of ATP synthase dimerization and oligomerisation is presented in Fig. 4.3 and shows that the e-, f- and g-subunits assembled in the membrane domain before the 6.8 kDa proteolipid-, A6L-, and a-subunits, which promote the formation of dimerisation competent ATP synthase. Four DAPIT subunits may mediate the oligomerisation of two dimers of ATP synthase to form a tetramer. The suppression of the e-subunit resulted in depletion of oligomeric ATP synthase, the ATP synthase dimer and also the ATP synthase monomer in mitochondrial membranes (Fig. 3.8). This is different to the result seen in Fig. S23 [138], where the suppression of the expression of the e-subunit resulted in the depletion of the oligomeric forms of ATP synthase, but the amount of the ATP synthase dimer remained unchanged.

Another difference observed between the two experiments was that monomeric ATP synthase was more severely depleted in Fig. 3.8 than in Fig. S23 [138]. A possible explanation for the difference could be that the siRNA used to deplete the e-subunit had a stronger effect on the cells used in Fig. 3.8 than in Fig. S23, or due to differences involved in using mitoplasts or mitochondrial membranes to perform the experiment. Δe-HAP1 mitochondrial membranes and mitoplasts should be analysed to assess this discrepancy. The e- and g-subunits were found to be required for the dimerisation of yeast ATP synthase, and were also required to form a dimerisation capable ATP synthase monomer [151]. According to Fig. 3.8 in this work, the e-subunit is required for stabilisation of the human ATP synthase dimer and monomer, consistent with the results in [151].

The oligomerisation capability of ATP synthase in mitochondrial membranes or mitoplasts from Δg-HAP1 cells was severely reduced (Fig. 3.21). Oligomerisation of ATP synthase with suppression of the g-subunit was affected to a similar degree as ATP synthase with e-subunit suppression, with oligomeric ATP synthase and the ATP synthase dimer depleted

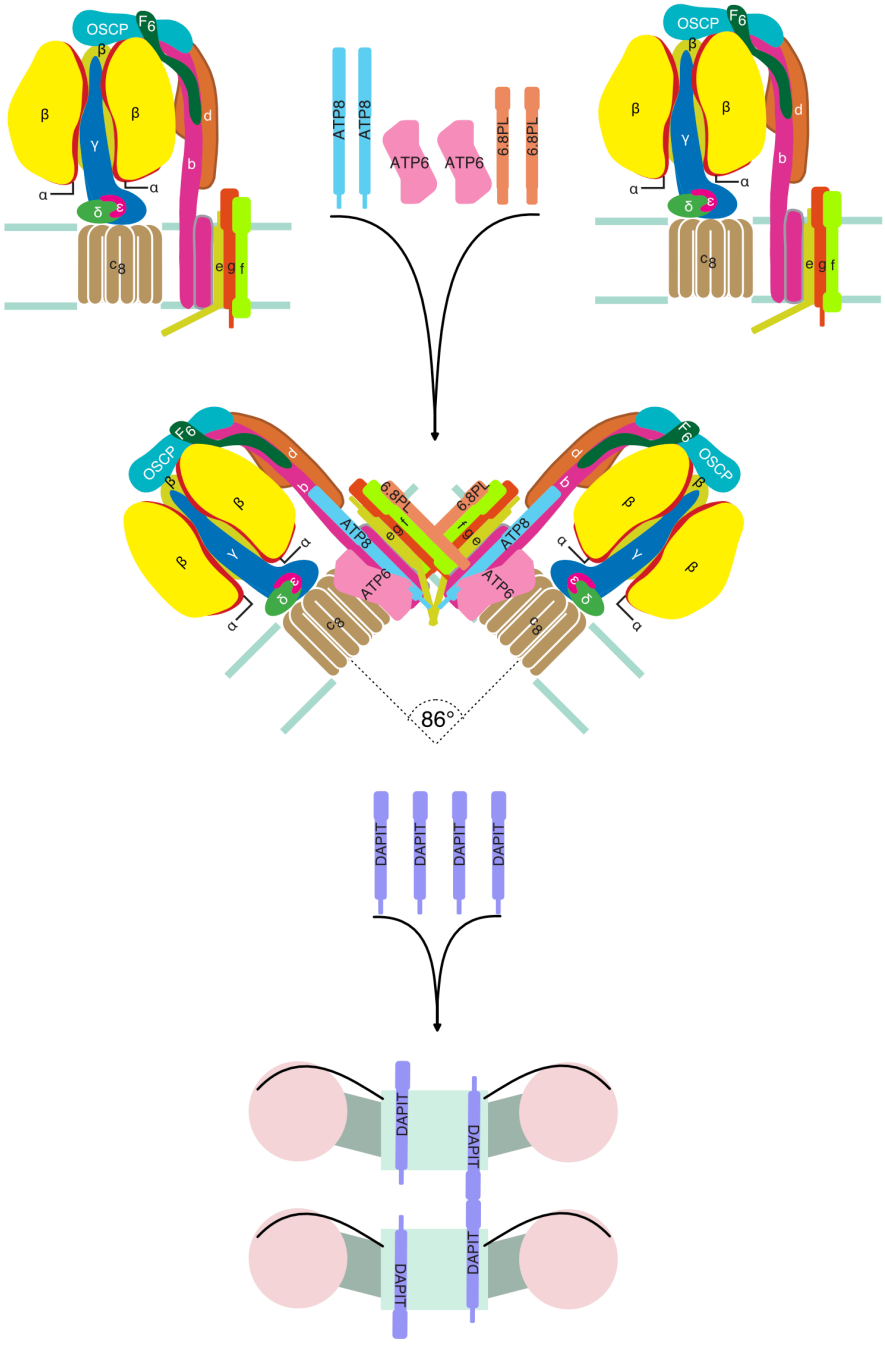

Fig. 4.3 Dimerisation and oligomerisation of ATP synthase. The formation of dimeric ATP synthase is dependent on the association of all the supernumerary subunits. The a-subunit is assembled after the supernumerary subunits. The Figure was adapted from Fig. S26 [138].

in both Fig. 3.8 (e suppression) and Fig. 3.20 (g suppression). This is different to the result for g-subunit suppression in Fig. S23 [138], where only ATP synthase oligomers were

depleted, but not the ATP synthase dimer. The effect upon oligomerisation of ATP synthase was much more severe in Δg-HAP1 mitochondrial membranes and mitoplasts (Fig. 3.21). There were no visible signs of the oligomeric forms of ATP synthase in either mitochondrial membranes or mitoplasts. The ATP synthase monomer was also not observed in mitochondrial membranes, and in mitoplasts, the monomer was severely depleted. The depletion of the ATP synthase monomer in Δg-HAP1 mitochondrial membranes and mitoplasts indicates that the g-subunit is required to stabilise the ATP synthase monomer and dimer.

In mitochondrial membranes with suppression of the f-subunit, oligomeric ATP synthase and dimeric ATP synthase were depleted (Fig. 3.14). This result is different to that presented in Fig. S23 [138], where the oligomers were modestly depleted and there was no effect observed upon the dimer. The depletion of oligomeric forms of ATP synthase and dimeric ATP synthase was much more severe in Δf-HAP1 mitochondrial membranes and mitoplasts than depletion of ATP synthase oligomers and dimers in mitochondrial membranes with suppression of the f-subunit. This is possibly due to the residual f-subunit protein still present in the siRNA treated sample during the experiment. The e-, f-, g-, DAPIT- and 6.8 kDa proteolipid-subunits are probably all required to form a 'dimerisation-competent, primed' ATP synthase. The common loss of subunits in the e-, f- and g-subunit suppressed or disrupted ATP synthase complexes were the a-, A6L-, DAPIT- and 6.8 kDa proteolipid-subunits (Figs. 3.6A and B, 3.10A and B and, 3.11A and B, 3.17A and B and 3.18A and B).

In ATP synthase where the DAPIT-subunit had been suppressed only the oligomeric forms of ATP synthase were depleted (Fig. 3.26), which corroborates with the profile of oligomeric ATP synthase seen in Fig. S23 [138]. However, the ATP synthase dimer was not separated into two discreet complexes in Fig. 2.25 as was the case in Fig. S23, and

instead was a more intense band that migrated faster than the ATP synthase dimer in the control lane. The loss of ATP synthase lacking DAPIT reported previously [152], has not been confirmed here. The evidence for the involvement of DAPIT in the oligomerisation of ATP synthase comes from blue native PAGE with immunodetection of the β-subunit. It is possible that ATP synthase is able to form oligomers, and that this is mediated by the DAPIT-subunit when ATP synthase has been solubilised from the IMM. However, this may not be the case in biological inner mitochondrial membranes where the membrane has not been disrupted with digitonin.

In ATP synthase depleted of the 6.8 kDa proteolipid-subunit, the oligomeric and dimeric ATP synthase were depleted (Fig. 3.29). The accumulation of monomeric ATP synthase may be the result of the decomposition of oligomeric and dimeric ATP synthase. This finding is different to that reported in Fig S23 [138], where the oligomers were not depleted to the extent they were in Fig. 3.29, and also the ATP synthase dimer appeared to be unaffected by suppression of the 6.8 kDa proteolipid-subunit (Fig. S23 [138]), whereas the dimer was depleted in Fig. 3.29. Differences in experimental set up may account for these discrepancies, as mitochondrial membranes were prepared in Fig. 3.28, whereas mitoplasts were prepared in Fig. S23.

4.4. The supernumerary subunits and the PTP

The mitochondrial permeability transition is a process that occurs in mammals, fish, amphibians, plants and fungi [153], suggesting that the physiological role of the permeability transition is an evolutionary conserved process. During the permeability transition, a pore is formed in the IMM which induces permeabilisation of the membrane to metabolites and solutes up to 1.5 kDa in size [154].

The permeability transition pore in mitochondria was first believed to be the result of Ca^{2+} activated phospholipases and acetyl coA synthetase that caused formation of a pore in the IMM [154]. It was later shown that pore formation and resealing of the mitochondria could still occur in the absence of ATP, acetyl-CoA and Mg^{2+}, which are required to activate the phospholipase and acetyl coA synthetase enzymes in the phospholipase model of pore formation [155]. Pore opening was shown to be a reversible, Ca^{2+} dependent phenomenon, where pore closure could be achieved by chelating Ca^{2+} [156]. The pore opening effect of Ca^{2+} was only observed in the presence of 2.5 mM P_i, and 35 nmol of Ca^{2+} per mg of protein. The molecular identity of the pore was investigated and assumed to consist of the voltage dependent anion channel (VDAC) and the adenine nucleotide transporter (ANT). Cyclophillin D was used to purify these components after it was found that pore opening could be inhibited by cyclosporin A, which binds to and inhibits cyclophillin D [157]. The identity of the protein constituents of the pore still remained (and continue to remain) elusive, after it was discovered that neither the ANT nor the VDAC were necessary components for establishing a pore [158, 159]. The search for the molecular identity of the mitochondrial PTP continued and in 2013, it was suggested that dimeric ATP synthase formed the PTP, after dimeric ATP synthase was purified from blue native gels and reconstituted into planar lipid bilayers, where electrophysiological measurements suggested that a pore was formed with identical electrophysiology to that measured in mitochondria [160]. It has also been reported that the c-subunit of ATP synthase forms the pore [161, 162], however, it has been shown that cells engineered with gene deletions for the three isoforms of subunit-c are still capable of pore formation and permeability transition [163]. The role of specific ATP synthase subunits in the formation of the mPTP is being investigated using gene-deletion experiments targeting each subunit of ATP synthase. Therefore, the Δf-HAP1 and Δg-HAP1 cells used in this work to investigate the

function of the f- and g-subunits can be used in the permeability transition pore assay to assess the involvement of the f- and g-subunits of ATP synthase in the formation of the mPTP.

4.5. Methodological considerations: siRNA versus CRISPR-Cas9

The investigation of protein function in cell biology is often conducted by removal of the protein of interest either completely or partially in the cases CRISPR-Cas9 genome editing [140], or siRNA [164], respectively. These processes emerged from the biological machinery required for the defence of a hosts bacterial DNA from invading viral DNA, in the case of CRISPR-Cas9 [165, 166], or from the regulation of gene expression by expressed microRNAs (miRNAs) or small interfering RNAs (siRNAs), in the case of siRNA [164]. There is a trade-off to be considered when using siRNA to suppress the expression of a protein. This is the choice between the dose used to suppress the expression of a protein, where too high a dose can result in undesirable off-target effects, and too little dose results in inefficient suppression of the protein. Even at doses that will result in off-target effects, the protein of interest still is not suppressed entirely. That is usually not the case with disruption of the expression of a gene using CRISPR-Cas9, where the protein of interest is in theory completely gone from the cell. One of the differences in the two methods relate to the transfection procedure. When siRNA is used, a plate of cells is transfected, and the whole population of transfected cells are grown and used for the experiment. However, with CRISPR-Cas9 mediated gene disruption, the plate of cells is transfected but then the cells are sorted into single cells by FACS and each cell is grown into a clonal colony, which is grown and screened to ensure the gene deletion status of the cell. Only after validation of the gene deletion status of the clonal cell population is the experiment performed. With siRNA, a high percentage of the mRNA transcripts encoding

the protein of interest should be degraded, but the remaining transcripts will result in a small amount of the protein of interest being translated. This consequence may be responsible for the occasionally differing effects resulting from experiments performed by siRNA or with Δf-HAP1 or Δg-HAP1 cells. For example, in the extracellular flux analysis of OCR performed with siRNA to suppress the expression of the f-subunit, and in Δf-HAP1 cells, the results are different. In siRNA treated cells, the mitochondrial OCR is only significantly changed during basal respiration and during accelerated respiration, whereas in Δf-HAP1 cells, the mitochondrial OCR is significantly changed during all three measurements, including during respiration where ATP synthase had been inhibited by oligomycin A. This is presumably because the small amount of the f-subunit that remains in cells treated with siRNA may still be functional and increases the amount of ATP synthase that is analogous to the control.

4.6. Conclusions and further work

The assembly pathway of ATP synthase has been further characterised by this work, where a previously presented pathway [138] suggested the assembly of the e- and g-subunits of ATP synthase were incorporated concurrently, whereas the findings in the present work point to a putative delineation in the incorporation of these subunits. The e-subunit is incorporated first, followed by the g-subunit. Subsequent steps are identical to the assembly pathway presented in [138].

The theoretical locations of the supernumerary subunits were further defined by characterisation of the subunit composition of ATP synthase after the individual suppression of expression of the e-, f-, g-, DAPIT- and 6.8 kDa proteolipid-subunits. This work points to the f-subunit residing near to the a- and A6L-subunits.

This work has pointed to the roles of all the nuclear encoded supernumerary subunits being required for the dimerisation of ATP synthase, except DAPIT, which is required for oligomerisation only. Once the e-, f- and g-subunits assemble, this is followed by the addition of the A6L-, DAPIT-, 6.8 kDa proteolipid- and a-subunits in order to form a dimerisation competent ATP synthase monomer.

The experiments conducted to investigate the functions of the supernumerary subunits using siRNA should be repeated with cells with disruption of the expression of these genes to investigate the effects on ATP synthase, where the complete removal of the protein occurs. The quantitative mass spectrometry experiments performed with immunopurified ATP synthase from cells with gene disruptions should be modified to prevent contamination of subunits from the control that are disrupted in the experimental condition. This could be done either by increasing the number of blank wells between experiments on the SDS-PAGE gel or by analysing each experiment on a different gel.

BN-PAGE coupled with 2 dimensional SDS-PAGE could be used to further characterise subcomplexes of ATP synthase. Cutting out sections of the BN-PAGE gel corresponding to the positions where the subcomplexes of ATP synthase migrate to and separating the subunits by SDS-PAGE with mass mapping would identify the subunit composition of ATP synthase subcomplexes from cells with disruptions of the supernumerary subunit-genes.

In order to investigate the roles of the supernumerary subunits of ATP synthase in the formation of the mitochondrial permeability transition pore, cells where the genes encoding each nuclear encoded supernumerary subunit individually should be analysed by the techniques used by He. *et al* [163].

There is also a need for a high-resolution structure of the subunits in the F_O domain in order to corroborate biochemical functional characterisation of the supernumerary subunits with structural features of each subunit in the F_O domain.

5. References

1. Nicholls, D. G. & Ferguson, S. (2013). Bioenergetics 4. *Elsevier*
2. den Hollander, J. A., Ugurbil, K., Brown, T. R., Bednar, M., Redfield, C. & Shulman, R. G. (1986). Studies of anaerobic and aerobic glycolysis in *Saccharomyces cerevisiae*. *Biochemistry* **25**, 203-211.
3. Li, X., Wu, F. & Beard, D. A. (2013). Identification of the kinetic mechanism of succinyl-CoA synthetase. *Biosci Rep* **33**, 145-163.
4. Wang, S. F., Si, Y. X., Wang, Z. J., Yin, S. J., Yang, J. M. & Qian, G. Y. (2012). Folding studies on muscle type of creatine kinase from *Pelodiscus sinensis*. *Int J Biol Macromol* **50**, 981-990.
5. Watt, I. N., Montgomery, M. G., Runswick, M. J., Leslie, A. G. W. & Walker, J. E. (2010). Bioenergetic cost of making an adenosine triphosphate molecule in animal mitochondria. *Proc. Natl. Acad. Sci. U. S. A.* **107**, 16823-16827.
6. Mitchell, P. (1979). Keilin's respiratory chain concept and its chemiosmotic consequences. *Science* **206**, 1148-1159.
7. Mitchell, P. (1961). Coupling of phosphorylation to electron and hydrogen transfer by a chemi-osmotic type of mechanism. *Nature* **191**, 144-148.
8. Mitra, K., Wunder, C., Roysam, B., Lin, G. & Lippincott-Schwartz, J. (2009). A hyperfused mitochondrial state achieved at G1-S regulates cyclin E build up and entry into S phase. *Proc. Natl. Acad. Sci. U. S. A.* **106**, 11960-11965.
9. Newmeyer, D. D. & Ferguson-Miller, S. (2003). Mitochondria: releasing power for life and unleashing the machineries of death. *Cell* **112**, 481-490.
10. Biasutto, L., Azzolini, M., Szabò, I. & Zoratti, M. (2016). The mitochondrial permeability transition pore in AD 2016: An update. *Biochim. Biophys. Acta* **1863**, 2515-2530.
11. Gakh, O., Ranatunga, W., Smith, D. Y., Ahlgren, E. C., Al-Karadaghi, S., Thompson,

J. R. & Isaya, G. (2016). Architecture of the Human Mitochondrial Iron-Sulfur Cluster Assembly Machinery. *J. Biol. Chem.* **291**, 21296-21321.

12. Ponka, P. (1997). Tissue-specific regulation of iron metabolism and heme synthesis: distinct control mechanisms in erythroid cells. *Blood* **89**, 1-25.
13. Meléndez-Hevia, E., Waddell, T. G. & Cascante, M. (1996). The puzzle of the Krebs citric acid cycle: assembling the pieces of chemically feasible reactions, and opportunism in the design of metabolic pathways during evolution. *J. Mol. Evol.* **43**, 293-303.
14. Embley, T. M. & Martin, W. (2006). Eukaryotic evolution, changes and challenges. *Nature* **440**, 623-630.
15. Martin, W. & Müller, M. (1998). The hydrogen hypothesis for the first eukaryote. *Nature* **392**, 37-41.
16. Rehling, P., Model, K., Brandner, K., Kovermann, P., Sickmann, A., Meyer, H. E., Kühlbrandt, W., Wagner, R., Truscott, K. N. & Pfanner, N. (2003). Protein insertion into the mitochondrial inner membrane by a twin-pore translocase. *Science* **299**, 1747-1751.
17. Chacinska, A., Koehler, C. M., Milenkovic, D., Lithgow, T. & Pfanner, N. (2009). Importing mitochondrial proteins: machineries and mechanisms. *Cell* **138**, 628-644.
18. Anderson, S., Bankier, A. T., Barrell, B. G., de Bruijn, M. H., Coulson, A. R., Drouin, J., Eperon, I. C., Nierlich, D. P., Roe, B. A., Sanger, F., Schreier, P. H., Smith, A. J., Staden, R. & Young, I. G. (1981). Sequence and organization of the human mitochondrial genome. *Nature* **290**, 457-465.
19. Palmieri, L., Lasorsa, F. M., Vozza, A., Agrimi, G., Fiermonte, G., Runswick, M. J., Walker, J. E. & Palmieri, F. (2000). Identification and functions of new transporters in yeast mitochondria. *Biochim. Biophys. Acta* **1459**, 363-369.

20. Runswick, M. J., Philippides, A., Lauria, G. & Walker, J. E. (1994). Extension of the mitochondrial transporter super-family: sequences of five members from the nematode worm, *Caenorhabditis elegans*. *DNA Seq* **4**, 281-291.

21. Kunji, E. R. & Robinson, A. J. (2010). Coupling of proton and substrate translocation in the transport cycle of mitochondrial carriers. *Curr Opin Struct Biol* **20**, 440-447.

22. Lill, R. & Kispal, G. (2000). Maturation of cellular Fe-S proteins: an essential function of mitochondria. *Trends Biochem. Sci.* **25**, 352-356.

23. Sano, S., Inoue, S., Tanabe, Y., Sumiya, C. & Koike, S. (1959). Significance of mitochondria for porphyrin and heme biosynthesis. *Science* **129**, 275-276.

24. Fiermonte, G., Dolce, V., Arrigoni, R., Runswick, M. J., Walker, J. E. & Palmieri, F. (1999). Organization and sequence of the gene for the human mitochondrial dicarboxylate carrier: evolution of the carrier family. *Biochem. J.* **344 Pt 3**, 953-960.

25. Saraste, M. & Walker, J. E. (1982). Internal sequence repeats and the path of polypeptide in mitochondrial ADP/ATP translocase. *FEBS Lett.* **144**, 250-254.

26. Okamoto, K. & Shaw, J. M. (2005). Mitochondrial morphology and dynamics in yeast and multicellular eukaryotes. *Annu. Rev. Genet.* **39**, 503-536.

27. Brereiter-Hahn, J. & Voth, M. (1994). Dynamics of mitochondria in living cells: shape changes, dislocations, fusion and fission of mitochondria. *Microscopy research and technique* **27**, 198-219.

28. Moore, A. S., Wong, Y. C., Simpson, C. L. & Holzbaur, E. L. (2016). Dynamic actin cycling through mitochondrial subpopulations locally regulates the fission-fusion balance within mitochondrial networks. *Nat Commun* **7**, 12886.

29. Otera, H., Wang, C., Cleland, M. M., Setoguchi, K., Yokota, S., Youle, R. J. & Mihara, K. (2010). Mff is an essential factor for mitochondrial recruitment of Drp1 during mitochondrial fission in mammalian cells. *J. Cell Biol.* **191**, 1141-1158.

30. Losón, O. C., Song, Z., Chen, H. & Chan, D. C. (2013). Fis1, Mff, MiD49, and MiD51 mediate Drp1 recruitment in mitochondrial fission. *Mol. Biol. Cell* **24**, 659-667.

31. Malka, F., Guillery, O., Cifuentes-Diaz, C., Guillou, E., Belenguer, P., Lombès, A. & Rojo, M. (2005). Separate fusion of outer and inner mitochondrial membranes. *EMBO Rep.* **6**, 853-859.

32. Song, Z., Ghochani, M., McCaffery, J. M., Frey, T. G. & Chan, D. C. (2009). Mitofusins and OPA1 mediate sequential steps in mitochondrial membrane fusion. *Mol. Biol. Cell* **20**, 3525-3532.

33. Frey, T. G. & Mannella, C. A. (2000). The internal structure of mitochondria. *Trends Biochem. Sci.* **25**, 319-324.

34. Davies, K. M., Strauss, M., Daum, B., Kief, J. H., Osiewacz, H. D., Rycovska, A., Zickermann, V. & Kühlbrandt, W. (2011). Macromolecular organization of ATP synthase and complex I in whole mitochondria. *Proc. Natl. Acad. Sci. U. S. A.* **108**, 14121-14126.

35. Strauss, M., Hofhaus, G., Schröder, R. R. & Kühlbrandt, W. (2008). Dimer ribbons of ATP synthase shape the inner mitochondrial membrane. *EMBO J.* **27**, 1154-1160.

36. Dudkina, N. V., Heinemeyer, J., Keegstra, W., Boekema, E. J. & Braun, H. P. (2005). Structure of dimeric ATP synthase from mitochondria: an angular association of monomers induces the strong curvature of the inner membrane. *FEBS Lett.* **579**, 5769-5772.

37. Arselin, G., Vaillier, J., Salin, B., Schaeffer, J., Giraud, M. F., Dautant, A., Brèthes, D. & Velours, J. (2004). The modulation in subunits e and g amounts of yeast ATP synthase modifies mitochondrial cristae morphology. *J. Biol. Chem.* **279**, 40392-40399.

38. Amutha, B., Gordon, D. M., Gu, Y. & Pain, D. (2004). A novel role of Mgm1p, a dynamin-related GTPase, in ATP synthase assembly and cristae formation/maintenance. *Biochem. J.* **381**, 19-23.

39. Crofts, A. R. (2004). The cytochrome bc1 complex: function in the context of structure. *Annu Rev Physiol* **66**, 689-733.

40. Fiedorczuk, K., Letts, J. A., Degliesposti, G., Kaszuba, K., Skehel, M. & Sazanov, L. A. (2016). Atomic structure of the entire mammalian mitochondrial complex I. *Nature* **538**, 406-410.

41. Zhu, J., Vinothkumar, K. R. & Hirst, J. (2016). Structure of mammalian respiratory complex I. *Nature* **536**, 354-358.

42. Huang, J. & Fraser, M. E. (2016). Structural basis for the binding of succinate to succinyl-CoA synthetase. *Acta Crystallogr D Struct Biol* **72**, 912-921.

43. Watmough, N. J. & Frerman, F. E. (2010). The electron transfer flavoprotein: ubiquinone oxidoreductases. *Biochim. Biophys. Acta* **1797**, 1910-1916.

44. Crofts, A. R., Holland, J. T., Victoria, D., Kolling, D. R., Dikanov, S. A., Gilbreth, R., Lhee, S., Kuras, R. & Kuras, M. G. (2008). The Q-cycle reviewed: How well does a monomeric mechanism of the bc(1) complex account for the function of a dimeric complex. *Biochim. Biophys. Acta* **1777**, 1001-1019.

45. Abramson, J., Svensson-Ek, M., Byrne, B. & Iwata, S. (2001). Structure of cytochrome c oxidase: a comparison of the bacterial and mitochondrial enzymes. *Biochim. Biophys. Acta* **1544**, 1-9.

46. Shoubridge, E. A. (2012). Supersizing the mitochondrial respiratory chain. *Cell Metab* **15**, 271-272.

47. Medvedev, E. S. & Stuchebrukhov, A. A. (2014). Mechanisms of generation of local ΔpH in mitochondria and bacteria. *Biochemistry (Mosc)* **79**, 425-434.

48. Lapuente-Brun, E., Moreno-Loshuertos, R., Acín-Pérez, R., Latorre-Pellicer, A., Colás, C., Balsa, E., Perales-Clemente, E., Quirós, P. M., Calvo, E., Rodríguez-Hernández, M. A., Navas, P., Cruz, R., Carracedo, Á., López-Otín, C., Pérez-Martos, A., Fernández-Silva, P., Fernández-Vizarra, E. & Enríquez, J. A. (2013). Supercomplex assembly determines electron flux in the mitochondrial electron transport chain. *Science* **340**, 1567-1570.

49. Letts JA, F., K, Sazanov, LA (2016). The architecture of respiratory supercomplexes. *Nature* **537**, 664-648.

50. Schägger, H. & Pfeiffer, K. (2001). The ratio of oxidative phosphorylation complexes I-V in bovine heart mitochondria and the composition of respiratory chain supercomplexes. *J. Biol. Chem.* **276**, 37861-37867.

51. Yu-Wai-Man, P., Griffiths, P. G., Hudson, G. & Chinnery, P. F. (2009). Inherited mitochondrial optic neuropathies. *J. Med. Genet.* **46**, 145-158.

52. Bonilla, E., Tanji, K., Hirano, M., Vu, T. H., DiMauro, S. & Schon, E. A. (1999). Mitochondrial involvement in Alzheimer's disease. *Biochim. Biophys. Acta* **1410**, 171-182.

53. Beck, S. J., Guo, L., Phensy, A., Tian, J., Wang, L., Tandon, N., Gauba, E., Lu, L., Pascual, J. M., Kroener, S. & Du, H. (2016). Deregulation of mitochondrial F_1F_O-ATP synthase via OSCP in Alzheimer's disease. *Nat Commun* **7**, 11483.

54. Züchner, S., Mersiyanova, I. V., Muglia, M., Bissar-Tadmouri, N., Rochelle, J., Dadali, E. L., Zappia, M., Nelis, E., Patitucci, A., Senderek, J., Parman, Y., Evgrafov, O., Jonghe, P. D., Takahashi, Y., Tsuji, S., Pericak-Vance, M. A., Quattrone, A., Battaloglu, E., Polyakov, A. V., Timmerman, V., Schröder, J. M., Vance, J. M. & Battologlu, E. (2004). Mutations in the mitochondrial GTPase mitofusin 2 cause Charcot-Marie-Tooth neuropathy type 2A. *Nat. Genet.* **36**, 449-451.

55. Gakh, O., Bedekovics, T., Duncan, S. F., Smith, D. Y., Berkholz, D. S. & Isaya, G. (2010). Normal and Friedreich ataxia cells express different isoforms of frataxin with complementary roles in iron-sulfur cluster assembly. *J. Biol. Chem.* **285**, 38486-38501.

56. Ghezzi, D. & Zeviani, M. (2012). Assembly factors of human mitochondrial respiratory chain complexes: physiology and pathophysiology. *Adv. Exp. Med. Biol.* **748**, 65-106.

57. Ghezzi, D., Goffrini, P., Uziel, G., Horvath, R., Klopstock, T., Lochmüller, H., D'Adamo, P., Gasparini, P., Strom, T. M., Prokisch, H., Invernizzi, F., Ferrero, I. & Zeviani, M. (2009). SDHAF1, encoding a LYR complex-II specific assembly factor, is mutated in SDH-defective infantile leukoencephalopathy. *Nat. Genet.* **41**, 654-656.

58. Dahl, H. H. (1998). Getting to the nucleus of mitochondrial disorders: identification of respiratory chain-enzyme genes causing Leigh syndrome. *Am. J. Hum. Genet.* **63**, 1594-1597.

59. Hoefs, S. J., Dieteren, C. E., Distelmaier, F., Janssen, R. J., Epplen, A., Swarts, H. G., Forkink, M., Rodenburg, R. J., Nijtmans, L. G., Willems, P. H., Smeitink, J. A. & van den Heuvel, L. P. (2008). NDUFA2 complex I mutation leads to Leigh disease. *Am. J. Hum. Genet.* **82**, 1306-1315.

60. McKenzie, M., Liolitsa, D., Akinshina, N., Campanella, M., Sisodiya, S., Hargreaves, I., Nirmalananthan, N., Sweeney, M. G., Abou-Sleiman, P. M., Wood, N. W., Hanna, M. G. & Duchen, M. R. (2007). Mitochondrial ND5 gene variation associated with encephalomyopathy and mitochondrial ATP consumption. *J. Biol. Chem.* **282**, 36845-36852.

61. Hao, H. X., Khalimonchuk, O., Schraders, M., Dephoure, N., Bayley, J. P., Kunst, H., Devilee, P., Cremers, C. W., Schiffman, J. D., Bentz, B. G., Gygi, S. P., Winge,

D. R., Kremer, H. & Rutter, J. (2009). SDH5, a gene required for flavination of succinate dehydrogenase, is mutated in paraganglioma. *Science* **325**, 1139-1142.

62. McLelland, G. L., Soubannier, V., Chen, C. X., McBride, H. M. & Fon, E. A. (2014). Parkin and PINK1 function in a vesicular trafficking pathway regulating mitochondrial quality control. *EMBO J.* **33**, 282-295.

63. Jonckheere, A. I., Smeitink, J. A. & Rodenburg, R. J. (2012). Mitochondrial ATP synthase: architecture, function and pathology. *J. Inherit. Metab. Dis.* **35**, 211-225.

64. Sgarbi, G., Baracca, A., Lenaz, G., Valentino, L. M., Carelli, V. & Solaini, G. (2006). Inefficient coupling between proton transport and ATP synthesis may be the pathogenic mechanism for NARP and Leigh syndrome resulting from the T8993G mutation in mtDNA. *Biochem. J.* **395**, 493-500.

65. Ware, S. M., El-Hassan, N., Kahler, S. G., Zhang, Q., Ma, Y. W., Miller, E., Wong, B., Spicer, R. L., Craigen, W. J., Kozel, B. A., Grange, D. K. & Wong, L. J. (2009). Infantile cardiomyopathy caused by a mutation in the overlapping region of mitochondrial ATPase 6 and 8 genes. *J. Med. Genet.* **46**, 308-314.

66. Palmer, D. N., Fearnley, I. M., Walker, J. E., Hall, N. A., Lake, B. D., Wolfe, L. S., Haltia, M., Martinus, R. D. & Jolly, R. D. (1992). Mitochondrial ATP synthase subunit c storage in the ceroid-lipofuscinoses (Batten disease). *Am. J. Med. Genet.* **42**, 561-567.

67. Mayr, J. A., Havlícková, V., Zimmermann, F., Magler, I., Kaplanová, V., Jesina, P., Pecinová, A., Nusková, H., Koch, J., Sperl, W. & Houstek, J. (2010). Mitochondrial ATP synthase deficiency due to a mutation in the ATP5E gene for the F_1 ε subunit. *Hum. Mol. Genet.* **19**, 3430-3439.

68. Wang, Z. G., White, P. S. & Ackerman, S. H. (2001). Atp11p and Atp12p are assembly factors for the F_1-ATPase in human mitochondria. *J. Biol. Chem.* **276**,

30773-30778.

69. Wong, L. J. (2007). Diagnostic challenges of mitochondrial DNA disorders. *Mitochondrion* **7**, 45-52.

70. Stock, D., Gibbons, C., Arechaga, I., Leslie, A. G. W. & Walker, J. E. (2000). The rotary mechanism of ATP synthase. *Curr Opin Struct Biol* 672-679.

71. Vinothkumar, K. R., Montgomery, M. G., Liu, S. & Walker, J. E. (2016). Structure of the mitochondrial ATP synthase from Pichia angusta determined by electron cryo-microscopy. *Proc. Natl. Acad. Sci. U. S. A.* **113**, 12709-12714.

72. Chen, R., Fearnley, I. M., Palmer, D. N. & Walker, J. E. (2004). Lysine 43 is trimethylated in subunit c from bovine mitochondrial ATP synthase and in storage bodies associated with Batten disease. *J. Biol. Chem.* **279**, 21883-21887.

73. Palmer, D. N. (2015). The relevance of the storage of subunit c of ATP synthase in different forms and models of Batten disease (NCLs). *Biochim. Biophys. Acta* **1852**, 2287-2291.

74. De Meirleir, L., Seneca, S., Lissens, W., De Clercq, I., Eyskens, F., Gerlo, E., Smet, J. & Van Coster, R. (2004). Respiratory chain complex V deficiency due to a mutation in the assembly gene ATP12. *J. Med. Genet.* **41**, 120-124.

75. Ackerman, S. H. (2002). Atp11p and Atp12p are chaperones for F_1-ATPase biogenesis in mitochondria. *Biochim. Biophys. Acta* **1555**, 101-105.

76. Halestrap, A. P. (2009). What is the mitochondrial permeability transition pore. *J Mol Cell Cardiol* **46**, 821-831.

77. Halestrap, A. P. & Pasdois, P. (2009). The role of the mitochondrial permeability transition pore in heart disease. *Biochim. Biophys. Acta* **1787**, 1402-1415.

78. Crompton, M. (1999). The mitochondrial permeability transition pore and its role in cell death. *Biochem. J.* **341**, 233-249.

79. Di Lisa, F. & Bernardi, P. (2006). Mitochondria and ischemia-reperfusion injury of the heart: fixing a hole. *Cardiovasc. Res.* **70**, 191-199.

80. Pell, V. R., Chouchani, E. T., Frezza, C., Murphy, M. P. & Krieg, T. (2016). Succinate metabolism: a new therapeutic target for myocardial reperfusion injury. *Cardiovasc. Res.* **111**, 134-141.

81. Chouchani, E. T., Pell, V. R., Gaude, E., Aksentijević, D., Sundier, S. Y., Robb, E. L., Logan, A., Nadtochiy, S. M., Ord, E. N., Smith, A. C., Eyassu, F., Shirley, R., Hu, C. H., Dare, A. J., James, A. M., Rogatti, S., Hartley, R. C., Eaton, S., Costa, A. S., Brookes, P. S., Davidson, S. M., Duchen, M. R., Saeb-Parsy, K., Shattock, M. J., Robinson, A. J., Work, L. M., Frezza, C., Krieg, T. & Murphy, M. P. (2014). Ischaemic accumulation of succinate controls reperfusion injury through mitochondrial ROS. *Nature* **515**, 431-435.

82. Walker, J. E. (2013). The ATP synthase: the understood, the uncertain and the unknown. *Biochem. Soc. Trans.* **41**, 1-16.

83. Koumandou, V. L. & Kossida, S. (2014). Evolution of the F_OF_1 ATP synthase complex in light of the patchy distribution of different bioenergetic pathways across prokaryotes. *PLoS Comput. Biol.* **10**, e1003821.

84. Walker, J. E., Lutter, R. E., Dupuis, J. A. & Runswick, M. J. (1991). Identification of the subunits of F_1F_O-ATPase from bovine heart mitochondria. *Biochemistry* **30**, 5369-5378.

85. Runswick, M. J., Bason, J. V., Montgomery, M. G., Robinson, G. C., Fearnley, I. M. & Walker, J. E. (2013). The affinity purification and characterization of ATP synthase complexes from mitochondria. *Open Biol.* **3**, 120160.

86. Liu, S., Charlesworth, T. J., Bason, J. V., Montgomery, M. G., Harbour, M. E., Fearnley, I. M. & Walker, J. E. (2015). The purification and characterization of ATP

synthase complexes from the mitochondria of four fungal species. *Biochem. J.* **468**, 167-175.

87. Collinson, I. R., Runswick, M. J., Buchanan, S. K., Fearnley, I. M., Skehel, J. M., van Raaij, M. J., Griffiths, D. E. & Walker, J. E. (1994). F_O membrane domain of ATP synthase from bovine heart mitochondria: purification, subunit composition, and reconstitution with F_1-ATPase. *Biochemistry* **33**, 7971-7978.

88. Gledhill, J. R., Montgomery, M. G., Leslie, A. G. W. & Walker, J. E. (2007). How the regulatory protein, IF_1, inhibits F_1-ATPase from bovine mitochondria. *Proc. Natl. Acad. Sci. U. S. A.* **104**, 15671-15676.

89. Bason, J. V., Montgomery, M. G., Leslie, A. G. W. & Walker, J. E. (2014). Pathway of binding of the intrinsically disordered mitochondrial inhibitor protein to F_1-ATPase. *Proc. Natl. Acad. Sci. U. S. A.* **111**, 11305-11310.

90. Walker, J. E., Collinson, I. R., Van Raaij, M. J. & Runswick, M. J. (1995). Structural analysis of ATP synthase from bovine heart mitochondria. *Methods Enzymol.* **260**, 163-190.

91. Lee, J., Ding, S., Walpole, T. B., Holding, A. N., Montgomery, M. G., Fearnley, I. M. & Walker, J. E. (2015). Organization of subunits in the membrane domain of the bovine F-ATPase revealed by covalent cross-linking. *J. Biol. Chem.* **290**, 13308-13320.

92. Baker, L. A., Watt, I. N., Runswick, M. J., Walker, J. E. & Rubinstein, J. L. (2012). Arrangement of subunits in intact mammalian mitochondrial ATP synthase determined by cryo-EM. *Proc. Natl. Acad. Sci. U. S. A.* **109**, 11675-11680.

93. Rubinstein, J. L., Walker, J. E. & Henderson, R. (2003). Structure of the mitochondrial ATP synthase by electron cryomicroscopy. *EMBO J.* **22**, 6182-6192.

94. Walker, J. E., Runswick, M. J. & Poulter, L. (1987). ATP synthase from bovine

mitochondria. The characterization and sequence analysis of two membrane-associated subunits and of the corresponding cDNAs. *J. Mol. Biol.* **197**, 89-100.

95. Buchanan, S. K. & Walker, J. E. (1996). Large-scale chromatographic purification of F_1F_O-ATPase and complex I from bovine heart mitochondria. *Biochem. J.* **318**, 343-349.

96. Collinson, I. R., Skehel, J. M., Fearnley, I. M., Runswick, M. J. & Walker, J. E. (1996). The F_1F_O-ATPase complex from bovine heart mitochondria: the molar ratio of the subunits in the stalk region linking the F_1 and F_O domains. *Biochemistry* **35**, 12640-12646.

97. Carbajo, R. J., Kellas, F. A., Runswick, M. J., Montgomery, M. G., Walker, J. E. & Neuhaus, D. (2005). Structure of the F_1-binding domain of the stator of bovine F_1F_O-ATPase and how it binds an α-subunit. *J. Mol. Biol.* **351**, 824-838.

98. Fearnley, I. M. & Walker, J. E. (1986). Two overlapping genes in bovine mitochondrial DNA encode membrane components of ATP synthase. *EMBO J.* **5**, 2003-2008.

99. Walker, J. E. L., RE Dupuis, JA Runswick, MJ (1991). Identification of the subunits of F_1F_O-ATPase from bovine heart mitochondria. *Biochemistry* 5369-5378.

100. Chen, R., Runswick, M. J., Carroll, J., Fearnley, I. M. & Walker, J. E. (2007). Association of two proteolipids of unknown function with ATP synthase from bovine heart mitochondria. *FEBS Lett.* **581**, 3145-3148.

101. Duncan, A. L., Robinson, A. J. & Walker, J. E. (2016). Cardiolipin binds selectively but transiently to conserved lysine residues in the rotor of metazoan ATP synthases. *Proc. Natl. Acad. Sci. U. S. A.* **113**, 8687-8692.

102. Stock, D., Leslie, A. G. W. & Walker, J. E. (1999). Molecular architecture of the rotary motor in ATP synthase. *Science* **286**, 1700-1705.

103. Arechaga, I., Butler, P. J. G. & Walker, J. E. (2002). Self-assembly of ATP synthase subunit c rings. *FEBS Lett.* **515**, 189-193.

104. Zhou, A., Rohou, A., Schep, D. G., Bason, J. V., Montgomery, M. G., Walker, J. E., Grigorieff, N. & Rubinstein, J. L. (2015). Structure and conformational states of the bovine mitochondrial ATP synthase by cryo-EM. *Elife* **4**, e10180.

105. Morales-Rios, E., Montgomery, M. G., Leslie, A. G. W. & Walker, J. E. (2015). Structure of ATP synthase from *Paracoccus denitrificans* determined by X-ray crystallography at 4.0 Å resolution. *Proc. Natl. Acad. Sci. U. S. A.* **112**, 13231-13236.

106. Collinson, I. R., van Raaij, M. J., Runswick, M. J., Fearnley, I. M., Skehel, J. M., Orriss, G. L., Miroux, B. & Walker, J. E. (1994). ATP synthase from bovine heart mitochondria. *In vitro* assembly of a stalk complex in the presence of F_1-ATPase and in its absence. *J. Mol. Biol.* **242**, 408-421.

107. Carbajo, R. J., Kellas, F. A., Yang, J. C., Runswick, M. J., Montgomery, M. G., Walker, J. E. & Neuhaus, D. (2007). How the N-terminal domain of the OSCP subunit of bovine F_1F_O-ATP synthase interacts with the N-terminal region of an α-subunit. *J. Mol. Biol.* **368**, 310-318.

108. Dickson, V. K., Silvester, J. A., Fearnley, I. M., Leslie, A. G. W. & Walker, J. E. (2006). On the structure of the stator of the mitochondrial ATP synthase. *EMBO J.* **25**, 2911-2918.

109. Abrahams, J. P., Leslie, A. G. W., Lutter, R. & Walker, J. E. (1994). Structure at 2.8 Å resolution of F_1-ATPase from bovine heart mitochondria. *Nature* **370**, 621-628.

110. Boyer, P. D. (1993). The binding change mechanism for ATP synthase-some probabilities and possibilities. *Biochim. Biophys. Acta* **1140**, 215-250.

111. Menz, R. I., Walker, J. E. & Leslie, A. G. W. (2001). Structure of bovine mitochondrial F_1-ATPase with nucleotide bound to all three catalytic sites:

implications for the mechanism of rotary catalysis. *Cell* **106**, 331-341.

112. Bowler, M. W., Montgomery, M. G., Leslie, A. G. W. & Walker, J. E. (2006). How azide inhibits ATP hydrolysis by the F-ATPases. *Proc. Natl. Acad. Sci. U. S. A.* **103**, 8646-8649.

113. Bowler, M. W., Montgomery, M. G., Leslie, A. G. W. & Walker, J. E. (2007). Ground state structure of F_1-ATPase from bovine heart mitochondria at 1.9 Å resolution. *J. Biol. Chem.* **282**, 14238-14242.

114. Rees, D. M., Montgomery, M. G., Leslie, A. G. W. & Walker, J. E. (2012). Structural evidence of a new catalytic intermediate in the pathway of ATP hydrolysis by F_1-ATPase from bovine heart mitochondria. *Proc. Natl. Acad. Sci. U. S. A.* **109**, 11139-11143.

115. Kabaleeswaran, V., Puri, N., Walker, J. E., Leslie, A. G. W. & Mueller, D. M. (2006). Novel features of the rotary catalytic mechanism revealed in the structure of yeast F_1 ATPase. *EMBO J.* **25**, 5433-5442.

116. Ackerman, S. H. & Tzagoloff, A. (1990). Identification of two nuclear genes (ATP11, ATP12) required for assembly of the yeast F_1-ATPase. *Proc. Natl. Acad. Sci. U. S. A.* **87**, 4986-4990.

117. Straffon, A. F., Prescott, M., Nagley, P. & Devenish, R. J. (1998). The assembly of yeast mitochondrial ATP synthase: subunit depletion in vivo suggests ordered assembly of the stalk subunits b, OSCP and d. *Biochim. Biophys. Acta* **1371**, 157-162.

118. Fujikawa, M., Sugawara, K., Tanabe, T. & Yoshida, M. (2015). Assembly of human mitochondrial ATP synthase through two separate intermediates, F_1-c-ring and b-e-g complex. *FEBS Lett.* **589**, 2707-2712.

119. Osman, C., Wilmes, C., Tatsuta, T. & Langer, T. (2007). Prohibitins interact genetically with Atp23, a novel processing peptidase and chaperone for the F_1F_O-

ATP synthase. *Mol. Biol. Cell* **18**, 627-635.

120. Rak, M., Gokova, S. & Tzagoloff, A. (2011). Modular assembly of yeast mitochondrial ATP synthase. *EMBO J.* **30**, 920-930.

121. Rühle, T. & Leister, D. (2015). Assembly of F_1F_O-ATP synthases. *Biochim. Biophys. Acta* **1847**, 849-860.

122. Wittig, I., Meyer, B., Heide, H., Steger, M., Bleier, L., Wumaier, Z., Karas, M. & Schägger, H. (2010). Assembly and oligomerization of human ATP synthase lacking mitochondrial subunits a and A6L. *Biochim. Biophys. Acta* **1797**, 1004-1011.

123. Nijtmans, L. G., Henderson, N. S., Attardi, G. & Holt, I. J. (2001). Impaired ATP synthase assembly associated with a mutation in the human ATP synthase subunit 6 gene. *J. Biol. Chem.* **276**, 6755-6762.

124. Paumard, P., Vaillier, J., Coulary, B., Schaeffer, J., Soubannier, V., Mueller, D. M., Brèthes, D., di Rago, J. P. & Velours, J. (2002). The ATP synthase is involved in generating mitochondrial cristae morphology. *EMBO J.* **21**, 221-230.

125. Ong, S. E., Blagoev, B., Kratchmarova, I., Kristensen, D. B., Steen, H., Pandey, A. & Mann, M. (2002). Stable isotope labeling by amino acids in cell culture, SILAC, as a simple and accurate approach to expression proteomics. *Mol. Cell. Proteomics* **1**, 376-386.

126. Wu, M., Neilson, A., Swift, A. L., Moran, R., Tamagnine, J., Parslow, D., Armistead, S., Lemire, K., Orrell, J., Teich, J., Chomicz, S. & Ferrick, D. A. (2007). Multiparameter metabolic analysis reveals a close link between attenuated mitochondrial bioenergetic function and enhanced glycolysis dependency in human tumor cells. *Am J Physiol Cell Physiol* **292**, C125-C136.

127. Skehan, P., Storeng, R., Scudiero, D., Monks, A., McMahon, J., Vistica, D., Warren, J. T., Bokesch, H., Kenney, S. & Boyd, M. R. (1990). New colorimetric cytotoxicity

assay for anticancer-drug screening. *J. Natl. Cancer Inst.* **82**, 1107-1112.

128. Smith, P. K., Krohn, R. I., Hermanson, G. T., Mallia, A. K., Gartner, F. H., Provenzano, M. D., Fujimoto, E. K., Goeke, N. M., Olson, B. J. & Klenk, D. C. (1985). Measurement of protein using bicinchoninic acid. *Anal. Biochem.* **150**, 76-85.

129. Klement, P., Nijtmans, L. G., Van den Bogert, C. & Houstěk, J. (1995). Analysis of oxidative phosphorylation complexes in cultured human fibroblasts and amniocytes by blue-native-electrophoresis using mitoplasts isolated with the help of digitonin. *Anal. Biochem.* **231**, 218-224.

130. Schägger, H. & von Jagow, G. (1991). Blue native electrophoresis for isolation of membrane protein complexes in enzymatically active form. *Anal. Biochem.* **199**, 223-231.

131. Laemmli, U. K. (1970). Cleavage of structural proteins during the assembly of the head of bacteriophage T4. *Nature* **227**, 680-685.

132. Shevchenko, A., Wilm, M., Vorm, O. & Mann, M. (1996). Mass spectrometric sequencing of proteins silver-stained polyacrylamide gels. *Anal. Chem.* **68**, 850-858.

133. Towbin, H., Staehelin, T. & Gordon, J. (1992). Electrophoretic transfer of proteins from polyacrylamide gels to nitrocellulose sheets: procedure and some applications. 1979. *Biotechnology* **24**, 145-149.

134. Shevchenko, A., Tomas, H., Havlis, J., Olsen, J. V. & Mann, M. (2006). In-gel digestion for mass spectrometric characterization of proteins and proteomes. *Nat. Protoc.* **1**, 2856-2860.

135. Perkins, D. N., Pappin, D. J., Creasy, D. M. & Cottrell, J. S. (1999). Probability-based protein identification by searching sequence databases using mass spectrometry data. *Electrophoresis* **20**, 3551-3567.

136. Cox, J. & Mann, M. (2008). MaxQuant enables high peptide identification rates, individualized p.p.b.-range mass accuracies and proteome-wide protein quantification. *Nat. Biotechnol.* **26**, 1367-1372.

137. Cox, J., Neuhauser, N., Michalski, A., Scheltema, R. A., Olsen, J. V. & Mann, M. (2011). Andromeda: a peptide search engine integrated into the MaxQuant environment. *J. Proteome Res.* **10**, 1794-1805.

138. Ford, H. (2016). Studies of the assembly of ATP synthase in human mitochondria. *PhD thesis, Cambridge University*

139. Tyanova, S., Temu, T., Sinitcyn, P., Carlson, A., Hein, M. Y., Geiger, T., Mann, M. & Cox, J. (2016). The Perseus computational platform for comprehensive analysis of (prote)omics data. *Nat Methods* **13**, 731-740.

140. Ran, F. A., Hsu, P. D., Wright, J., Agarwala, V., Scott, D. A. & Zhang, F. (2013). Genome engineering using the CRISPR-Cas9 system. *Nat. Protoc.* **8**, 2281-2308.

141. International, H. G. S. C. (2004). Finishing the euchromatic sequence of the human genome. *Nature* **431**, 931-945.

142. Zeng, X., Barros, M. H., Shulman, T. & Tzagoloff, A. (2008). ATP25, a new nuclear gene of Saccharomyces cerevisiae required for expression and assembly of the Atp9p subunit of mitochondrial ATPase. *Mol. Biol. Cell* **19**, 1366-1377.

143. Tzagoloff, A., Barrientos, A., Neupert, W. & Herrmann, J. M. (2004). Atp10p assists assembly of Atp6p into the F_O unit of the yeast mitochondrial ATPase. *J. Biol. Chem.* **279**, 19775-19780.

144. Kucharczyk, R., Zick, M., Bietenhader, M., Rak, M., Couplan, E., Blondel, M., Caubet, S. D. & di Rago, J. P. (2009). Mitochondrial ATP synthase disorders: molecular mechanisms and the quest for curative therapeutic approaches. *Biochim. Biophys. Acta* **1793**, 186-199.

145. Hahn, A., Parey, K., Bublitz, M., Mills, D. J., Zickermann, V., Vonck, J., Kühlbrandt, W. & Meier, T. (2016). Structure of a complete ATP Synthase dimer reveals the molecular basis of inner mitochondrial membrane morphology. *Mol. Cell* **63**, 445-456.

146. Lytovchenko, O., Naumenko, N., Oeljeklaus, S., Schmidt, B., von der Malsburg, K., Deckers, M., Warscheid, B., van der Laan, M. & Rehling, P. (2014). The INA complex facilitates assembly of the peripheral stalk of the mitochondrial F_1F_o-ATP synthase. *EMBO J.* **33**, 1624-1638.

147. Stroud, D. A. & Ryan, M. T. (2014). Stalking the mitochondrial ATP synthase: Ina found guilty by association. *EMBO J.* **33**, 1617-1618.

148. Walpole, T. B., Palmer, D. N., Jiang, H., Ding, S., Fearnley, I. M. & Walker, J. E. (2015). Conservation of complete trimethylation of lysine-43 in the rotor ring of c-subunits of metazoan adenosine triphosphate (ATP) synthases. *Mol. Cell. Proteomics* **14**, 828-840.

149. Buchet, K. & Godinot, C. (1998). Functional F_1-ATPase essential in maintaining growth and membrane potential of human mitochondrial DNA-depleted rho^0 cells. *J. Biol. Chem.* **273**, 22983-22989.

150. Appleby, R. D., Porteous, W. K., Hughes, G., James, A. M., Shannon, D., Wei, Y. H. & Murphy, M. P. (1999). Quantitation and origin of the mitochondrial membrane potential in human cells lacking mitochondrial DNA. *Eur. J. Biochem.* **262**, 108-116.

151. Wagner, K., Rehling, P., Sanjuán Szklarz, L. K., Taylor, R. D., Pfanner, N. & van der Laan, M. (2009). Mitochondrial F_1F_O-ATP synthase: the small subunits e and g associate with monomeric complexes to trigger dimerization. *J. Mol. Biol.* **392**, 855-861.

152. Ohsakaya, S., Fujikawa, M., Hisabori, T. & Yoshida, M. (2011). Knockdown of

DAPIT (diabetes-associated protein in insulin-sensitive tissue) results in loss of ATP synthase in mitochondria. *J. Biol. Chem.* **286**, 20292-20296.

153. Azzolin, L., von Stockum, S., Basso, E., Petronilli, V., Forte, M. A. & Bernardi, P. (2010). The mitochondrial permeability transition from yeast to mammals. *FEBS Lett.* **584**, 2504-2509.

154. Broekemeier, K. M., Schmid, P. C., Schmid, H. H. & Pfeiffer, D. R. (1985). Effects of phospholipase A2 inhibitors on ruthenium red-induced Ca^{2+} release from mitochondria. *J. Biol. Chem.* **260**, 105-113.

155. Crompton, M. & Costi, A. (1988). Kinetic evidence for a heart mitochondrial pore activated by Ca^{2+}, inorganic phosphate and oxidative stress. A potential mechanism for mitochondrial dysfunction during cellular Ca2+ overload. *Eur. J. Biochem.* **178**, 489-501.

156. Al-Nasser, I. & Crompton, M. (1986). The reversible Ca^{2+}-induced permeabilization of rat liver mitochondria. *Biochem. J.* **239**, 19-29.

157. Crompton, M., Virji, S. & Ward, J. M. (1998). Cyclophilin-D binds strongly to complexes of the voltage-dependent anion channel and the adenine nucleotide translocase to form the permeability transition pore. *Eur. J. Biochem.* **258**, 729-735.

158. Kokoszka, J. E., Waymire, K. G., Levy, S. E., Sligh, J. E., Cai, J., Jones, D. P., MacGregor, G. R. & Wallace, D. C. (2004). The ADP/ATP translocator is not essential for the mitochondrial permeability transition pore. *Nature* **427**, 461-465.

159. Krauskopf, A., Eriksson, O., Craigen, W. J., Forte, M. A. & Bernardi, P. (2006). Properties of the permeability transition in VDAC1(-/-) mitochondria. *Biochim. Biophys. Acta* **1757**, 590-595.

160. Giorgio, V., von Stockum, S., Antoniel, M., Fabbro, A., Fogolari, F., Forte, M., Glick, G. D., Petronilli, V., Zoratti, M., Szabó, I., Lippe, G. & Bernardi, P. (2013). Dimers

of mitochondrial ATP synthase form the permeability transition pore. *Proc. Natl. Acad. Sci. U. S. A.* **110**, 5887-5892.

161. Alavian, K. N., Beutner, G., Lazrove, E., Sacchetti, S., Park, H. A., Licznerski, P., Li, H., Nabili, P., Hockensmith, K., Graham, M., Porter, G. A. & Jonas, E. A. (2014). An uncoupling channel within the c-subunit ring of the F_1F_O ATP synthase is the mitochondrial permeability transition pore. *Proc. Natl. Acad. Sci. U. S. A.* **111**, 10580-10585.
162. Bonora, M., Bononi, A., De Marchi, E., Giorgi, C., Lebiedzinska, M., Marchi, S., Patergnani, S., Rimessi, A., Suski, J. M., Wojtala, A., Wieckowski, M. R., Kroemer, G., Galluzzi, L. & Pinton, P. (2013). Role of the c subunit of the F_O ATP synthase in mitochondrial permeability transition. *Cell Cycle* **12**, 674-683.
163. He, J., Ford, H. C., Carroll, J., Ding, S., Fearnley, I. M. & Walker, J. E. (2017). Persistence of the mitochondrial permeability transition in the absence of subunit c of human ATP synthase. *PNAS* **Early Edition**, 1-6.
164. Shabalina, S. A. & Koonin, E. V. (2008). Origins and evolution of eukaryotic RNA interference. *Trends Ecol Evol* **23**, 578-587.
165. Mojica, F. J. & Montoliu, L. (2016). On the Origin of CRISPR-Cas Technology: From Prokaryotes to Mammals. *Trends Microbiol.* **24**, 811-820.
166. Mojica, F. J., Díez-Villaseñor, C., García-Martínez, J. & Soria, E. (2005). Intervening sequences of regularly spaced prokaryotic repeats derive from foreign genetic elements. *J. Mol. Evol.* **60**, 174-182.

Appendix I – Reagents and chemicals

Reagent	Product code	Source
1-palmitoyl-2-oleoyl-sn-glycero-3-phosphocholine	840051C	Avanti Polar Lipids, AL, USA
1-palmitoyl-2-oleoyl-sn-glycero-3-phosphoethanolamine	850757C	Avanti Polar Lipids, AL, USA
1-palmitoyl-2-oleoyl-sn-glycero-3-phosphoglycerol	840457C	Avanti Polar Lipids, AL, USA
10-20% acrylamide gradient Tris-glycine SDS PAGE gel	EC61355BOX	ThermoFisher Scientific, Hemel Hempstead, UK
143B osteosarcoma cells	CRL-8303	ATCC, Teddington, UK
2-Deoxy-D-glucose	1001469905	ThermoFisher Scientific, Hemel Hempstead, UK
3-12 % acrylamide gradient bis-Tris native PAGE gel	BN1003BOX	ThermoFisher Scientific, Hemel Hempstead, UK
A8 NC slide	942-0003	ChemoMetec, Lillerod, Denmark
Acetic acid	20104334	VWR Chemicals, Lutterworth, UK
Acetonitrile	H33387	Alfa Aesar, Heysham, UK
Acrylamide/bis-acrylamide 20% w/v 37.5:1 solution	20-2100-10	Severn Biotech, Kidderminster, UK
All blue prestained precision plus protein standards	161-0373	Biorad, Hemel Hempstead, UK
AllStars negative control siRNA	1027281	QIAGEN, Manchester, UK
alpha-cyano-4-hydroxy-trans-cinnamic acid	476870-2G	Sigma-Aldrich, Poole, UK
Ammonium persulfate	A3678-25G	Sigma-Aldrich, Poole, UK
Antimycin A	B16715	Seahorse Bioscience, MA, USA
ATP	1191-50GM	Millipore, MA, USA
ATP synthase immunocapture kit	ab109715	AbCam, Cambridge, UK
ATP synthase subunit 6.8 kDa antibody	147041AP	ProteinTech Europe, Manchester, UK
ATP synthase subunit-6.8 kDa PL qPCR forward primer	8002836950-003*	Sigma-Aldrich, Poole, UK
ATP synthase subunit-6.8 kDa PL qPCR probe	8002836900-002*	Sigma-Aldrich, Poole, UK
ATP synthase subunit-6.8 kDa PL qPCR reverse primer	8002836950-006*	Sigma-Aldrich, Poole, UK
ATP synthase subunit-DAPIT antibody	177161AP	ProteinTech Europe, Manchester, UK
ATP synthase subunit-DAPIT qPCR forward primer	8002836950-001*	Sigma-Aldrich, Poole, UK
ATP synthase subunit-DAPIT qPCR probe	8002836900-001*	Sigma-Aldrich, Poole, UK
ATP synthase subunit-DAPIT qPCR reverse primer	8002836950-002*	Sigma-Aldrich, Poole, UK
ATP synthase subunit-e antibody	HPA035010	Sigma-Aldrich, Poole, UK
ATP synthase subunit-e qPCR forward primer	8003294134-003*	Sigma-Aldrich, Poole, UK
ATP synthase subunit-e qPCR probe	8003294101-001*	Sigma-Aldrich, Poole, UK
ATP synthase subunit-e qPCR reverse primer	8003294134-004*	Sigma-Aldrich, Poole, UK
ATP synthase subunit-f antibody	In-House	MRC-MBU, Cambridge, UK
ATP synthase subunit-f qPCR forward primer	8003294134-001*	Sigma-Aldrich, Poole, UK
ATP synthase subunit-f qPCR probe	8003294101-002*	Sigma-Aldrich, Poole, UK
ATP synthase subunit-f qPCR reverse primer	8003294134-002*	Sigma-Aldrich, Poole, UK
ATP synthase subunit-f synthetic oligonucleotide guide RNA1-bottom	8021207207-000140*	Sigma-Aldrich, Poole, UK
ATP synthase subunit-f synthetic oligonucleotide guide RNA1-top	8021207207-000130*	Sigma-Aldrich, Poole, UK
ATP synthase subunit-f synthetic oligonucleotide guide RNA2-bottom	8021207207-000160*	Sigma-Aldrich, Poole, UK
ATP synthase subunit-f synthetic oligonucleotide guide RNA2-top	8021207207-000150*	Sigma-Aldrich, Poole, UK
ATP synthase subunit-f synthetic oligonucleotide guide RNA5-bottom	8021207207-000180*	Sigma-Aldrich, Poole, UK

Reagent	Product code	Source
ATP synthase subunit-f synthetic oligonucleotide guide RNA6-bottom	8021207207-000200*	Sigma-Aldrich, Poole, UK
ATP synthase subunit-f synthetic oligonucleotide guide RNA6-top	8021207207-000190*	Sigma-Aldrich, Poole, UK
ATP synthase subunit-f synthetic oligonucleotide guide RNA9-bottom	8021207207-000220*	Sigma-Aldrich, Poole, UK
ATP synthase subunit-f synthetic oligonucleotide guide RNA9-top	8021207207-000210*	Sigma-Aldrich, Poole, UK
ATP synthase subunit-g antibody	In-House	MRC-MBU, Cambridge, UK
ATP synthase subunit-g qPCR forward primer	8003684726-007*	Sigma-Aldrich, Poole, UK
ATP synthase subunit-g qPCR prone	8003684775-002*	Sigma-Aldrich, Poole, UK
ATP synthase subunit-g qPCR reverse primer	8003684726-008*	Sigma-Aldrich, Poole, UK
BCA assay kit	23228	ThermoFisher Scientific, Hemel Hempstead, UK
Benzonase	D00146087	EMD Chemicals, Darmstadt, Germany
Beta actin antibody	A2228	Sigma-Aldrich, Poole, UK
Beta actin qPCR forward primer	HA04346403-010*	Sigma-Aldrich, Poole, UK
Beta actin qPCR probe	HA04346405-002*	Sigma-Aldrich, Poole, UK
Beta actin qPCR reverse primer	HA04346404-002*	Sigma-Aldrich, Poole, UK
Boric acid	31146-500G	Sigma Aldrich UK
Bromophenol blue	B/P620/44	ThermoFisher Scientific, Hemel Hempstead, UK
BSA	23288	ThermoFisher Scientific, Hemel Hempstead, UK
Calcium chloride	100704Y	VWR Chemicals, Lutterworth, UK
Cas9	M0386S	New England Biolabs, MA, USA
Cell scraper	83.183	Sarstedt, Numbrecht, Germany
Cells to CT kit	AM1729	ThermoFisher Scientific, Hemel Hempstead, UK
Chicken secondary antibody	A9046	Sigma-Aldrich, Poole, UK
Complete protease inhibitor tablets	11844600	Sigma-Aldrich, Poole, UK
Coomassie R-250	C/P540/46	ThermoFisher Scientific, Hemel Hempstead, UK
Cryovial	377267	ThermoFisher Scientific, Hemel Hempstead, UK
D-glucose	G0/500/53	ThermoFisher Scientific, Hemel Hempstead, UK
DDM	09003-C	Glycon Biochemicals, Luckenwalde, Germany
Dialised FBS	F0392-500ML	Sigma-Aldrich, Poole, UK
Digitonin	300410	Sigma-Aldrich, Poole, UK
DMEM	41966-052	ThermoFisher Scientific, Hemel Hempstead, UK
DMSO	D2438-5X10ML	Sigma-Aldrich, Poole, UK
DNA ladder	15613-029	ThermoFisher Scientific, Hemel Hempstead, UK
DNAse I buffer	B0303S	ThermoFisher Scientific, Hemel Hempstead, UK
dPBS	14190-094	ThermoFisher Scientific, Hemel Hempstead, UK
DTT	DTT010	ThermoFisher Scientific, Hemel Hempstead, UK
ECL reagent	RPN2232	GE Healthcare, Amersham, UK
EDTA	EDTA6000	Formedium, Norfolk, UK
Ethanol	02875-2.5L	Sigma-Aldrich, Poole, UK
FBS	F0392	Sigma-Aldrich, Poole, UK
FCCP	B16715	Seahorse Bioscience, MA, USA
Freezing container	5100-0001	ThermoFisher Scientific, Hemel Hempstead, UK
Fuji Super RX-N X-ray film	47410 19289	FUJIFILM, Bedford, UK

Reagent	Product code	Source
Glycerol	24388320	VWR Chemicals, Lutterworth, UK
Glycine	30-21-60	Severn Biotech, Kidderminster, UK
HAP1 chronic myelogenous leukemia cells	C665	Horizon Discovery, Cambridge, UK
HBSS	14170088	ThermoFisher Scientific, Hemel Hempstead, UK
Heavy L-arginine	CNLM-539-H-PK	Cambridge Isotope Laboratories, MA, USA
Heavy L-lysine	CNLM-291-H-PK	Cambridge Isotope Laboratories, MA, USA
HPLC water	W/0106/17	ThermoFisher Scientific, Hemel Hempstead, UK
Hydrochloric acid	SG.1.18	ThermoFisher Scientific, Hemel Hempstead, UK
Iodoacetamide	RPN6302	GE Healthcare, Amersham, UK
KOD hot start DNA polymerase	71086-4	Millipore, Darmstadt, Germany
L-Proline	88430	ThermoFisher Scientific, Hemel Hempstead, UK
LB ampicillin agar plates	LMM0202	Formedium, Norfolk, UK
LB medium	LMM0102	Formedium, Norfolk, UK
Light L-Arginine	A8094	Sigma-Aldrich, Poole, UK
Light L-Lysine	L8662	Sigma-Aldrich, Poole, UK
Lipofectamine-2000	11668019	ThermoFisher Scientific, Hemel Hempstead, UK
Lipofectamine-3000	L3000008	ThermoFisher Scientific, Hemel Hempstead, UK
Magnesium chloride	101494V	VWR Chemicals, Lutterworth, UK
Marvel skimmed milk powder	3021601	Sigma-Aldrich, Poole, UK
Methanol	M/4000/17	ThermoFisher Scientific, Hemel Hempstead, UK
Micro-Spin column	89879	ThermoFisher Scientific, Hemel Hempstead, UK
Mouse secondary antibody	NXA931	GE Healthcare, Amersham, UK
Native mark	LC0725	ThermoFisher Scientific, Hemel Hempstead, UK
Native PAGE cathode buffer additive	BN2002	ThermoFisher Scientific, Hemel Hempstead, UK
Native PAGE electrophoresis buffer	BN2001	ThermoFisher Scientific, Hemel Hempstead, UK
Native sample buffer	BN20032	ThermoFisher Scientific, Hemel Hempstead, UK
NDUFS1 antibody	12444-1-AP	ProteinTech Europe, Manchester, UK
NEB 5-alpha high efficency competent E. coli cells	C2987P	New England Biolabs, MA, USA
Nuclease free water	129114	QIAGEN, Manchester, UK
Oligomycin A	942-003	Seahorse Bioscence, MA, USA
OptiMEM	51985-026	ThermoFisher Scientific, Hemel Hempstead, UK
PBS	PBS100L	Formedium, Norfolk, UK
Pellet paint co-precipitant	69049-3	ThermoFisher Scientific, Hemel Hempstead, UK
Penicillin/Streptomycin	15140122	ThermoFisher Scientific, Hemel Hempstead, UK
Phosphate buffered saline	PBS100L	Formedium, Norfolk, UK
Propan-2-ol	20842.323	VWR Chemicals, Lutterworth, UK
pSpCas9(BB)-2A-GFP plasmid	PX458	Addgene, Teddington, UK
PVDF membrane	IPVH00010	Millipore, MA, USA
QIAGEN DNA miniprep kit	27104	QIAGEN, Manchester, UK
Rabbit secondary antibody	31460	ThermoFisher Scientific, Hemel Hempstead, UK
RNAse free DNAse I	AM2222	ThermoFisher Scientific, Hemel Hempstead, UK

Reagent name	Product code	Source
Rotenone	101706-100	Seahorse Bioscence, MA, USA
SDS	S/P530/53	ThermoFisher Scientific, Hemel Hempstead, UK
Sequencing grade trypsin	11418475001	Sigma-Aldrich, Poole, UK
SILAC DMEM	12132410	ThermoFisher Scientific, Hemel Hempstead, UK
SILAC IMDM	88423	ThermoFisher Scientific, Hemel Hempstead, UK
SOC outgrowth medium	B9020S	New England Biolabs, MA, USA
Sodium acetate	27649.297	VWR Chemicals, Lutterworth, UK
Sodium carbonate decahydrate	S/2760/53	ThermoFisher Scientific, Hemel Hempstead, UK
Sodium chloride	NAC02	Formedium, Norfolk, UK
Sodium hydrogen carbonate	S/4240/53	ThermoFisher Scientific, Hemel Hempstead, UK
Sodium pyruvate	S8636	Sigma-Aldrich, Poole, UK
Solution 13	910-3013	ChemoMetec, Lillerod, Denmark
Spin-X microcellulose filter tubes	8163	Sigma-Aldrich, Poole, UK
Succinate dehydrogenase chain B antibody	A002868	Atlas Antibodies, Stockholm, Sweden
Sulforhodamine B	1367499	Kodak, Watford, UK
Synthetic oligonucleotide scaffold RNA plasmid	66565	Addgene, Teddington, UK
Synthetic oligonucleotide siRNA (ATP synthase subunit-6.8 kDa)	SI00319585*	QIAGEN, Manchester, UK
Synthetic oligonucleotide siRNA (ATP synthase subunit-DAPIT)	SI00758079*	QIAGEN, Manchester, UK
Synthetic oligonucleotide siRNA (ATP synthase subunit-e)	1027415*	QIAGEN, Manchester, UK
Synthetic oligonucleotide siRNA (ATP synthase subunit-f)	SI03211054*	QIAGEN, Manchester, UK
Synthetic oligonucleotide siRNA (ATP synthase subunit-g)	8017355335*	Sigma-Aldrich, Poole, UK
T4 kinase	M5201S	New England Biolabs, MA, USA
T4 kinase buffer	B0201S	New England Biolabs, MA, USA
T7 ligase	M03185	New England Biolabs, MA, USA
T7 ligation buffer	E26215	New England Biolabs, MA, USA
TCEP	1001240154	Sigma-Aldrich, Poole, UK
TEMED	1000862779	Sigma-Aldrich, Poole, UK
Tissue culture plates 10 cm	353003	VWR Chemicals, Lutterworth, UK
Tissue culture plates 15 cm	2021-01	ThermoFisher Scientific, Hemel Hempstead, UK
Tissue culture plates 6 well	3526	Corning Inc. NY, USA
Tissue culture plates 96 well	3595	Corning Inc. NY, USA
Trichloroacetic acid	T4885-2KG	Sigma-Aldrich, Poole, UK
Trifluoroacetic acid	74564-10ML-F	Sigma-Aldrich, Poole, UK
Tris base	T15031KG	Sigma-Aldrich, Poole, UK
Trypsin-EDTA dissociation reagent	15400-054	ThermoFisher Scientific, Hemel Hempstead, UK
Tween-20	17767-B	Sigma-Aldrich, Poole, UK
Uridine	U3003-5G	Sigma-Aldrich, Poole, UK
Western blotting tank	1703930	Biorad, Hemel Helpstead, UK
XCell SureLock electrophoresis tank	EI0001	ThermoFisher Scientific, Hemel Hempstead, UK
XF assay medium	102365-100	Seahorse Bioscence, MA, USA
XF Callibration buffer pH 7.4	100840-100	Seahorse Bioscence, MA, USA
XFe24 cell culture plate	100777-004	Seahorse Bioscence, MA, USA

Reagent name	Product code	Source
XFe24 extracellular flux assay kit (probe plate)	102340-100	Seahorse Bioscence, MA, USA

Reagents with a '*' were custom products

Appendix II – Constituents of buffers

Buffer	**Constituents**	**Section**
Cell lysis buffer	10 mM Tris HCl pH 7.4, 0.2% w/v SDS, Roche protease inhibitors (1 tablet/50 mL) contains phenylmethane sulphonyl fluoride, Pefabloc SC, Pefabloc SC plus, E-64, aprotinin, leupeptin, α-$_2$-macroglobulin	2.6.8
Coomassie blue gel stain	0.2% w/v Coomassie R-250, 50% v/v methanol, 7% v/v acetic acid	2.4.6, 2.5.1
Destain	50% v/v methanol, 7% v/v acetic acid	2.4.6, 2.5.1
DNA loading buffer	10% v/v glycerol, 20 mM Tris HCl pH 7.4, 5 mM EDTA, 0.01% w/v bromophenol blue, 0.2% w/v SDS	2.3.2, 2.6.5
Freezing solution	40% v/v DMEM or IMDM, 50% v/v FBS, 10% v/v DMSO	2.2.6, 2.6.7
Laemmli SDS PAGE electrophoresis buffer (10X)	3.84 M glycine, 0.5 M Tris base, 69.3 mM SDS, pH 6.8	2.4.6, 2.6.8
Matrix solution (MALDI TOF)	10 mg/mL a-cyano-4-hydroxy-trans-cinnamic acid, 60% v/v acetonitrile, 1% v/v trifluoroacetic acid	2.5.2
Milk/PBS Tween solution	5% w/v Marvel skimmed milk powder, 140 mM NaCl, 0.2 mM $PO43^-$, 0.1% v/v Tween 20, pH 7.4	2.4.7
Native PAGE cathode buffer	1:20 aqueous dilution of cathode buffer additive, 1:20 aqueous dilution of electrophoresis buffer, pH 8.3	2.4.4
Native PAGE anode buffer	1:20 aqueous dilution of electrophoresis buffer, pH 8.3	2.4.4
PBS	140 mM NaCl, 0.2 mM $PO4^{3-}$, pH 7.4	2.2.1, 2.6.6, 2.2.5
PBS Tween	140 mM NaCl, 0.2 mM $PO43^-$, 0.1% v/v Tween 20, pH 7.4	2.4.7, 2.6.7
PBS with protease inhibitors	140 mM NaCl, 0.2 mM $PO43^-$, 0.1% v/v Tween 20, Roche protease inhibitors (1 tablet/50 mL) contains phenylmethane sulfonyl fluoride, Pefabloc SC, Pefabloc SC plus, E-64, Aprotinin, leupeptin, α-$_2$-macroglobulin, pH 7.4	2.2.5, 2.4.1, 2.4.2
Peptide extraction solution	60% v/v acetonitrile, 4% v/v formic acid	2.5.2, 2.5.3
SDS PAGE gel loading buffer pH 6.8 (4X)	40% v/v glycerol, 4 mM EDTA, 200 mM Tris-HCl pH 6.8, 4% w/v SDS	2.4.6, 2.6.8
SDS PAGE gel loading buffer pH 8 (4X)	40% v/v glycerol, 4 mM EDTA, 200 mM Tris-HCl pH 8, 4% w/v SDS	2.5.1
SDS PAGE separating gel	12-22% w/v acrylamide (gradient), 375 mM Tris-HCl pH 8.8, 0.1% w/v SDS, 0.0007% TEMED, 0.0003% ammonium persulphate	2.4.5

Buffer	Constituents	Section
SDS PAGE stacking gel	4% w/v acrylamide, 65 mM Tris-HCl pH 6.8, 0.05% w/v SDS, 0.0007% TMED, 0.0003% w/v ammonium persulphate	2.4.5
Sulforhodamine B solution	0.4% w/v sulphorhodamine B, 1% v/v acetic acid	2.2.7
TBE electrophoresis buffer	90 mM Tris-boric acid, 1 mM EDTA, pH 8.0	2.3.2, 2.6.5
Trypsin digestion buffer	20 mM Tris-HCl pH 8.0, 5 mM $CaCl_2$	2.5.2, 2.5.3
Trypsin digestion solution	12.5 ng/μL sequencing grade trypsin in trypsin digestion buffer	2.5.2, 2.5.3
Western blotting SDS carbonate buffer	10 mM sodium hydrogen carbonate, 3 mM sodium carbonate, 0.025% w/v SDS, pH 9.9	2.4.7
Western blotting native carbonate buffer	10 mM sodium hydrogen carbonate, 3 mM sodium carbonate, pH 9.9	2.4.7

Table S1. Peptide mass mapping of human ATP synthase subunits from 143B cells used in Figs. 3.5, 3.9, 3.16, 3.22 and 3.26.

Immunopurified ATP synthase subunits were separated by SDS-PAGE and Coomassie stained. Individual bands were excised from the gel and digested with trypsin or chymotrypsin for subunit-c. The peptides were analysed by MALDI TOFTOF mass spectrometry.

Protein	Protein ID	Peptides (N-C-term)	Score (p=<0.05)	Observed Mr	Expected Mr	Calculated Mr
α	P25705	R.ILGADTSVDLEETGR.V	72	1575.8016	1574.7943	1574.7788
		R.VLSIGDGIAR.V	26	1000.5681	999.5608	999.5713
		R.TGAIVDVPVGEELLGR.V	91	1624.9058	1623.8985	1623.8832
		K.AVDSLVPIGR.G	49	1026.5853	1025.578	1025.5869
		R.QMSLLLR.R	22	860.4755	859.4682	859.4949
		R.EAYPGDVFYLHSR.L	94	1553.7551	1552.7478	1552.731
		K.GIRPAINVGLSVSR.V	38	1438.865	1437.8577	1437.8416
		K.LELAQYR.E	39	892.4663	891.459	891.4814
		R.EVAAFAQFGSDLDAATQQLLSR.G	114	2338.1326	2337.1253	2337.1601
		K.QGQYSPMAIEEQVAVIYAGVR.G	83	2309.1316	2308.1243	2308.1521
		K.FENAFLSHVVSQHQALLGTIR.A	49	2367.1943	2366.187	2366.2495
β	P06576	R.LVLEVAQHLGESTVR.T	116	1650.8815	1649.8742	1649.9101
		R.TIAMDGTEGLVR.G	65	1262.6215	1261.6142	1261.6336
		K.IPVGPETLGR.I	57	1038.5869	1037.5796	1037.5869
		R.IMNVIGEPIDER.G	84	1385.6914	1384.6841	1384.702
		K.AHGGYSVFAGVGER.T	115	1406.6606	1405.6533	1405.6739
		K.VALVYGQMNEPPGAR.A	64	1601.782	1600.7747	1600.8031
		K.VALVYGQMNEPPGAR.A + Oxidation (M)	44	1617.7772	1616.7699	1616.7981

Protein	Protein ID	Peptides (N-C-term)	Score (p=<0.05)	Observed Mr	Expected Mr	Calculated Mr
β	P06576	R.VALTGLTVAEYFR.D	57	1439.7587	1438.7514	1438.782
		R.AIAELGIYPAVDPLDSTSR.I	98	1988.0032	1986.9959	1987.0262
		R.IMDPNIVGSEHYDVAR.G	110	1815.8413	1814.834	1814.8621
		K.SLQDIIAILGMDELSEEDKLTVSR.A	125	2675.3938	2674.3865	2674.3735
		R.FLSQPFQVAEVFTGHMGK.L	76	2022.9808	2021.9735	2022.0033
γ	P36542	K.HLLIGVSSDR.G	60	1096.6023	1095.595	1095.6037
		K.EVMLVGIGDKIR.G	14	1329.7355	1328.7282	1328.7486
		K.EVMLVGIGDKIR.G + Oxidation (M)	45	1345.7283	1344.721	1344.7435
		R.THSDQFLVAFK.E	96	1292.6411	1291.6338	1291.6561
		K.NASEMIDKLTLTFNR.T	86	1752.8694	1751.8621	1751.8876
		K.NASEMIDKLTLTFNR.T + Oxidation (M)	65	1768.8634	1767.8561	1767.8825
IgG	P01642	R.ASQSIGTSIHWYQQR.T	94	1761.978	1760.9707	1760.8594
		K.YASESISGIPSR.F	85	1266.712	1265.7047	1265.6252
b	P24539	R.YGLIPEEFFQFLYPK.T	90	1890.8699	1889.8626	1889.9604
		R.HYLFDVQR.N	68	1077.5244	1076.5171	1076.5403
		R.NNIAMALEVTYR.E	61	1394.6123	1393.605	1393.7023
OSCP	P48047	K.LVRPPVQVYGIEGR.Y	57	1582.8601	1581.8528	1581.8991
		R.FSPLTTNLINLLAENGR.L	127	1872.9762	1871.9689	1872.0105
		R.LSNTQGVVSAFSTMMSVHR.G	59	2051.9707	2050.9634	2050.9928
		R.LSNTQGVVSAFSTMMSVHR.G + Oxidation (M)	21	2067.9717	2066.9644	2066.9878
		K.SFLSQGQVLK.L	52	1106.5984	1105.5911	1105.6132
		K.TDPSILGGMIVR.I	40	1258.6495	1257.6422	1257.6751
		K.TDPSILGGMIVR.I + Oxidation (M)	28	1274.6398	1273.6325	1273.67
d	O75947	K.TIDWVAFAEIIPQNQK.A	121	1872.9885	1871.9812	1871.9781

Protein	Protein ID	Peptides (N-C-term)	Score (p=<0.05)	Observed Mr	Expected Mr	Calculated Mr
d	O75947	K.SWNETLTSR.L	30	1093.5205	1092.5132	1092.52
		K.KYPYWPHQPIENL.-	76	1684.8433	1683.836	1683.8409
a	P00846	R.LITTQQWLIK.L	62	1243.7179	1242.7106	1242.7336
δ	P30049	K.AQAELVGTADEATR.A	55	1431.6611	1430.6538	1430.7001
g	O75964	K.TPALVNAAVTYSKPR.L	76	1587.8561	1586.8488	1586.878
		R.LATFWYYAK.V	24	1162.574	1161.5667	1161.5859
		K.VELVPPTPAEIPR.A	41	1417.7802	1416.7729	1416.7977
F_6	P18859	K.LFVDKIR.E	17	890.5505	889.5432	889.5385
		R.QTSGGPVDASSEYQQELER.E	92	2080.9265	2079.9192	2079.9345
f	P56134	K.LGELPSWILMR.D + Oxidation (M)	24	1330.6936	1329.6863	1329.7115
e	P56385	R.YNYLKPR.A	15	953.529	952.5218	952.513
A6L	P03928	K.NYNKPWEPK.W	53	1175.5671	1174.5598	1174.5771
DAPIT	Q96IX5	M.AGPESDAQYQFTGIK.K	108	1611.8262	1610.8189	1610.7576
		K.YFNSYTLTGR.M	48	1221.6627	1220.6554	1220.5826
c	P05496	Y.ARNPSLKQQLF.S + Trimethyl (K)	32	1343.7771	1342.7698	1342.7721
ε	P56382	R.QAGLSYIR.F	50	907.5135	906.5062	906.4923
		R.DALKTEFK.A	55	951.4856	950.4783	950.5073

Table S2. Peptide mass mapping of human control and Δf-HAP1 ATP synthase subunits used in Fig. 3.9. Immunopurified ATP synthase subunits from control HAP1 cells and Δf-HAP1 cells were separated by SDS-PAGE and Coomassie stained. Individual bands were excised from the gel and digested with trypsin or chymotrypsin in the case of subunit-c. The peptides were analysed by MALDI TOFTOF mass spectrometry.

Protein	Protein ID	Peptides (N-C-term)	Score (p=<0.05)	Observed Mr	Expected Mr	Calculated Mr
Control						
α	P25705	R.TGAIVDVPVGEELLGR.V	133	1624.8735	1623.8662	1623.8832
		R.ISVREPMQTGIK.A	51	1358.7233	1357.716	1357.7388
		K.AVDSLVPIGR.G	66	1026.5868	1025.5795	1025.5869
		R.EAYPGDVFYLHSR.L	107	1553.7346	1552.7273	1552.731
		K.LELAQYR.E	38	892.4937	891.4864	891.4814
		R.EVAAFAQFGSDLDAATQQLLSR.G	87	2338.2654	2337.2581	2337.1601
		K.QGQYSPMAIEEQVAVIYAGVR.G	82	2309.2786	2308.2713	2308.1521
		K.FENAFLSHVVSQHQALLGTIR.A	40	2367.3594	2366.3521	2366.2495
β	P06576	R.LVLEVAQHLGESTVR.T	96	1650.9366	1649.9293	1649.9101
		R.TIAMDGTEGLVR.G	124	1262.6577	1261.6504	1261.6336
		R.IMNVIGEPIDER.G	89	1385.7244	1384.7171	1384.702
		K.VALVYGQMNEPPGAR.A	86	1601.8311	1600.8238	1600.8031
		R.VALTGLTVAEYFR.D	56	1439.8069	1438.7996	1438.782
		R.DQEGQDVLLFIDNIFR.F	57	1922.0371	1921.0298	1920.9581
		R.IPSAVGYQPTLATDMGTMQER.I	96	2266.1731	2265.1658	2265.077
		R.AIAELGIYPAVDPLDSTSR.I	109	1988.0493	1987.042	1987.0262
		R.IMDPNIVGSEHYDVAR.G	127	1815.8784	1814.8711	1814.8621
		K.SLQDIIAILGMDELSEEDKLTVSR.A	139	2675.5227	2674.5154	2674.3735

Protein	Protein ID	Peptides (N-C-term)	Score (p=<0.05)	Observed Mr	Expected Mr	Calculated Mr
γ	P36542	R.IYGLGSLALYEK.A	99	1326.7048	1325.6975	1325.7231
		K.HLLIGVSSDR.G	84	1096.6499	1095.6426	1095.6037
		R.THSDQFLVAFK.E	96	1292.6501	1291.6428	1291.6561
		K.NASEMIDKLTLTFNR.T	93	1752.9474	1751.9401	1751.8876
		K.NASEMIDKLTLTFNR.T + Oxidation (M)	72	1768.8804	1767.8731	1767.8825
		K.LTLTFNR.T	24	864.523	863.5157	863.4865
IgG	P01642	R.ASQSIGTSIHWYQQR.T	138	1761.92	1760.9127	1760.8594
		K.YASESISGIPSR.F	89	1266.6268	1265.6195	1265.6252
b	P24539	R.YGLIPEEFFQFLYPK.T	99	1890.9637	1889.9564	1889.9604
		K.KYGPFVADFADK.L	48	1357.6434	1356.6361	1356.6714
		K.YGPFVADFADK.L	62	1229.5483	1228.541	1228.5764
		K.QASIQHIQNAIDTEK.S	127	1695.8215	1694.8142	1694.8587
		R.HYLFDVQR.N	79	1077.5846	1076.5773	1076.5403
		R.NNIAMALEVTYR.E	57	1394.7386	1393.7313	1393.7023
		R.NNIAMALEVTYR.E + Oxidation (M)	49	1410.6627	1409.6554	1409.6973
		R.LDYHISVQNMMR.R	80	1506.7422	1505.7349	1505.7119
		R.LDYHISVQNMMR.R + 2 Oxidation (M)	19	1538.6437	1537.6364	1537.7017
		K.EQEHMINWVEK.H	84	1442.6256	1441.6183	1441.666
		K.HVVQSISTQQEK.E	53	1383.6741	1382.6668	1382.7154
OSCP	P48047	K.LVRPPVQVYGIEGR.Y	66	1583.0537	1582.0464	1581.8991
		K.VAASVLNPYVK.R	64	1160.6371	1159.6298	1159.6601
		R.FSPLTTNLINLLAENGR.L	124	1873.1711	1872.1638	1872.0105
		R.LSNTQGVVSAFSTMMSVHR.G	43	2052.1074	2051.1001	2050.9928
		K.SFLSQGQVLK.L	52	1106.6141	1105.6068	1105.6132
		K.TDPSILGGMIVR.I	67	1258.7515	1257.7442	1257.6751

Protein	Protein ID	Peptides (N-C-term)	Score (p=<0.05)	Observed Mr	Expected Mr	Calculated Mr
OSCP	P48047	K.TDPSILGGMIVR.I + Oxidation (M)	46	1274.692	1273.6847	1273.67
d	O75947	K.TIDWVAFAEIIPQNQK.A	124	1873.0718	1872.0645	1871.9781
		K.SWNETLTSR.L	74	1093.5862	1092.5789	1092.52
		R.LAALPENPPAIDWAYYK.A	99	1932.0472	1931.0399	1930.9828
		K.AGLVDDFEKK.F	32	1121.5892	1120.5819	1120.5764
		K.NLIPFDQMTIEDLNEAFPETK.L	83	2465.0962	2464.0889	2464.1832
		K.NLIPFDQMTIEDLNEAFPETK.L + Oxidation (M)	48	2481.0286	2480.0213	2480.1781
		K.KYPYWPHQPIENL.-	79	1684.96	1683.9527	1683.8409
		K.YPYWPHQPIENL.-	69	1556.8456	1555.8383	1555.7459
a	P00846	R.LITTQQWLIK.L	69	1243.7802	1242.7729	1242.7336
δ	P30049	K.AQAELVGTADEATR.A	111	1431.8485	1430.8412	1430.7001
		R.IEANEALVK.A	42	986.4989	985.4916	985.5444
f	P56134	K.LGELPSWILMR.D	65	1314.8575	1313.8502	1313.7166
		K.LGELPSWILMR.D + Oxidation (M)	45	1330.7722	1329.7649	1329.7115
		R.DFSPSGIFGAFQR.G	63	1428.8441	1427.8368	1427.6834
IF1	Q9UII2	K.HHEEEIVHHK.K	55	1294.64	1293.6327	1293.6214
		K.HHEEEIVHHKK.E	56	1422.7673	1421.76	1421.7164
g	O75964	K.TPALVNAAVTYSKPR.L	145	1588.1099	1587.1026	1586.878
		R.LATFWYYAK.V	67	1162.6484	1161.6411	1161.5859
		K.VELVPPTPAEIPR.A	70	1418.0217	1417.0144	1416.7977
		K.KIVNSAQTGSFK.Q	64	1279.8025	1278.7952	1278.6932
		K.IVNSAQTGSFK.Q	17	1151.6528	1150.6455	1150.5982
F_6	P18859	R.QTSGGPVDASSEYQQELER.E	173	2081.0811	2080.0738	2079.9345

Protein	Protein ID	Peptides (N-C-term)	Score (p=<0.05)	Observed Mr	Expected Mr	Calculated Mr
e	P56385	-.MVPPVQVSPLIK.L	41	1307.7751	1306.7678	1306.7683
		-.MVPPVQVSPLIK.L + Oxidation (M)	41	1323.7833	1322.776	1322.7632
		M.VPPVQVSPLIK.L	59	1176.6781	1175.6708	1175.7278
		R.YNYLKPR.A	30	953.5331	952.5258	952.513
DAPIT	Q96IX5	M.AGPESDAQYQFTGIK.K	108	1611.8262	1610.8189	1610.7576
		K.YFNSYTLTGR.M	48	1221.6627	1220.6554	1220.5826
A6L	P03928	K.MLNTNYHLPPSPKPMK.M + Oxidation (M)	28	1883.9686	1882.9613	1882.9433
		K.NYNKPWEPK.W	48	1175.5834	1174.5761	1174.5771
6.8		K.ASAPAPGHH.-	47	844.3781	843.3708	843.3987
ε	P56382	R.QAGLSYIR.F	50	907.5135	906.5062	906.4923
		R.DALKTEFK.A	55	951.4856	950.4783	950.5073
c	P05496	K.FIGAGAATVGVAGSGAGIGTVFGSLIIGYAR.N	185	2810.5803	2809.573	2809.5127
Δf						
α	P25705	R.ILGADTSVDLEETGR.V	52	1575.7924	1574.7851	1574.7788
		R.VLSIGDGIAR.V	58	1000.6217	999.6144	999.5713
		R.TGAIVDVPVGEELLGR.V	123	1624.9122	1623.9049	1623.8832
		K.AVDSLVPIGR.G	64	1026.64	1025.6327	1025.5869
		R.QMSLLLR.R	32	860.569	859.5618	859.4949
		R.EAYPGDVFYLHSR.L	107	1553.7738	1552.7665	1552.731
		K.GIRPAINVGLSVSR.V	17	1438.8564	1437.8491	1437.8416
		K.LELAQYR.E	40	892.5522	891.545	891.4814
		R.EVAAFAQFGSDLDAATQQLLSR.G	90	2338.2651	2337.2578	2337.1601
		K.QGQYSPMAIEEQVAVIYAGVR.G	84	2309.2795	2308.2722	2308.1521

Protein	Protein ID	Peptides (N-C-term)	Score (p=<0.05)	Observed Mr	Expected Mr	Calculated Mr
α	P25705	K.FENAFLSHVVSQHQALLGTIR.A	31	2367.3457	2366.3384	2366.2495
β	P06576	R.LVLEVAQHLGESTVR.T	101	1650.7437	1649.7364	1649.9101
		R.TIAMDGTEGLVR.G	117	1262.5286	1261.5213	1261.6336
		R.IMNVIGEPIDER.G	85	1385.5762	1384.5689	1384.702
		K.AHGGYSVFAGVGER.T	115	1406.5563	1405.549	1405.6739
		K.VALVYGQMNEPPGAR.A	101	1601.6509	1600.6436	1600.8031
		R.VALTGLTVAEYFR.D	54	1439.6506	1438.6433	1438.782
		R.DQEGQDVLLFIDNIFR.F	55	1921.822	1920.8147	1920.9581
		R.IPSAVGYQPTLATDMGTMQER.I	112	2265.915	2264.9077	2265.077
		R.AIAELGIYPAVDPLDSTSR.I	109	1987.8179	1986.8106	1987.0262
		R.IMDPNIVGSEHYDVAR.G	131	1815.6686	1814.6613	1814.8621
		K.SLQDIIAILGMDELSEEDKLTVSR.A	143	2675.2141	2674.2068	2674.3735
γ	P36542	R.IYGLGSLALYEK.A	99	1326.7742	1325.7669	1325.7231
		K.HLLIGVSSDR.G	94	1096.6573	1095.65	1095.6037
		R.THSDQFLVAFK.E	89	1292.707	1291.6997	1291.6561
		R.KPPTFGDASVIALELLNSGYEFDEGSIIFNK.F	18	3370.9238	3369.9165	3370.6973
		K.NASEMIDKLTLTFNR.T	100	1753.0558	1752.0485	1751.8876
		K.LTLTFNR.T	29	864.4434	863.4361	863.4865
IgG	P01642	R.ASQSIGTSIHWYQQR.T	138	1761.9146	1760.9073	1760.8594
		K.YASESISGIPSR.F	61	1266.6421	1265.6348	1265.6252
b	P24539	R.YGLIPEEFFQFLYPK.T	97	1890.9695	1889.9622	1889.9604
		K.QASIQHIQNAIDTEK.S	119	1695.8459	1694.8386	1694.8587
		K.SQQALVQK.R	29	901.4849	900.4776	900.5029
		R.HYLFDVQR.N	71	1077.5983	1076.591	1076.5403
		R.NNIAMALEVTYR.E	51	1394.7522	1393.7449	1393.7023

Protein	Protein ID	Peptides (N-C-term)	Score (p=<0.05)	Observed Mr	Expected Mr	Calculated Mr
b	P24539	R.NNIAMALEVTYR.E + Oxidation (M)	58	1410.6865	1409.6792	1409.6973
		R.LDYHISVQNMMR.R	94	1506.7694	1505.7621	1505.7119
		R.LDYHISVQNMMR.R + 2 Oxidation (M)	26	1538.6814	1537.6741	1537.7017
		K.EQEHMINWVEK.H	68	1442.6458	1441.6385	1441.666
		K.HVVQSISTQQEK.E	67	1383.7032	1382.6959	1382.7154
OSCP	P48047	K.LVRPPVQVYGIEGR.Y	59	1583.0765	1582.0692	1581.8991
		R.YATALYSAASK.Q	52	1145.5635	1144.5562	1144.5764
		K.VAASVLNPYVK.R	78	1160.6448	1159.6375	1159.6601
		R.FSPLTTNLINLLAENGR.L	149	1873.1957	1872.1884	1872.0105
		R.LSNTQGVVSAFSTMMSVHR.G	65	2052.1421	2051.1348	2050.9928
		K.SFLSQGQVLK.L	59	1106.6141	1105.6068	1105.6132
		K.TDPSILGGMIVR.I	79	1258.7667	1257.7594	1257.6751
		K.TDPSILGGMIVR.I + Oxidation (M)	49	1274.7141	1273.7068	1273.67
d	O75947	K.TIDWVAFAEIIPQNQK.A	125	1873.0857	1872.0784	1871.9781
		K.SWNETLTSR.L	78	1093.593	1092.5857	1092.52
		R.LAALPENPPAIDWAYYK.A	93	1932.062	1931.0547	1930.9828
		K.AGLVDDFEKK.F	44	1121.5977	1120.5904	1120.5764
		K.YTAQVDAEEKEDVK.S	77	1624.8783	1623.871	1623.7628
		K.NLIPFDQMTIEDLNEAFPETK.L	77	2465.05	2464.0427	2464.1832
		K.NLIPFDQMTIEDLNEAFPETK.L + Oxidation (M)	44	2481.0068	2479.9995	2480.1781
		K.KYPYWPHQPIENL	73	1684.9785	1683.9712	1683.8409
		K.YPYWPHQPIENL.	80	1556.8713	1555.864	1555.7459
		R.YGLIPEEFFQFLYPK.T	62	1890.9778	1889.9705	1889.9604
		R.HYLFDVQR.N	46	1077.597	1076.5897	1076.5403
		R.NNIAMALEVTYR.E	30	1394.7948	1393.7875	1393.7023

Protein	Protein ID	Peptides (N-C-term)	Score (p=<0.05)	Observed Mr	Expected Mr	Calculated Mr
d	O75947	R.NNIAMALEVTYR.E + Oxidation (M)	50	1410.6984	1409.6911	1409.6973
		R.LDYHISVQNMMR.R	31	1506.8153	1505.808	1505.7119
		K.HVVQSISTQQEK.E	79	1383.7186	1382.7113	1382.7154
δ	P30049	K.AQAELVGTADEATR.A	103	1431.8805	1430.8732	1430.7001
		R.IEANEALVK.A	44	986.4968	985.4895	985.5444
IF1	Q9UII2	K.HHEEEIVHHK.K	65	1294.6735	1293.6662	1293.6214
		K.HHEEEIVHHKK.E	66	1422.7676	1421.7603	1421.7164
g	O75964	K.TPALVNAAVTYSKPR.L	140	1587.9495	1586.9422	1586.878
		R.LATFWYYAK.V	74	1162.5815	1161.5742	1161.5859
		R.LATFWYYAKVELVPPTPAEIPR.A	64	2561.426	2560.4187	2560.373
		K.VELVPPTPAEIPR.A	85	1417.8776	1416.8703	1416.7977
		K.KIVNSAQTGSFK.Q	61	1279.6898	1278.6825	1278.6932
		K.IVNSAQTGSFK.Q	17	1151.5876	1150.5803	1150.5982
F6	P18859	K.LFVDKIR.E	40	890.5409	889.5337	889.5385
		R.QTSGGPVDASSEYQQELER.E	150	2081.0071	2079.9998	2079.9345
		K.QMFGNADMNTFPTFK.F + Oxidation (M)	51	1764.7867	1763.7794	1763.7647
		K.FEDPKFEVIEKPQA.-	89	1676.8555	1675.8482	1675.8457
e	P56385	-.MVPPVQVSPLIK.L	40	1307.7518	1306.7445	1306.7683
		-.MVPPVQVSPLIK.L + Oxidation (M)	44	1323.7537	1322.7464	1322.7632
		M.VPPVQVSPLIK.L	84	1176.6956	1175.6883	1175.7278
		R.YNYLKPR.A	35	953.5449	952.5376	952.513
		R.ELAEDDSILK.-	36	1132.5681	1131.5608	1131.5659
ε	P56382	R.QAGLSYIR.Y	38	907.5105	906.5032	906.4923
		R.DALKTEFK.A	31	951.4632	950.4559	950.5073

Protein	Protein ID	Peptides (N-C-term)	Score (p=<0.05)	Observed Mr	Expected Mr	Calculated Mr
c	P05496	K.FIGAGAATVGVAGSGAGIGTVFGSLIIGYAR.N	80	2810.3396	2809.3323	2809.5127

Table S3. Peptide mass mapping of human control and HAP1 Δg ATP synthase subunits used in Fig. 3.16. Immunopurified ATP synthase subunits from control HAP1 cells and Δg-HAP1 cells were separated by SDS-PAGE and Coomassie stained. Individual bands were excised from the gel and digested with trypsin or chymotrypsin in the case of subunit-c. The peptides were analysed by MALDI TOFTOF mass spectrometry.

Protein	Protein ID	Peptides (N-C-term)	Score (p=<0.05)	Observed Mr	Expected Mr	Calculated Mr
Control						
α	P25705	R.TGAIVDVPVGEELLGR.V	133	1624.8735	1623.8662	1623.8832
		R.ISVREPMQTGIK.A	51	**1358.7233**	1357.716	1357.7388
		K.AVDSLVPIGR.G	66	1026.5868	1025.5795	1025.5869
		R.EAYPGDVFYLHSR.L	107	1553.7346	1552.7273	1552.731
		K.LELAQYR.E	38	892.4937	891.4864	891.4814
		R.EVAAFAQFGSDLDAATQQLLSR.G	87	2338.2654	2337.2581	2337.1601
β	P06576	R.LVLEVAQHLGESTVR.T	110	1650.8716	1649.8643	1649.9101
		K.VLDSGAPIKIPVGPETLGR.I	128	1919.0558	1918.0485	1918.0888
		R.IMNVIGEPIDERGPIK.T	68	1780.9196	1779.9123	1779.9553
		K.AHGGYSVFAGVGER.T	146	1406.6449	1405.6376	1405.6739
		K.VALVYGQMNEPPGAR.A	79	1601.769	1600.7617	1600.8031
		R.AIAELGIYPAVDPLDSTSR.I	43	1987.9911	1986.9838	1987.0262
		R.IMDPNIVGSEHYDVAR.G	119	1815.8237	1814.8164	1814.8621
		R.FLSQPFQVAEVFTGHMGK.L	56	2022.9624	2021.9551	2022.0033
γ	P36542	R.IYGLGSLALYEK.A	79	1326.7354	1325.7281	1325.7231
		K.HLLIGVSSDR.G	79	1096.6064	1095.5991	1095.6037
		K.EVMLVGIGDKIR.G + Oxidation (M)	34	1345.7555	1344.7482	1344.7435

Protein	Protein ID	Peptides (N-C-term)	Score (p=<0.05)	Observed Mr	Expected Mr	Calculated Mr
γ	P36542	R.THSDQFLVAFK.E	79	1292.6687	1291.6614	1291.6561
		R.THSDQFLVAFKEVGR.K	51	1733.9117	1732.9044	1732.8897
		K.NASEMIDKLTLTFNR.T	58	1752.9076	1751.9003	1751.8876
		K.NASEMIDKLTLTFNR.T + Oxidation (M)	72	1768.9017	1767.8944	1767.8825
		R.QAVITKELIEIISGAAALD.-	178	1955.1119	1954.1046	1954.0986
IgG	P01642	R.ASQSIGTSIHWYQQR.T	122	1761.8146	1760.8073	1760.8594
b	P24539	R.YGLIPEEFFQFLYPK.T	48	1890.884	1889.8767	1889.9604
		R.HYLFDVQR.N	71	1077.5033	1076.496	1076.5403
OSCP	P48047	K.LVRPPVQVYGIEGR.Y	53	1582.799	1581.7917	1581.8991
		K.TDPSILGGMIVR.I	39	1258.5985	1257.5912	1257.6751
d	O75947	K.TIDWVAFAEIIPQNQK.A	83	1872.9907	1871.9834	1871.9781
		K.AIASSLKSWNETLTSR.L	141	1763.9187	1762.9114	1762.9213
		K.SWNETLTSR.L	59	1093.5168	1092.5095	1092.52
		R.LAALPENPPAIDWAYYK.A	78	1931.9774	1930.9701	1930.9828
		R.LAALPENPPAIDWAYYKANVAK.A	100	2415.2766	2414.2693	2414.2634
		K.KYPYWPHQPIENL.-	75	1684.8322	1683.8249	1683.8409
a	P00846	R.LITTQQWLIK.L	63	1243.7249	1242.7176	1242.7336
		R.LITTQQWLIKLTSK.Q	48	1672.9767	1671.9694	1671.9923
δ	P30049	K.ANLEKAQAELVGTADEATR.A	35	1986.9972	1985.9899	1986.0018
		K.AQAELVGTADEATR.A	28	1431.6836	1430.6763	1430.7001
		R.AEIQIRIEANEALVK.A	81	1696.9349	1695.9276	1695.9519
f	P30049	K.LLEVKLGELPSWILMR.D	46	1897.0764	1896.0691	1896.0906
		K.LLEVKLGELPSWILMR.D + Oxidation (M)	13	1913.0635	1912.0562	1912.0856
		K.LGELPSWILMR.D	68	1314.6991	1313.6918	1313.7166
		K.LGELPSWILMR.D + Oxidation (M)	43	1330.6926	1329.6853	1329.7115

Protein	Protein ID	Peptides (N-C-term)	Score (p=<0.05)	Observed Mr	Expected Mr	Calculated Mr
		R.DFSPSGIFGAFQR.G	50	1428.6604	1427.6531	1427.6834
g	O75964	R.NLVEKTPALVNAAVTYSKPR.L	63	2171.2083	2170.201	2170.211
		K.TPALVNAAVTYSKPR.L	105	1587.8588	1586.8515	1586.878
		R.LATFWYYAKVELVPPTPAEIPR.A	134	2561.3979	2560.3906	2560.373
		K.VELVPPTPAEIPR.A	32	1417.7789	1416.7716	1416.7977
F_6	P18859	R.QTSGGPVDASSEYQQELER.E	173	2081.0811	2080.0738	2079.9345
e	P56385	-.MVPPVQVSPLIKLGR.Y + Oxidation (M)	40	1649.9478	1648.9405	1648.9698
		R.YSALFLGVAYGATR.Y	90	1488.7585	1487.7512	1487.7773
		R.YSALFLGVAYGATRYNYLKPR.A	32	2423.3049	2422.2976	2422.2797
		R.YNYLKPR.A	29	953.512	952.5047	952.513
DAPIT	Q96IX5	M.AGPESDAQYQFTGIK.K	108	1611.8262	1610.8189	1610.7576
		K.YFNSYTLTGR.M	48	1221.6627	1220.6554	1220.5826
		R.IARELAEDDSILK.-	22	1472.767	1471.7597	1471.7882
A6L	P03928	K.MKNYNKPWEPK.W	40	1434.703	1433.6957	1433.7125
		K.NYNKPWEPK.W	45	1175.5696	1174.5623	1174.5771
6.8	P56378	K.NIWIPMKPYYTK.V	37	1553.7871	1552.7798	1552.8112
		K.NIWIPMKPYYTK.V + Oxidation (M)	25	1569.7751	1568.7678	1568.8061
		K.ASAPAPGHH.-	40	844.4214	843.4141	843.3987
ε	P56382	R.QAGLSYIR.F	48	907.5072	906.4999	906.4923
c	P05496	K.FIGAGAATVGVAGSGAGIGTVFGSLIIGYAR.N	185	2810.5803	2809.573	2809.5127
Δg						
α	P25705	R.TGAIVDVPVGEELLGR.V	47	1624.8656	1623.8583	1623.8832
		R.VGLKAPGIIPR.I	64	1120.7135	1119.7062	1119.7128

Protein	Protein ID	Peptides (N-C-term)	Score (p=<0.05)	Observed Mr	Expected Mr	Calculated Mr
α	P25705	R.ISVREPMQTGIK.A	23	1358.7311	1357.7238	1357.7388
		K.AVDSLVPIGRGQR.E	36	1367.7572	1366.7499	1366.7681
		K.TSIAIDTIINQKR.F	46	1472.822	1471.8147	1471.8358
		R.EAYPGDVFYLHSR.L	100	1553.7181	1552.7108	1552.731
		R.EAYPGDVFYLHSRLLER.A	59	2065.0349	2064.0276	2064.0428
		R.EVAAFAQFGSDLDAATQQLLSR.G	99	2338.1714	2337.1641	2337.1601
β	P06576	R.LVLEVAQHLGESTVR.T	125	1650.8978	1649.8905	1649.9101
		K.VLDSGAPIKIPVGPETLGR.I	140	1919.0836	1918.0763	1918.0888
		R.IMNVIGEPIDERGPIK.T	68	1780.9454	1779.9381	1779.9553
		K.AHGGYSVFAGVGER.T	145	1406.6665	1405.6592	1405.6739
		K.VALVYGQMNEPPGAR.A	70	1601.7943	1600.787	1600.8031
		K.VALVYGQMNEPPGAR.A + Oxidation (M)	32	1617.7891	1616.7818	1616.7981
		R.AIAELGIYPAVDPLDSTSR.I	60	1988.0189	1987.0116	1987.0262
		R.IMDPNIVGSEHYDVAR.G	109	1815.8505	1814.8432	1814.8621
		R.FLSQPFQVAEVFTGHMGK.L	68	2022.9944	2021.9871	2022.0033
γ	P30049	R.IYGLGSLALYEK.A	61	1326.7269	1325.7196	1325.7231
		K.HLLIGVSSDR.G	52	1096.5951	1095.5878	1095.6037
		K.EVMLVGIGDKIR.G + Oxidation (M)	17	1345.7483	1344.741	1344.7435
		R.THSDQFLVAFKEVGR.K	61	1733.9043	1732.897	1732.8897
		R.KPPTFGDASVIALELLNSGYEFDEGSIIFNKFR.S	82	3674.73	3673.7227	3673.8668
		K.NASEMIDKLTLTFNR.T	56	1752.9023	1751.895	1751.8876
		K.NASEMIDKLTLTFNR.T + Oxidation (M)	47	1768.8937	1767.8864	1767.8825
		R.QAVITKELIEIISGAAALD.-	174	1955.1071	1954.0998	1954.0986
IgG	P01642	R.ASQSIGTSIHWYQQR.T	127	1761.8616	1760.8543	1760.8594
b	P24539	R.YGLIPEEFFQFLYPK.T	63	1890.9073	1889.9	1889.9604

Protein	Protein ID	Peptides (N-C-term)	Score (p=<0.05)	Observed Mr	Expected Mr	Calculated Mr
b	P24539	R.HYLFDVQR.N	71	1077.5059	1076.4986	1076.5403
		R.NNIAMALEVTYRER.L	8	1679.7727	1678.7654	1678.846
d	O75947	K.TIDWVAFAEIIPQNQK.A	96	1872.9851	1871.9778	1871.9781
		K.AIASSLKSWNETLTSR.L	123	1763.9146	1762.9073	1762.9213
		K.SWNETLTSR.L	40	1093.5117	1092.5044	1092.52
		R.LAALPENPPAIDWAYYK.A	56	1931.9736	1930.9663	1930.9828
		R.LAALPENPPAIDWAYYKANVAK.A	106	2415.27	2414.2627	2414.2634
		K.KYPYWPHQPIENL.-	70	1684.8285	1683.8212	1683.8409
δ	P30049	K.ANLEKAQAELVGTADEATR.A	6	1987.0112	1986.0039	1986.0018
		R.AEIQIRIEANEALVK.A	29	1696.9585	1695.9512	1695.9519
Trypsin	P00760	K.SIVHPSYNSNTLNNDIMLIKLK.S	125	2514.377	2513.3697	2513.3311
		K.SIVHPSYNSNTLNNDIMLIKLK.S + Oxidation (M)	42	2530.355	2529.3477	2529.3261

Appendix IV – SILAC data

The data Tables containing the data that were used to make Figs. 3.6, 3.10. 3.11, 3.17, 3.18, 3.23 and 2.24 are provided with this web link. https://lighthouse.mrc-mbu.cam.ac.uk/cplcj2/thesis

The password is corstenthesis. The titles of the Tables are listed below.

Table S4. Proteins identified in immunopurified ATP synthase depleted of the e-subunit using siRNA.

Table S5. Proteins identified in mitoplasts of cells depleted of the e-subunit with siRNA.

Table S6. Proteins identified in immunopurified ATP synthase depleted of the f-subunit using siRNA.

Table S7. Proteins identified mitoplasts depleted of the f-subunit using siRNA.

Table S8. Protein ratios of ATP synthase subunits from mitoplasts depleted of the f-subunit in Fig. 3.10D that were calculated manually.

Table S9. Proteins identified in immunopurified Δf-HAP1 ATP synthase.

Table S10. Proteins identified in mitoplasts from Δf-HAP1 cells.

Table S11. Proteins identified in immunopurified ATP synthase depleted of the g-subunit using siRNA.

Table S12. Protein ratios from immunopurified ATP synthase depleted of the g-subunit that were calculated manually from peptide data.

Table S13. Proteins identified in mitoplasts from 143B cells depleted of the g-subunit.

Table S14. Proteins identified in immunopurified Δg-HAP1 ATP synthase.

Table S15. Proteins identified in mitoplasts from Δg-HAP1 cells.

Table S16. Proteins identified in immunopurified ATP synthase depleted of the DAPIT-subunit using siRNA.

Table S17. Proteins identified in mitoplasts from 143B cells depleted of the DAPIT-subunit were analysed by mass spectrometry and SILAC.

Table S18. Proteins identified in immunopurified ATP synthase depleted of the 6.8 kDa proteolipid-subunit using siRNA.

Table S19. Protein ratios in immunocaptured ATP synthase depleted of the 6.8 kDa proteolipid-subunit that were manually calculated from peptide data.

Table S20. Proteins identified in mitoplast material from 143B cells with suppression of the 6.8 kDa proteolipid-subunit.

Table S21. Protein ratios from 6.8 kDa proteolipid depleted mitoplasts that were calculated manually from peptide data.

Table S22. Peptide data from the MaxQuant evidence file used to manually calculate protein ratios from f-subunit suppressed mitoplasts.

Table S23. Peptide data from the MaxQuant evidence file used to manually calculate protein ratios from g-subunit suppressed immunopurified ATP synthase.

Table S24. Peptide data from the MaxQuant evidence file used to manually calculate protein ratios from 6.8 kDa proteolipid-subunit suppressed immunopurified ATP synthase.

Table S25. Peptide data from the MaxQuant evidence file used to manually calculate protein ratios from 6.8 kDa proteolipid-subunit suppressed mitoplasts.

Appendix V – Reference Figures

The Figures in Appendix V were created by Holly Ford, and were part of their thesis [138].

The Figures below were referred to in this thesis.

Fig. S22. Sequence alignment of the isoforms of IF_1. The amino acid sequences of the different IF_1 isoforms that were variously identified in quantitative mass spectrometry Figures (Figs. 3.6, 3.10, 3.11, 3.17, 3.18, 3.23 and 3.27). The Figure is referred also to as Fig. S22 in [138].

```
 IF1-P  MAVTALAARTWLGVWGVRTMQARGFGSDQSENVDRGAGSIREAGGAFGKREQA
IF1-M1  ------------------------FGSDQSENVDRGAGSIREAGGAFGKREQA
IF1-M2  -------------------------GSDQSENVDRGAGSIREAGGAFGKREQA
IF1-M3  --------------------------SDQSENVDRGAGSIREAGGAFGKREQA
                                   ***************************

 IF1-P  EEERYFRAQSREQLAALKKHHEEEIVHHKKEIERLQKEIERHKQKIKMLKHDD
IF1-M1  EEERYFRAQSREQLAALKKHHEEEIVHHKKEIERLQKEIERHKQKIKMLKHDD
IF1-M2  EEERYFRAQSREQLAALKKHHEEEIVHHKKEIERLQKEIERHKQKIKMLKHDD
IF1-M3  EEERYFRAQSREQLAALKKHHEEEIVHHKKEIERLQKEIERHKQKIKMLKHDD
        ************************************************************
```

Fig. S23. Analysis of native protein complexes of ATP synthase from 143B cells depleted of the e-, f-, g-, DAPIT- and 6.8 kDa proteolipid-subunits. Mitoplasts were prepared and solubilised with digitonin then analysed by BN-PAGE. The Figure legend was written by [138] and is included at the bottom of the Figure.

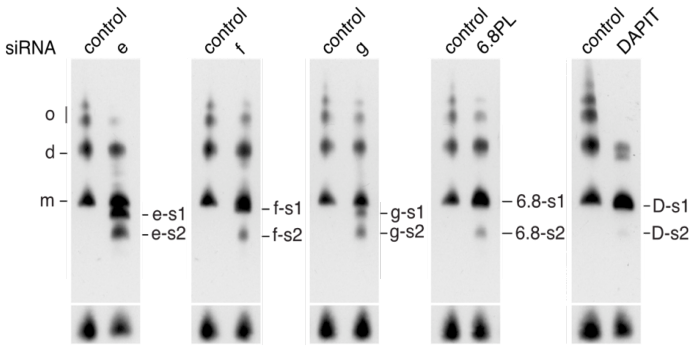

Figure 3.31 The effect of depletion of the supernumerary subunits on the assembly of ATP synthase. 143B cells were transfected with 100 nM siRNA targeting e, f, g, 6.8PL and DAPIT or a scrambled control sequence. Mitoplasts were prepared 96 h later, then fractionated by BN-PAGE and ATP synthase complexes detected with an antibody against the α-subunit; o, d and m denote oligomers, dimers and monomers of ATP synthase respectively. Subcomplexes are denoted e-s1, e-s2, f-s1, f-s2, g-s1, g-s2, 6.8-s1, 6.8-s2, D-s1 and D-s2. Citrate synthase (CS) was employed as a loading control.

Fig. S24. Relative quantitation of proteins using SILAC and mass spectrometry in 143B cells that were depleted of the DAPIT- and 6.8 kDa proteolipid-subunits with siRNA. ATP synthase was immunopurified, subunits separated by SDS-PAGE followed by in-gel digestion of proteins, which were analysed by LC-MS/MS mass spectrometry. The Figure was referred to as Figure 3.33 in [138] and in this thesis. The Figure legend written by [138] is included at the bottom of the Figure.

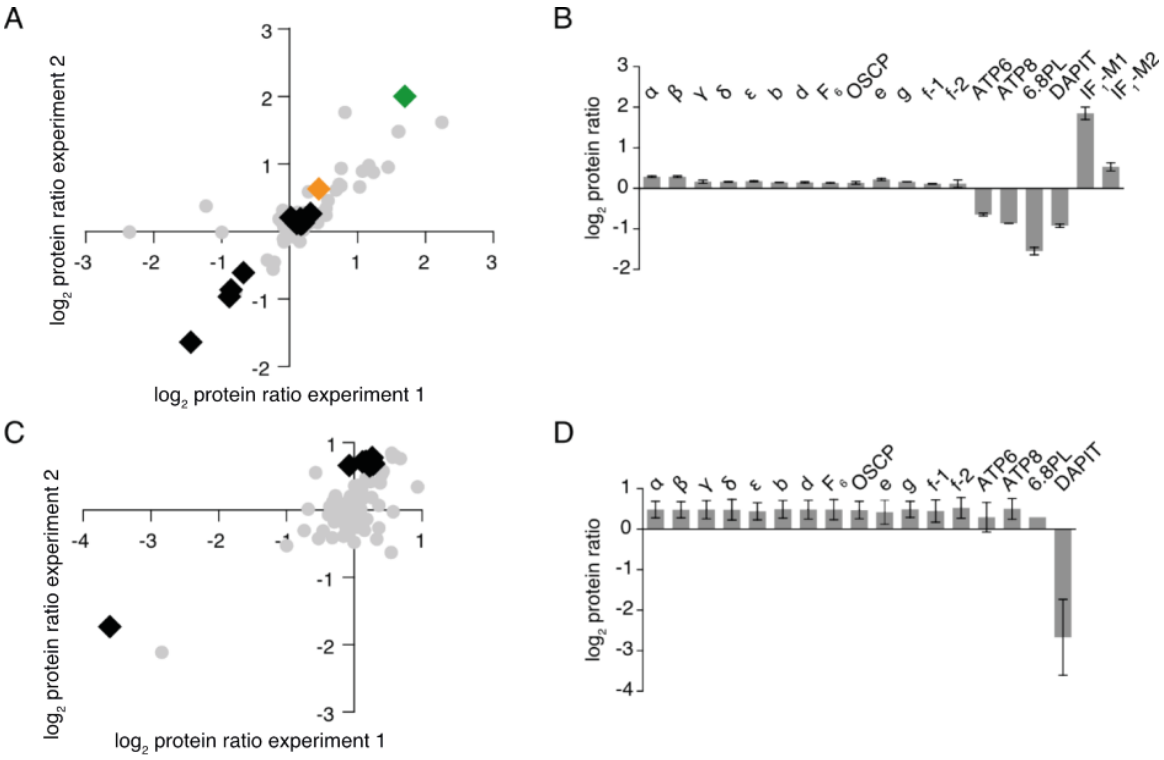

Figure 3.33 Relative quantitation of SILAC labelled samples analogous to those in Figure 3.32. A and **B**, 6.8PL depletion; **C** and **D**, DAPIT depletion. In panels A and C, ATP synthase was immunopurified from mitoplasts from SILAC labelled control and subunit-depleted cells. Samples were fractionated by SDS-PAGE and analysed by quantitative mass spectrometry. ATP synthase subunits (17 and 18, in parts A and C respectively) are black, IF_1-M1 is green, IF_1-M2 is orange and all other proteins (63 and 104, in parts A and C respectively) are grey. 6 and 8 proteins are outside the limits of the axes in the upper left quadrants of A and C respectively. Parts B and D show summaries of the relative changes in levels of ATP synthase subunits in parts A and C respectively. Bars represent median values of both relative abundance ratios of subunits. Error bars show the range of the two values.

Fig. S25. The new assembly model of human ATP synthase [138]**.** The Figure legend was written by [138] and is at the bottom of the Figure.

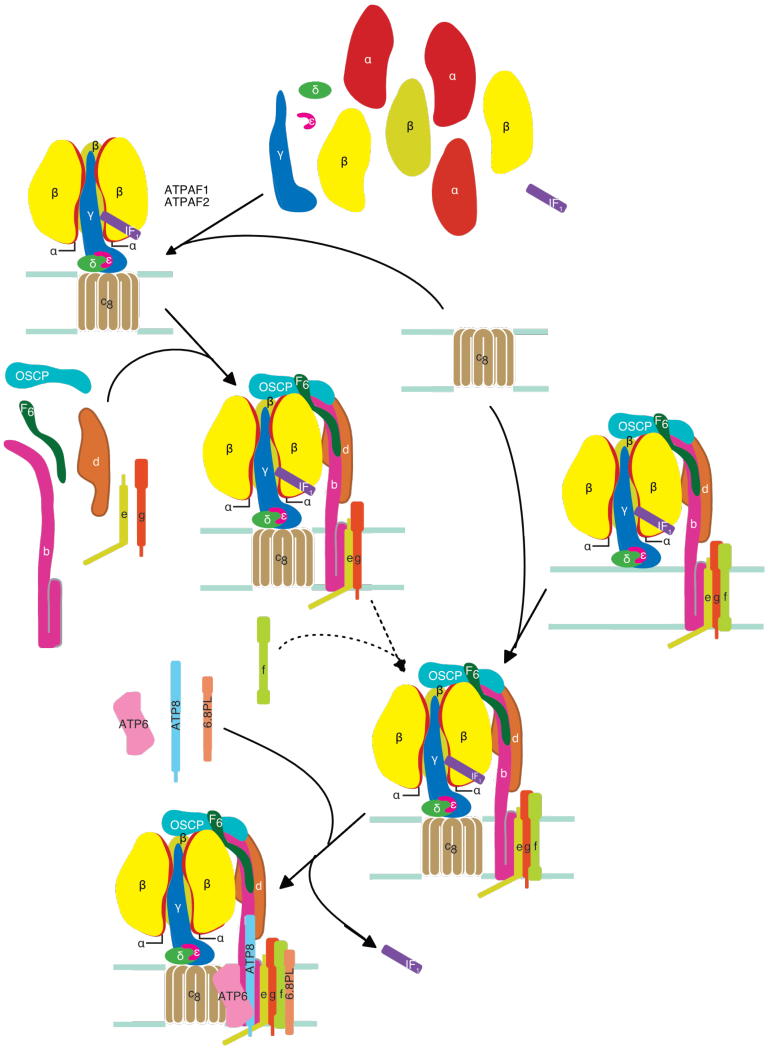

Figure 4.1 New model of the assembly of human ATP synthase. The c subunits can assemble with either F_1 domain subunits alone, forming an F_1-c8+IF_1 intermediate, or with a subcomplex comprising the F_1 domain, the peripheral stalk, and subunits e, f and g, forming an ATP synthase lacking subunits ATP6, ATP8, 6.8PL and DAPIT. This is alternatively formed by the association of peripheral stalk subunits b, d, OSCP and F_6, and subunits e, g and f with the F_1-c8 subcomplex, with subunit f likely to be incorporated last (indicated by dotted arrows). Subunits ATP6, ATP8 and 6.8PL are incorporated co-dependently to form a monomer lacking only DAPIT. IF_1 is highly associated with all F_1 domains in sub-assemblies, but dissociates once subunits ATP6, ATP8 and 6.8PL join the enzyme which is then coupled to the pmf.